

Azərbaycan Milli Elmlər Akademiyası
Fizika-Riyaziyyat və Texnika Elmləri Bölməsi
Fizika İnstitutu

1-2

Fizika

Cild

XI

2005

Bakı * Elm

THE USE OF ZEOLITE FOR ADSORPTION PURIFICATION OF THE LEATHER MANUFACTURING WATERS AT THE ELECTRIC DISCHARGE INFLUENCE

M.A. GASANOV

*Institute of Physics of National Academy of Sciences of Azerbaijan,
Az-1143, H. Javid av., 33*

The investigation results of the purification process of manufacturing waters of leather -processing with the application of the electro-discharge influence are given in the paper.

The optimal mode of the absorbing purification of manufacturing waters with the help of the zeolite of the trend NaM_{Tb} , activated by the influence of the electric discharge of the barrier type has been revealed.

The suggested method can be interest for the manufactures of the leather -processing.

The scientific-technological progress and connected with it the large scale of the industrial human activity led to the big positive transformations in the world, to the creation of the strong industrial and agricultural potentials, to the wide development of all kinds of transport, to irrigation and melioration of big ground areas, to the creation of the systems of the artificial climate.

Moreover, the state of the environment has been worsened. The pollution of the atmosphere, basins and soil by the solid, liquid and gaseous wastes achieves huge sizes, the exhaustion of the irreplaceable natural resources and firstly of the minerals and sweet water takes place [1].

That's why the nature protection from the pollution has become the one of the important global problems.

The intensive use of the waters of the different sources in the industry for the technical use and also the discharge of the waste waters in the nature basins needs the maximal their purification from the different harmful impurities.

It is need to note, that manufacturing waters of the different plant facilities are very different by the compositions, containing different impurities. In the result of this, it is impossible to suggest some universal purification methods, providing the satisfactory purity of the cleanable waters of the different compositions.

There are several methods for the purification of the manufacturing waters: physico-chemical, biological, mechanical and others.

The physico-chemical methods of the purification are: coagulation, flotation, absorption, ion exchange, extraction, rectification, crystallization, desorption and others. These methods are used for the removal of the thin-dispersed suspended particles (solid and liquid), soluble gases, mineral and organic substances from the manufacturing waters. The choice of this or that purification method (or several methods) is carried out taking into account sanitary and technological demands, making to purified manufacturing waters with the purpose of their further use, and also taking into account the quantity of manufacturing waters and pollution concentration in them, the presence of the needed material and energetical resources and process economy [2,3].

The investigation results of the purification processes of manufacturing waters of the leather manufacture with the application of the absorption method are described in the given paper.

In the paper the zeolite by the trend NaM_{Tb} is used in the capacity of the absorbents. The activation with the application of the electric discharge of the barrier type was

carried out with the goal of increase of the zeolite absorption capability.

It had been established earlier zeolites absorb very effectively the impurities from the hydrocarbon liquids, they reveal the barrier role in respect of some mineral oil: xylene, toluene, benzol, phenol and others after electric-discharge activation [4-7].

At the electric-discharge activation the filter cycle increases, but water flow on the ablution of the filtering layer decreases. The decrease of the drop rate of the filtering velocity at the repeated cycles has been also established.

The thermal treatment of the zeolite absorbents of the trend NaM_{Tb} at 800°C with the pumping during five hours was carried out on the preparatory step of the investigations. Further the samples of the absorbents were treated by the electric-discharge activation. The electric-discharge activation of the absorbents was carried out in the special discharge camera, the construction of which allowed to excite the electric charge of the barrier type in the interelectrode space.

The treatment by the barrier charge was carried out at the alternating voltage 17 kV, discharge current 100 mA, time duration of the treatment was 30 minutes.

The principal electric schema is presented in the fig.1.

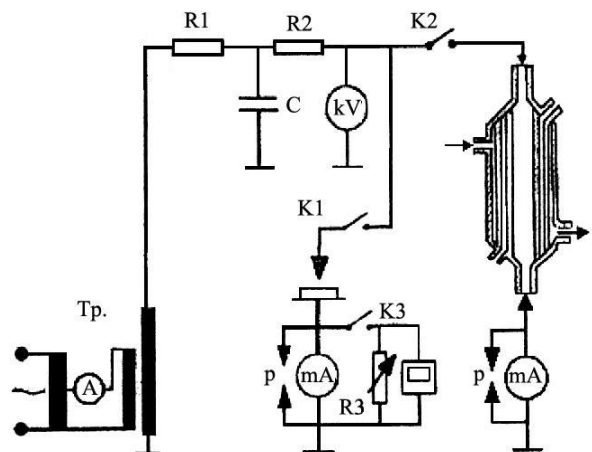


Fig.1

After discharge treatment the zeolite absorbents of the trend NaM_{Tb} were putted in the special glassy reactor and the tests of manufacturing water of the leather manufacture were gone through them.

The technological schema of the experiment carrying out is presented in the fig.2.

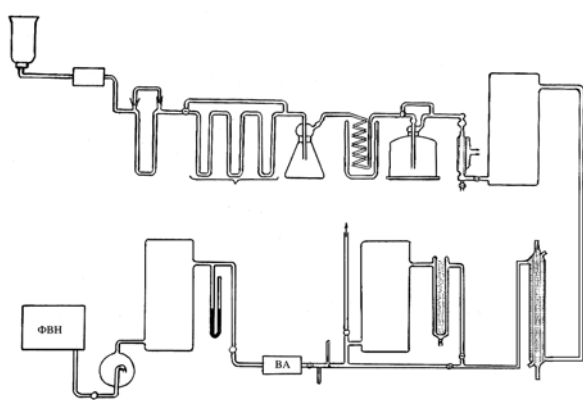


Fig. 2.

After carrying out of the purification processes, each water test with the test of the initial (crude) water was treated by the chemical analysis.

The results of the carrying out of the investigations are presented in the table. From the comparison of the data analysis follows, that content of such impurities as and others has been decreased significantly in the result of the purification.

Thus, it is established, that application of the influence of the barrier discharge at these conditions also increases significantly the efficiency of the absorbing purification of the given manufacturing waters.

The suggested method presents itself the perspective technology of the purification of manufacturing waters of leather -processing.

Table 1.
The results of the chemical analysis of the water tests from the impurities.

Name of indexes	Measurement units	Impurity content in water		
		Initial	Crude	Electro-reduced NaM _{Tb}
pH (hydrogen ion exponent)	Un	12,5	12,05	11,8
Electric conductivity mS/sm	mg/l	46400	40800	35600
TDS (total dissolved solids)	Ppm (mg/l)	40600	35000	3000
Σ_{ion} Mineralization	mg/l	43188		
Dry residue (105%)	mg/l	42425	39040	38210
Dry residue (150%)	mg/l	36875	33882	22000
Thick residue (600%)	mg/l	25285	23120	20700
PPPcalcination %	mg/l	40,4	40,8	39,8
PPP losses	mg/l	43,4	39	25
Turbidity (optical density)	un/cm	3,8	2,5	0
HCO ₃ ⁻	mg/l	18,4	16	0
CO ₃ ²⁻	mg/l	6000	444	354
OH-	mg/l	272	170	100
Ca ²⁺	mg/l	521	60	40
Na ⁺	mg/l	17377	14851	13220
NH ₄ ⁺	mg/l	875	212,7	0
NaHCO ₃	mg/l	10388	5000	100
Na ₂ CO ₃	mg/l	10388	5000	100
NaOH	mg/l	196	170	80
Ca(OH) ₂	mg/l	592,6	200	0
NH ₄ Cl	mg/l	2598,2	1234,8	0
Sera compounds, oxidated by iodine (on H ₂ S)	mg/l	32846	2846,7	0
$\sum H_2S + HS^- + S^{2-}$	mg/l	6166	4831	4250
S ²⁻	mg/l	809	282	221
HS ⁻	mg/l	5499	5240	461
PO ₄ ³⁻	mg/l	130	130	70
Chlorides, Cl-	mg/l	90000	5261	4885
Na ₂ S	mg/l	167,45	100	50
SiO ₃ ²⁻	mg/l	8048	7349	10

- [1] F. Meynk, G. Shtogg, G. Kolshuter. «Ochistka promishlennikh stochnikh vod». Leningrad.1963 p.535-555 (in Russian).
- [2] Yu.I. Tarasevich, F.D. Ovcharenko. Adsorbent, ikh poluchenije, svoystva i primeneniye.1976 p.848 pod.red. M.M. Dubinina. (in Russian).
- [3] V.A. Proskuryakov, L.I. Shmidt. Ochistka stochnikh vod v khimicheskoy promishlennosti. L. Khimiya, 1977, p.464. (in Russian).
- [4] Ch.M. Dzhavarli, A.A. Buniyatzzade, K.B. Kurbanov, M.A. Gasanov i dr. Elektronnaya obrabotka materialov. 1992, №1, p.43-45. (in Russian)
- [5] A.M. Gashimov, K.Kh. Dzhalalob, E.V. Dmitriyev, R.N. Mekhtizade. Elektronnaya obrabotka materialov. 2000, №4, c.57-58. (in Russian)
- [6] A.M. Gashimov, K.B. Kurbanov, M.A. Gasanov, I.G. Zakiyeva. Izv. NAN Azerb.Resp. ser. fiz.-tekhn. i matem nauk 2004, №2, p.81-83.
- [7] M.A. Gasanov. Power engineering problems. Baku, 2004, №3, p. 58-61.

М.Ә. Нәсәнов

**ARAKƏSMƏLİ QAZBOŞALMASININ TƏSİRİ ŞƏRAİTİNDƏ DƏRİ, SƏNAYE TULLANTI SULARININ
SEOLİTDƏ TƏMİZLƏNMƏSİ**

Məqalədə dəri sənaye tullanti sularının aşqarlardan temizlənməsinə dair tədqiqatlardan alınmış nəticələr şərh edilmişdir. Göstərilmişdir ki, arakəsməli elektrik qaz boşalmasında aktivləşdirilmiş NaM_{Tb} markalı sintetik seolitdən keçirilən dəri sənaye tullanti sularının təmizlənməsinin optimal nəticələri müəyyənləşdirilmişdir.

М.А. Гасанов

**ИСПОЛЬЗОВАНИЕ ЦЕОЛИТА ДЛЯ АДСОРБИОННОЙ ОЧИСТКИ КОЖЕВЕННЫХ
ПРОИЗВОДСТВЕННЫХ СТОЧНЫХ ВОД ПРИ ВОЗДЕЙСТВИИ ЭЛЕКТРИЧЕСКИХ РАЗРЯДОВ**

В статье приводятся результаты исследований процесса очистки сточных вод кожевенного производства с применением электроразрядного воздействия.

Выявлен оптимальный режим адсорбционной очистки сточных вод с помощью цеолитов марки NaM_{Tb} , активированного воздействием на них электрического разряда барьерного вида.

Предложенный метод может представлять интерес для предприятий кожевенного производства.

Received: 23.02.05

THE CURRENTS, LIMITED BY VOLUME CHARGE IN THE CHALCOGENIDE GLASSY SEMICONDUCTORS OF Se-Te SYSTEM

S.I. MEKHTIEVA, A.L. ISAYEV, E.A. MAMEDOV, Z.A. AGAMALIYEV

*Institute of Physics of National Academy of Sciences of Azerbaijan,
Az-1143, H. Javid av., 33*

In the stationary regime, the measurements of VAC of pure containing chlorine impurities (0,001; 0,005; 0,01; 0,1 at.%) of HGS system $\text{Se}_{100-x} \text{Te}_x$ ($x = 0; 1; 2,5; 5; 10$ at.%) in the structure of the type $\text{Te} - \text{Se}_{100-x} \text{Te}_x - \text{Al}$, have been carried out. It is established, that in the given structure, the current going mechanism is caused by the currents, limited by space charge and definite parameters (concentration and activation energy), controlling the transfer of electric charges. It is also established, that the tellurium addition in the amorphous selenide, bigger than 2 at. %, causes the increase of the increase of density state of negatively charged defects D .

Introduction.

The complex investigation of optical and photoelectric properties of chalcogenide glassy semiconductors (HGS) of Se-Te system [1-3] showed that change of chemical composition and input of impurities of halogens strongly influences on the energy spectrum of electronic states near the boundary of permitted bands and in the chink of mobility also. It must influence on material properties connected with the electric charge transfer. The aim of the present work is the revealing of current going mechanism in (HGS) of Se-Te system. With this purpose the volt-ampere characteristics (VAC) of HGS of $\text{Se}_{100-x} \text{Te}_x$ ($x=0; 1; 2,5; 5; 10$ at.%) system and HGS of $\text{Se}_{95} \text{Te}_5$ system also, containing the chlorine impurities (0,001; 0,005; 0,01; 0,1 at.%) have been measured.

Experiment technique.

The samples for measurements had structure by the type "sandwich" and presented themselves films, prepared by thermal evaporation in the vacuum at the residual pressure 10^{-6} mm. of mercury. The polished glass substrates have been used on which the lower electrode from aluminum or In_2O_3 was applied. The upper electrode was film from tellurium, evaporated on the layer of the investigated material in the vacuum. The chemical composition of the film was the same, as in the suspended matter. The substrate temperature was controlled with the help of thermocouple.

VAC of the samples were measured on the direct current in the darkness. The polarity of applied voltage is "plus" on the tellurium electrode.

Experimental results and their analysis.

VAC of HGS samples of system $(\text{Se}_{100-x} \text{Te}_x)$ ($x = 0; 1; 5; 10$ at.%) and HGS of $\text{Se}_{95} \text{Te}_5$ system, containing the impurities of chlorine (0,001; 0,005; 0,01; 0,1 at.%) correspondingly are given on the fig.1 and 2. Thicknesses of all samples are equal 10 mcm.

As it is seen, VAC contains from the several strongly expressed straight-line portions, corresponding to the degree dependence of current I on applied voltage V in the double logarithmic scale. The first portion corresponds to Ohm law (i.e. dependence $I \sim V^n$, where $n=1$). The quadratic dependence of the current on the voltage ($n=1,8-2$) is observed on the second portion and on the third portion the current increases with the voltage in the degree $n>2$. VAC of HGS samples of Se-Te system with the tellurium concentration about 2 - 5 at.% have the two portions with quadratic and degree dependences of the current on the voltage, where $n>2$. VAC of HGS of $\text{Se}_{95} \text{Te}_5$ system at the different temperatures are

shown in the fig.3. As it is seen from the figure, the voltage corresponding to VAC bending between ohmic and quadratic portions increases with the temperature increase.

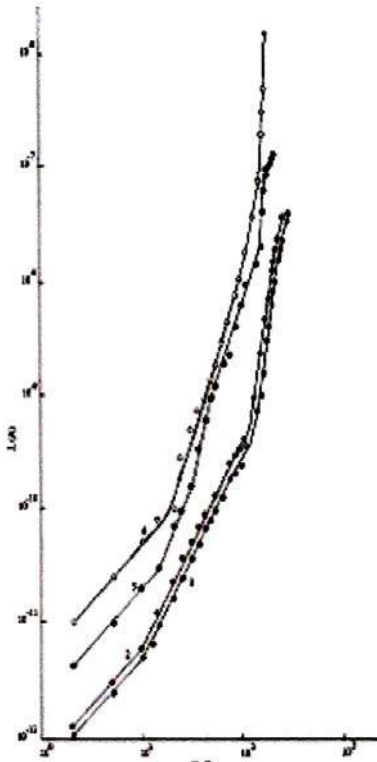


Fig.1. The volt-ampere characteristics of Se-Te system at the room temperature for the compositions 1 - Se;
2 - $\text{Se}_{99} \text{Te}_1$; $\text{Se}_{95} \text{Te}_5$; $\text{Se}_{90} \text{Te}_{10}$.

Such VAC behaviour is characteristic for the currents, limited by volume charge (CLVC), at the presence of the levels of hole attachment, situated lower than Fermi F_0 level, i.e. the condition $(F_0 - E_i)/kT > 1$ is fulfilled. The observable peculiarities of VAC prove that energy position and concentration of attachment levels depend on the chemical composition and on the concentration of inputted atoms of chlorine impurities.

In a particular, in HGS of $\text{Se}_{95} \text{Te}_5$ system the observable peculiarities of VAC testify the existence of the two groups of trap centers, located between ceiling of valence band and Fermi level. In the frameworks of CLVC theory, the attempt, in order to explain the given peculiarities VAC has been done.

At the small values of the voltage applied of the sample the charge carrier injection from electrode is small and layer

THE CURRENTS, LIMITED BY VOLUME CHARGE IN THE CHALCOGENIDE GLASSY SEMICONDUCTORS OF Se-Te SYSTEM

conductivity stays ohmic because of the presence some quantity of the equilibrium charge carriers. Using the following obtained value

$$I = \mu e n_v V / L \quad (1)$$

$$n = N_v \exp(- (F_0 - E_v) / kT). \quad (2)$$

of concentration of the equilibrium holes n from formula(1) the position of Fermi level ($F_0 - F_v$) with the help of the formula (2) is obtained

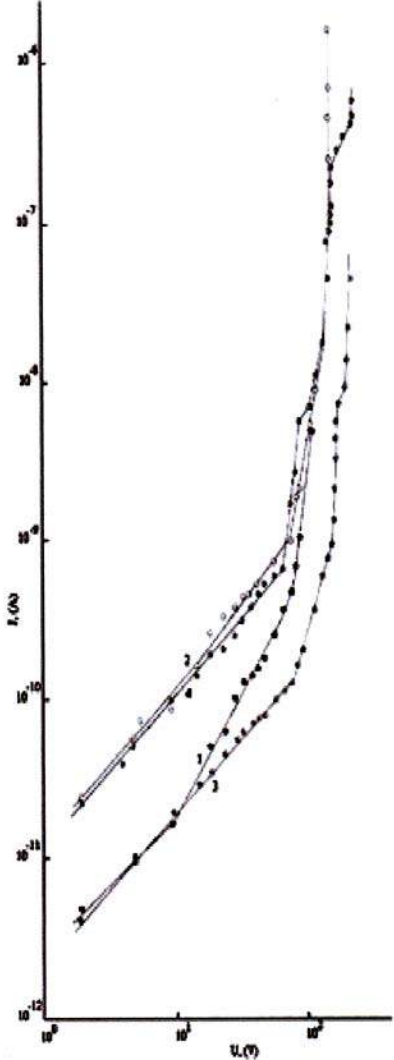


Fig.2. The volt-ampere characteristics of formula composition with chlorine impurity: 1- $\text{Se}_{95}\text{Te}_5\text{Cl}_{0,001}$; 2- $\text{Se}_{95}\text{Te}_5\text{Cl}_{0,005}$; 3- $\text{Se}_{95}\text{Te}_5\text{Cl}_{0,01}$; 4- $\text{Se}_{95}\text{Te}_5\text{Cl}_{0,1}$.

. Here μ is hole mobility; e is elementary charge, L is distance between electrodes, V is applied voltage, I is current density, Nv is effective density of the states in the valence band, kT is heat energy. The obtained values for the all samples are presented in the table.

At the voltage increase, because of the charge carrier injection from electrode, the hole concentration increases, and when they become bigger, than concentration of equilibrium holes, then the current subordinates to the law [4]:

$$I = \epsilon \mu V^2 / L^3, \quad (3)$$

where ϵ is statical dielectric constant of the material.

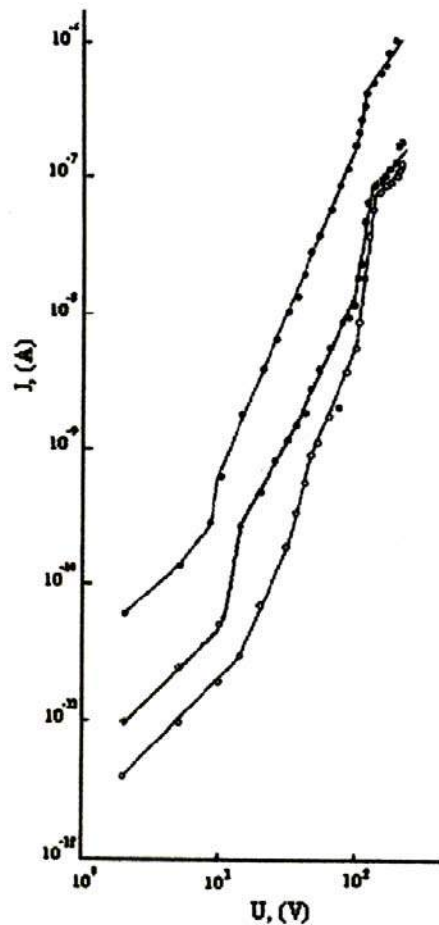


Fig.3. The volt-ampere characteristics of $\text{Se}_{95}\text{Te}_5$ composition at the room temperatures 20K, 35K, and 55K, correspondingly (from bottom to top)

In the case, when traps are existed, the parameter θ is input, defining the part of free charge carriers on the total charges:

$$\theta = N_v / N_t \exp(-E_T / kT), \quad (4)$$

where N_t is concentration of small traps, E_T is activation energy of the traps.

In this case VAC are described by the equation (3), but for μ it is need to use expression $\mu = \theta \mu_o$, where μ_o is mobility of free charge carriers.

The transversal voltage between portions, subordinating to ohmic and quadratic laws, is defined by the expression:

$$V_I = e n_t L^2 / 2\epsilon, \quad (5)$$

where n_t is thermal equilibrium concentration of charge carriers. At $V > V_I$, the traps gradually fill up and at the defined voltage value become totally filled. According to CLSC theory, voltage, at which the total trap filling begins, is defined by the expression

$$V_2 = e N_t L^2 / 2\epsilon. \quad (6)$$

With the help of the equation (6), the concentration N_t of traps, which is 10^{13} - 10^{14} cm^{-3} has been calculated. The trap parameters (concentration and activation energy) were

calculated b by the formula(6), and also from the temperature dependence of θ . The obtained results are presented in the table 1.

Table 1.
The traps parameters of HGS of Se-Te system.

Material	$F_0 - E_v$, eV	E_{t1} , eV	N_{t1} , cm^{-3}	E_{t2} , eV	N_{t2} , cm^{-3}
Se	1,09	0,87	2×10^{13}	—	—
Se ₉₉ Te ₁	1,08	0,81	5×10^{15}	—	—
Se _{98,5} Te _{1,5}	1,05	0,80	2×10^{17}	—	—
Se ₉₅ Te ₅	1,05	0,84	2×10^{16}	0,67	$5 \cdot 10^{18}$
Se ₉₀ Te ₁₀	1,02	0,82	1×10^{16}	—	—
Se ₉₅ Te ₅ Cl _{0,001}	1,05	0,86	1×10^{16}	0,75	10^{18}
Se ₉₅ Te ₅ Cl _{0,005}	1,05	0,80	2×10^{16}	0,70	10^{18}
Se ₉₅ Te ₅ Cl _{0,01}	1,05	0,80	5×10^{15}	—	—
Se ₉₅ Te ₅ Cl _{0,1}	1,05	0,80	2×10^{15}	—	—

At the calculations the following number values of parameters of the investigated materials, are used: $N_v = 9,5 \cdot 10^{19} \text{ cm}^{-3}$ [5], $\varepsilon = 5,5 \cdot 10^{-11} \text{ F/m}$ [6], $\mu_o = 10^{-3} \text{ m}^2/\text{V sec}$. [7].

As it is seen from the table, at the addition of the tellurium in selenium, the concentration of local states strongly increases (bigger, than in 100 times), but if tellurium concentration 5 at.%, the second group of localized states, situated near to the ceiling of valence band, appears. From the work [8] it is known, that tellurium, inputted in selenium, destroys selenium chains, in the result of which they become

shorter and concentration of broken bonds increases. Obviously, these broken bonds are traps for holes. It is established by us [1-2] that tellurium additions in the amorphous selenium bigger than 2 at.%, causes the increase of the state density of negatively charged defects D. The decrease of the trap concentrations at the addition of the electronegative chlorine impurity in HGS of Se-Te system allows us to proceed, that hole traps in the given HGS material connect with the negatively charged defects D.

- [1] S.I. Mekhtiyeva, A.I. Isayev, E.A. Mamedov. Materiali konferencii, posvyashchennoy 80-letiyu G.A. Aliyeva, Baku, 2003.
- [2] S.I. Mekhtiyeva, A.I. Isayev, E.A. Mamedov. Materiali konferencii Amorfniye mikrokristallicheskiye poluprovodniki. S. Peterburg, 2002.
- [3] S.I. Mehdiyeva, N.I. Ibragimov, A.I. Isayev, E.A. Mamedov. Turkish Journal of Physics, 2002, 26, 449-452.
- [4] M. Lampert, P. Mark. Injekcionniye toki v tverdikh telakh. M. Mir, 1973.
- [5] W.E. Spear. Proc. Phys. Soc., 1960, 76, 822.
- [6] F. Eckart, A. Rabenhorst, Ann. d. Phys., 19, 381, 1957.
- [7] N.Mott, E. Devis. Elektronniye processi v nekrystallicheskikh veshhestvakh. Moskow, Mir, 1982. (in Russian)
- [8] S.I. Mekhtiyeva, D.Sh. Abdinov. Razvitiye fiziki selena. Baku, Elm, 2000. (in Russian).

S.İ. Mehdiyeva, A.İ. İsayev, G.A. Məmmədov, Z.A. Aqamaliyev

Se-Te XALKOQENİD ŞÜŞƏVARI YARIMKEÇİRİCİ SİSTEMLƏRDƏ HƏCMLİ YÜKLƏ MƏHDUDLAŞDIRILMIŞ CƏRƏYANLAR

Stasionar rejimde təmiz və xlor aşşarları (0,001; 0,005; 0,01; 0,1 at.%) əlavə edilmiş şüşəvari xalkogenid yarımkəçirici Se_{100-x}Te_x sistemi əsasında hazırlanın Te - Se_{100-x}Te_x - Al strukturunun volt-amper xarakteristikası tədqiq edilmişdir. Müəyyən edilmişdir ki, həmin strukturda yük daşıyıcıların köçürülmə mehanizmi həcmi yüksərlər məhdudlaşan cəryanlarla əlaqədardır, və köçürülmə prosesini idarə edən lokal halların parametrləri (konsentrasiyası və aktivləşmə enerjisi) təyin olunmuşdur. Həmçinin müəyyən olunmuşdur ki, amorf selene əlavə edilmiş tellurun miqdarı 2%-dan böyük olduqda, mənfi yüklü defektlərin konsentrasiyası artır.

С.И. Мехтиева, А.И. Исаев, Э.А. Мамедов, З.А. Агамалиев

ТОКИ, ОГРАНИЧЕННЫЕ ОБЪЕМНЫМ ЗАРЯДОМ, В ХАЛЬКОГЕНИДНЫХ СТЕКЛООБРАЗНЫХ ПОЛУПРОВОДНИКАХ СИСТЕМЫ Se – Te

В стационарном режиме были проведены измерения вольтамперных характеристик (BAX) чистых и содержащих примеси хлора (0,001; 0,005; 0,01; 0,1 ат.%) ХСП систем Se_{100-x}Te_x (x = 0; 1; 2,5; 5; 10 ат.%) в структуре типа Te - Se_{100-x}Te_x - Al. Установлено, что в указанной структуре механизм токопрохождения обусловлен токами, ограниченными объемным зарядом, и определены параметры (концентрация и энергия активации), контролирующие перенос электрических зарядов. Также установлено, что добавка теллура в аморфный селен, превышающая 2 ат.%, способствует увеличению плотности состояний отрицательно заряженных дефектов D⁻.

Received: 23.02.05

THE SPECIFIC HEAT OF THE SURFACE FORMATION OF LIQUIDS

E.A. EYVAZOV, A.A. ABUSHOVA, Y.M. ABASOV

*The Azerbaijan Pedagogy University
Baku, Az-1000, U.Hajibekov. str.,4*

A.U. MAKHMUDOV

*Baku State University
Baku, Az-1145, Z.Halilov str.,23*

The semi-phenomenological method, allowing one to establish the temperature dependence of the specific heat of the surface formation (SHS) of liquids on the base of density value at two arbitrary temperatures is considered.

The given method is applied to the liquid alkaline metals and the correlation between thermal direction coefficient, SHS, bond energy and liquid molecular mass is established

The processes, carrying out on the two phases interface are special and differ from volume phenomena significantly. The osculating phases are divided by the narrow transitive layer, the atomic (molecular) structure of which strongly differs from structures of divided phases. In a particular, the interatomic distances in the subsurface layers of crystal (liquid) are in average on ~10% more, than in the volume. That's why the physical parameters, with the help of which the volume phenomena are described, aren't enough for surface phenomena and it is need to introduce the new characteristics, connected with the surface immediately. One of such values is the specific heat of the surface formation (SHS), which means energy physically, needed for isothermal formation of free unit surface. As all values characterizing the thermodynamic properties of the surface are expressed by the surface tension and it connects immediately with the specific heat of the surface formation, so the urgency of investigation of the last one becomes more significant.

In spite of the many theoretical and experimental investigations [see 1-4], because of the complexity of the structure of subsurface layer and unknowing of the potential of intermolecular interaction, nowadays the uniform approach to the surface phenomena in liquids doesn't exist.

In the given article some practically suitable semi-phenomenological method of the establishment of temperature dependence of the specific heat of the surface formation of liquids is suggested.

With the help of the potential method [5] and also thermodynamical cycles one [6] it can be shown that the temperature dependence of the surface tension coefficient of liquids (σ) in the general case is defined as follows

$$\frac{d\sigma}{dT} = - \frac{q}{T}, \quad (1)$$

where q is the heat quantity, absorbing at the reversible isothermal change of unit surface area and is equal to the difference of the specific surface energy and the work at the isothermal expansion of the interface on the unit. (This value is often called by the specific heat of the surface formation). From another hand, the thermal direction coefficient of the surface tension of many liquids is well expressed by the following expression [7]:

$$\frac{d\sigma}{dT} = -B \left(\frac{\rho}{\mu} \right)^{2/3}, \quad (2)$$

where ρ is the liquid density; μ is the liquid molecular mass. $B=2,1 \text{ g}\cdot\text{cm}^2/\text{sec}^2\cdot\text{grad}$. is the numerical coefficient. From the formulae (1) and (2), we have:

$$q = 2,1 \frac{\rho}{\mu} T^{2/3} = A \cdot \rho^{2/3} \cdot T, \quad (3)$$

where $A=2,1 \mu^{2/3}$ is the constant value for the given liquid (table 2).

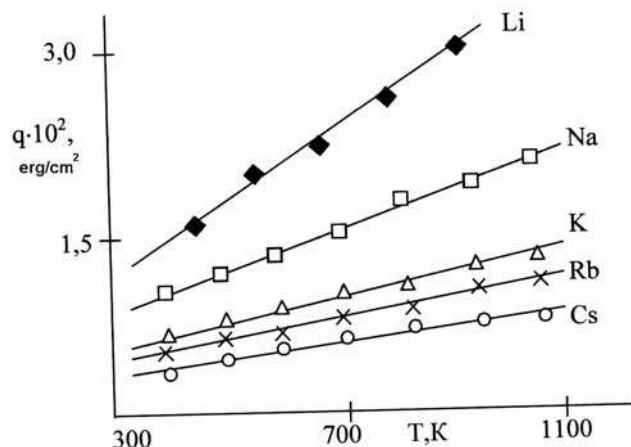


Fig.1. The temperature dependence of the specific heat of the surface formation of liquid alkaline metals.

As it is followed from the formula (3), the heat of the surface formation depends on the temperature. Knowing the temperature dependence of the liquid density with the help of formula (3), we can establish the analytical form of dependence $q=q(T)$. With the help of experimental values of liquid alkaline metals density, taken from the formula [8] at the different temperatures, we have calculated q values. The corresponding results are given in the fig.1. As it is seen, in the temperature interval $400\text{K} \leq T \leq 1100\text{K}$ for all chosen

liquids, the dependence $q=q(T)$ has linear character, i.e. the specific heat of the surface formation of liquid alkaline metals with the temperature increase increases according to the linear law. As the given linearity doesn't mean the temperature independence of the thermal angular coefficient of the heat of the surface formation, i.e. $\alpha_T = \frac{dq}{dT} = \text{const}$, so it is obviously, that

$$q(T) = \alpha_T T + C. \quad (4)$$

For the finding of integration constant C , we assume, that at the arbitrary temperature $T=T_r$, the heat of the surface formation, calculated by means of the known density $\rho=\rho_r$, is equal q_r . Then from the formula (4), we have:

$$q(T) = q_r + \alpha_T (T - T_r). \quad (5)$$

The formula (5) is the analytical expression of above mentioned linear dependence $q=q(T)$ and allows to establish the temperature dependence of the specific heat of the surface formation of liquids by means of the density values at two arbitrary temperatures. Indeed, let's suppose that at the temperatures T_1 and T_2 , the density is equal to ρ_1 and ρ_2 correspondingly. Then with the help of the formulae (5) and (3), after simple transformations, we obtain:

$$q(T) = 2.1 \cdot \mu^{-2/3} \left[\rho_1^{2/3} T_1 + \frac{T - T_1}{T_2 - T_1} (\rho_2^{2/3} T_2 - \rho_1^{2/3} T_1) \right] \quad (6)$$

(In the formula (6), it is supposed, that $T_2 > T_1$, i.e. $\rho_2 < \rho_1$).

SHS of liquid direction metals, calculated on the formulae (3) (q_3) and (6) (q_6).

T, K	Na		K		Rb		q_6/q_3		
	q_3	q_6	q_3	q_6	q_3	q_6	Na	K	Rb
400	98.29	98.28	63.48	63.49	54.51	54.52	0.9999	1.0001	1.0001
500	120.72	120.71	77.83	77.84	67.13	67.13	0.9999	1.0001	1.0000
600	142.27	143.14	91.53	92.19	78.76	79.75	1.0061	1.0072	1.0126
700	162.92	165.57	104.58	106.54	89.77	92.37	1.0162	1.0187	1.0283
800	182.82	188.00	116.97	120.89	101.83	104.99	1.0283	1.0335	1.0310
900	201.66	210.43	128.66	135.24	113.60	117.61	1.0435	1.0511	1.0353
1000	219.58	232.86	139.63	149.59	125.32	130.23	1.0605	1.0713	1.0392

The specificity is the decrease of the thermal angular coefficient α_T with the increase molecular mass of alkaline metals. Formally, such dependence follows from the formula (6), according to $\alpha_T \sim \mu^{-2/3}$ (fig.2). One of the probable physical causes of α_T decrease at the increase of molecular mass, is

It is clear, that formula (6) has universal character, i.e. it is suitable for all normal liquids.

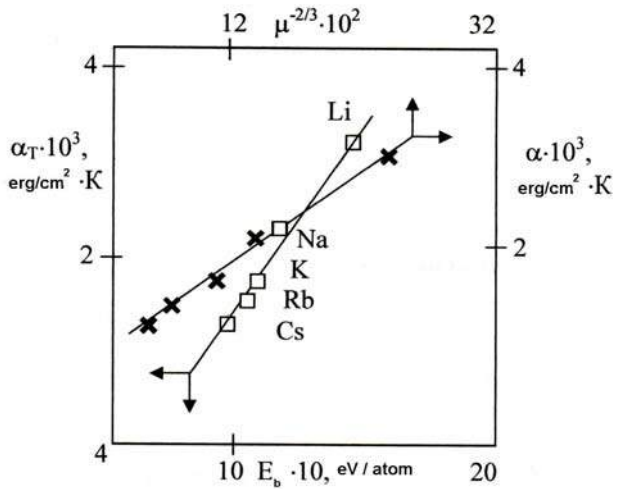


Fig.2. The dependence of thermal angular coefficient (α_T) on the bond energy (E_b) and molecular masses (μ) of liquid alkaline metals.

As it follows from the above mentioned, at the presence of the density data in the wide temperature interval it is necessary the specific heat of surface formation to calculate on the formula (3); and on the two density values, the dependence $q=q(T)$ can be established on the formula (6). For the liquid alkaline metals q values, calculated by the both methods, well coincide (table 1).

Table 1.

the decrease of bond energy at the transition from lithium to cesium, i.e. it is obviously, that the more strong the bond between atoms, the more big the energy is needed for the formation of unit surface. The values of bond energy E_b , taken from the formula (9), are given in the table 2.

Table 2.

The values of some parameters for alkaline elements.

	Li	Na	K	Rb	Cs
μ	6.94	23	39.10	85.50	132.9
$A \cdot 10$	5.73	2.59	18.20	1.80	0.81
$\alpha_T \cdot 10^2, \text{erg/cm}^2 \cdot \text{K}$	32.03	20.61	13.17	11.82	9.66
$E_b \cdot 10^{-10}, \text{eV}$ [9]	15.80	11.30	9.50	8.90	8.10
T_{m}, K [7]	453	371	350	313	302

The dependence α_T on bond energy is shown on the fig.2. As it is seen, our exposition about correlation between α_T and E_b takes place really.

It is note, that described in the present work the semi-phenomenological approach allows us to establish also the temperature dependence of liquid surface tension on two density values.

THE SPECIFIC HEAT OF THE SURFACE FORMATION OF LIQUIDS

- Thus, in the given paper, the semi-phenomenological method of the definition of the specific heat of the surface formation (SHS) of liquids on the base of density values at two arbitrary temperatures is suggested. By this method, the temperature dependence of the

specific heat of the surface formation of liquid alkaline metals has been calculated and correlation between the thermal direction coefficient, SHS, bond energy and liquid molecular mass is established.

-
- [1] S. Ono, S. Kondo .Molekulyarnaya teoriya poverkhnostnogo natyajeniya jidkostey. M. 1963. (in Russian)
 - [2] K.Rsherman. Phys.Res.Letters, 1969, 15, 141, p.157-162.
 - [3] K. Krakston. Fizika jidkogo sostoyaniya. M. 1978. (in Russian)
 - [4] Rezibua Pyer, De Lener. Klassicheskaya kineticheskaya teoriya jidkostey i gazov. M. 1980. (in Russian)
 - [5] L.D. Landau, E.M. Lifshic. Statisticheskaya fizika. M. 1976. (in Russian).
 - [6] I.P.Bazarov. Termodinamika. M. 1969, 95. (in Russian).
 - [7] Tablici fizicheskikh velichin. Spravochnik pod. red. akad. Kikoina. M. 1976, 160. (in Russian).
 - [8] N.B. Vargaftik. Spravochnik po teplofizicheskim svoystvam gazov i jidkostey. M. 1972, 237. (in Russian).
 - [9] Ch. Kittel. Vvedeniye v fiziku tvyordogo tela. M. 1978, 113. (in Russian)

E.Ə. Eyvazov, A.U. Mahmudov, A.A. Abuşova, Y.M. Abbasov

MAYELƏRİN XÜSUSİ SƏTHƏMƏLƏGƏLMƏ İSTİLİYİ

İşdə iki ixtiyari müxtəlif temperaturda mayenin sıxlığını bilməklə xüsusi səthəmələgəlmə istiliyinin (XSİ) temperatur asılılığını hesablamamağa imkan verən yarım fenomenoloji metod verilir. Bu metodla qəlevi metalların mayelerinin XSİ-nin termik bucaq əmsali ilə mayenin rabiə enerjisi arasında korrelyasiya olduğu aşkarlanmışdır.

Э.А. Эйвазов, А.У. Махмудов, А.А. Абушова, Я.М. Абасов

УДЕЛЬНАЯ ТЕПЛОТА ПОВЕРХНОСТООБРАЗОВАНИЯ ЖИДКОСТЕЙ

Рассматривается полуфеноменологический метод, позволяющий на основании значений плотности при двух произвольных температурах установить температурную зависимость удельной теплоты поверхностиообразования (УТП) жидкостей.

Предложенный метод применен к жидким щелочным металлам и установлена корреляция между термическим угловым коэффициентом, УТП, энергией связи и молекулярной массой жидкости.

Received: 23.02.2005

THE INVESTIGATION OF THE PECULIARITIES OF THE INTERNAL FRICTION AND THE SHEAR MODULUS IN THE LEAD TELLURIDE MONOCRYSTAL

O. DAVARASHVILI, M. ENUKASHVILI, N. KEKELIDZE

*The Tbilisi State University name of Javakhishvili,
3801286 Tbilisi, Chavchavadze ave., 1*

G. DARSAVELIDZE, L. GABRICHIDZE, E. KUTELIYA

*Institute of metallurgy and materiology name of A.Tavadze, AS of Georgia,
380060, Tbilisi, Kazbegi str., 15*

V.P. ZLOMANOV, O.I. TANANAЕVA

The Moscow State University name of M.V. Lomonosov

N. AHMEDZADE

*Institute of Physics of Academy of Sciences of Azerbaijan
Baku - 1143, H.Javid av. 33*

L. TECER

Karaelmaz University, Zonguldak, Turkey

T. MAMEDOV

Gazi University, Ankara, Turkey

The internal friction and the shear modulus have been investigated in PbTe crystals, undopped and dopped by chromium till the temperature 650°C. It has been established at the first time, that the shear modulus increases at the room temperature in the dopped PbTe almost in 2,5 times, and the elastic limit increases in 5-6 times.

The lead telluride, belonging to the narrow-band semiconductor materials, is widely used in the modern semiconductor technique for the production of lasers and photodetectors in the infrared-ray spectrum region, and also for the production of the high-effective thermoelectric transducers. The investigation of the types of the structural defects and their thermal stability, their influence on the structural-sensitive mechanical properties will cause the expansion of the possibilities of their use in many respects.

Such kind of the investigation can be carried out successfully with the use of the acoustic spectroscopy methods, allowing us to define the absolute values of elastic constants, to estimate activation parameters of the different defects and their contribution in the formation of the mechanical properties.

As the last investigations show [1], these questions are very actual in the compound and solid solutions of A^{IV}B^{VI} in the connection with the diffusion error in the heterostructures and the inelastic phenomena, connected with them.

In the present paper for the solution of such kind of problems the method of the low-frequency internal friction at the torsional oscillations has been used. The method has the high sensitivity to the change of the crystal elastic properties, allows us to carry out the measurements in the wide ranges of the temperature change and the amplitudes of the vibrational deformation. The choice of this method is also caused by the fact, that it differs by the high sensitivity to the different defects of the crystal lattice (planar and point defects). The relaxation times of the processes, connected for example with the dislocation defects, interacting with the vacancies or

atoms of the impurities, can have the values, which are close to the period of oscillation of the torsion pendulum. This allows us to get the information about the nature of the relaxation processes of the dissipation of energy of the mechanical oscillations, caused by the real structure of crystals.

The PbTe crystals (~ 0,1at. %) undopped and dopped by chromium, are chosen as the objects of the investigation. Earlier in the samples, dopped by chromium at T=80K, the increase of the elastic constants more than in two times with the comparison of the undopped PbTe, was revealed [2].

The measurements of the internal friction and dynamic shear modulus are carried out in the vacuum on the installation of the internal friction with the direct torsion pendulum at the oscillation frequency 1-5 Hz in the temperature interval from the room temperature till 650°C. The samples' sizes are 0.5·0.5·(10-15)mm³, the velocity of the temperature change is 2 grad/min. The amplitude vibrational deformation was changing in the interval 5·10⁻⁵-10⁻³.

The value of the internal friction was defined by the formula [3]:

$$Q^{-1} = \ln (A_n / A_{n+N}) / \pi N , \quad (1)$$

where N is the number of the free-damped oscillations at the decrease of the light deflection amplitude on the optical scale from A_n till A_{n+m}. The precision of estimation of the value is IF~5%. The absolute value of the shear modulus at the room temperature was defined by the method of the comparison

with the etalon sample (aluminum of high purity) of identical sizes by the formula

$$G = G_{et} f^2 / f_{et}^2, \quad (2)$$

where G and f , G_{et} and f_{et} are values of the shear modulus and oscillation frequency of the investigated and etalon samples correspondingly. At the construction of the curves of the shear modulus, its proportionality to the square of oscillation frequency: $G \sim f^2$ was used.

The activation energy was defined by the Vesta-Marx method on the known values of the temperature T_{max} and oscillation frequency f_{max} from the experiment at the maximum of the relaxation internal friction [3]:

$$H = RT_{max} \ln(KT_{max} / hf_{max}), \quad (3)$$

where K and h are Boltzmann and Plank constants correspondingly, R is the gas constant.

The relative deformation was defined at the torsional oscillations by the formula:

$$r = NL / lR, \quad (4)$$

where r is the radius of the circumscribed circle of the sample cross-section, l is the sample length, R is the distance from the sample till the optical reference system, L is the deflection of the light ray on the optical scale.

The temperature spectrum IF of the monocrystal undopped sample PbTe at the oscillation frequency $\sim 5\text{Hz}$ characterizes by the maximums at the temperatures 240 and 340K (fig.1).

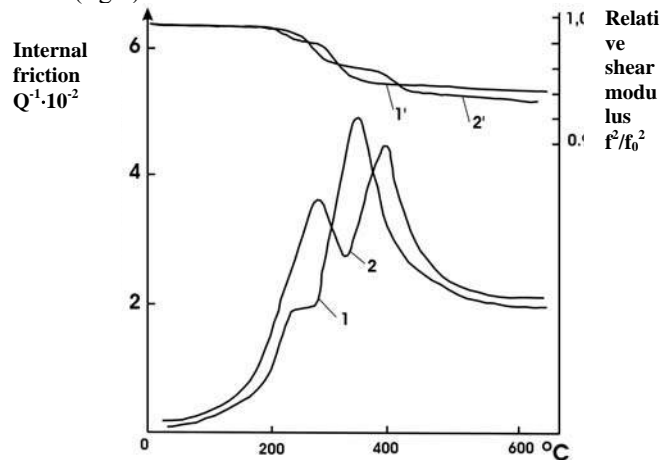


Fig.1. The temperature dependence of the internal friction and relative shear modulus (1,2) of monocrystalline PbTe. 1,1 - PbTe (undopped), 2,2 - PbTe:Cr.

They appear on the IF phone, the level of which increases strongly in the temperature region $>400^\circ\text{C}$. The decrease of the shear modulus is observed in the neighborhood of the IF temperature maximums. The last one, excepting the given maximal wanes, decreases approximately linearly at the increase of the sample temperature. At the further measurement of the IF spectrums and shear modulus in the cooling process the significant changes were not observed with the comparison with the initial spectrums. In the repeated experiment, carried out on the heating and the cooling, the former characteristics of given temperature spectrums mainly conserved. This fact proves the thermal stability of the maximums and IF phone in the PbTe samples. It is need to notice, that spectrum of the temperature dependence are registered in the mode, when the internal friction Q^{-1} is the amplitude-independent.

According to the calculation by the formula (3), IF maximums at 240 and 340°C are characterized by the values of activation energy 1,23 and 1,49 eV correspondingly. From the exponential dependence of the frequency relaxation factor on the back absolute temperature $r' = r_0 \exp(H/KT_{max})$ the frequency factors were equal $1,7 \cdot 10^{10}$ and $6 \cdot 10^{12} \text{s}^{-1}$, correspondingly. The equality at the maximum $2\pi f_{max} = r'$, where r is relaxation time is used at the calculation.

The absolute value of the shear modulus was equal $1,21 \cdot 10^{11} \text{ din/cm}^2$. It didn't change at the further experiments, carried out after the sample's heating till 650°C in the measurement process of IF and f^2 . When $Q^{-1}(E)$ depends on the amplitude, then the separation of the dislocation segments from the fixed points begins in the case of the crystals with low potential barrier or the separation of the twists begins on the dislocations in the case of the crystals having high Payers barrier. The interface of the amplitude-independent and -dependent regions of Q^{-1} is referred to the critical amplitude deformation. It is equal $9,3 \cdot 10^{-4}$ for the undopped PbTe (fig.2, table).

In the temperature IF spectrum of PbTe sample, dopped by chromium, measured at the frequency $\sim 5\text{Hz}$, the above mentioned maximums are revealed at the relative high temperatures 265 and 385°C. They appear on the phone, having the lowered intensity in the comparison with the undopped sample. And in this case IF maximums have the higher thermal stability, i.e. the extract at 600°C during 2,5 hours practically doesn't influence on their temperature position and intensity. The shear modulus decreases in the temperature region of IF maximums. Its decrease is higher in the region of the second maximum, characterizing by the relative high intensity. The absolute value of the shear modulus of the dopped sample is $-2,96 \cdot 10^{11} \text{ din/cm}^2$.

Table.

Physic-mechanical characteristics of the lead telluride monocrystalline samples.

Sample's type	Shear modulus 10^{11} din/cm^2	Critical amplitude of deformation	Temperature of IF maximums, °C	Activation energy, eV	Frequency factor, s^{-1}
PbTe (undopped)	1,21	$9,3 \cdot 10^{-4}$	240	1,23	$1,7 \cdot 10^{10}$
			340	1,49	$6 \cdot 10^{12}$
PbTe: Cr	2,96	$2,9 \cdot 10^{-3}$	265	1,30	$3 \cdot 10^{10}$
			385	1,60	$2,8 \cdot 10^{13}$

The activation characteristics of IF maximums in the dopped sample also have the relative high values 1,3 eV and

$1,3 \cdot 10^{10} \text{s}^{-1}$ for the maximum at 265°C and 1,6 eV and $2,8 \cdot 10^{10} \text{s}^{-1}$ for the second maximum at 385°C.

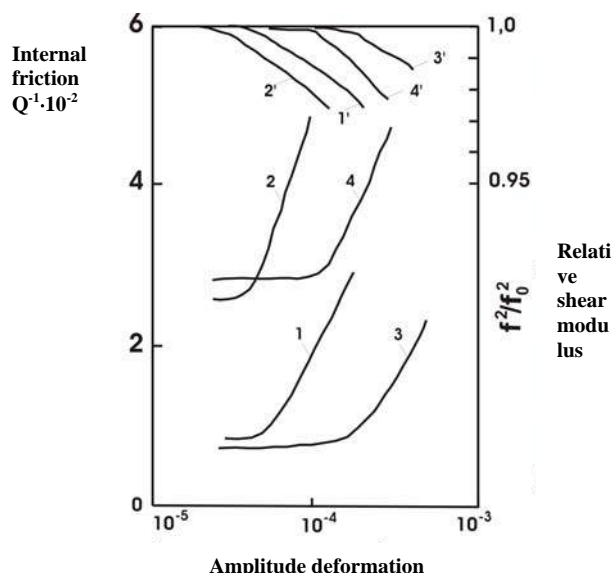


Fig.2. The amplitude dependence of the internal friction (1-4) and relative shear modulus (1-4)
PbTe (undopped): 1,1 -IF and shear modulus at the room temperature, 2,2 - at 300°C
PbTe:Cr3,3 - IF and shear modulus at the room temperature, 4,4 - at 300°C.

The initial spectrums of IF and shear modulus in the temperature interval from room till 650°C and in the case of

- [1] O.I.Davarashvili, M.I.Enukashvili, N.P.Kekelidze etc.
Georgian Engineering News, 2002, 2, 7.
- [2] A.N. Vasilyev, Yu. P. Gaydukov, V.P. Zlomanov i dr. Ne-organicheskiye materiali, 1988, 19, 2, 237.(in Russian).
- [3] V.S. Postnikov. Vnutrenneye treniye v metallakh.

chromium doping reveal the strong dependence on the oscillation amplitude (fig.2). The decrease of the value of the critical amplitude deformation, at which the strong increase of IF increase or the decrease of shear modulus, is observed on the amplitude dependences of IF and shear modulus at the increase of the temperature of their measurement. Such change of the critical amplitude is character for the thermoactivated process of the dislocation separation on the relative weak fixed points [4].

The calculations of the elastic limit by the formula $\sigma = 2C_{44} \cdot (3-4 \cdot C_{44}/C_{11}) \cdot \epsilon_{cur}$ show, that in PbTe sample, dopped by chromium, the elastic limit increases not the less, than in 5-6 times in the comparison with the undopped one. Here it is noted, that $C_{44} = G = 29,6 \cdot 10^{10}$ din/cm², $C_{11} = 104 \cdot 10^{10}$ din/cm² [5] and $143 \cdot 10^{10}$ din/cm² for the undopped and dopped samples correspondingly. The existence of the lowered values of the critical amplitudes at the increased temperatures shows, that dislocation limit also decreases at the increase of the sample's temperature. According to the results of the measurements its decrease is significant at the temperatures >200°C. The annealing at 600°C during 2,5 hours insignificantly increases the value of the critical amplitude at the different temperatures. Therefore, the given thermal treatment practically doesn't influence on the absolute values of shear modulus and dislocation elastic limit, i.e. doesn't cause the significant changes of the real structure of the dopped sample.

- Moscow, Metallurgiya, 1974, 351s. (in Russian).
- [4] M.A. Krishtal, S.A. Golovin. Analiticheskiye vozmojnosti metoda vnutrennego treniya. Moscow, Nauka, 1973, s.178-190. (in Russian).
- [5] A.A. Chudinov. FTT, 1962, 4, 3, 755. (in Russian).

**O.İ. Davarashvili, M.İ. Enukaşvili, N.P. Kekelidze, Q.Ş. Darsavelidze, L.L. Qabriçidze, E.R. Kuteliya,
V.P. Zlomanov, O.İ. Tananayeva, T.S. Mamedov, N.D. Əhmədzadə, L.N. Teser**

PbTe MONOKRİSTALLARININ DAXİLİ SÜRTÜNMƏ VƏ SÜRÜŞMƏ MODULUNUN XÜSUSİYYƏTLƏRİNİN TƏDQİQİ

PbTe və xromlu kristallarının daxili sürtünmə sürüşmə modulu 650°C temperaturuna qədər tədqiq edilmişdir. Xromlu PbTe kristalında müəyyən edilmişdir ki, sürüşmə modulu otaq temperaturunda 2,5 dəfə, elastiklik sərhəddi isə 5-6 dəfə artır.

**О.И. Даварашвили, М.И. Енукашвили, Н.П. Кекелидзе, Г.Ш. Дарсавелидзе, Л.Л. Габричидзе, Э.Р. Кутелия,
В.П. Злomanов, О.И. Тананаева, Т.С. Мамедов, Н.Д. Ахмедзаде, Л.Н. Тесер**

ИССЛЕДОВАНИЕ ОСОБЕННОСТЕЙ ВНУТРЕННЕГО ТРЕНИЯ И МОДУЛЯ СДВИГА В МОНОКРИСТАЛЛАХ ТЕЛЛУРИДА СВИНЦА

В нелегированных и легированных хромом кристаллах PbTe исследованы внутреннее трение и модуль сдвига вплоть до температур 650°C. Впервые установлено, что модуль сдвига при комнатной температуре возрастает в легированном PbTe почти в 2.5 раза, а предел упругости- в 5-6 раз.

Received: 25.02.2005

THE THEORETICAL MODEL OF THE MET1-ARG16 SEGMENT STRUCTURE FROM N-TERMINUS OF TYROSINE HYDROXYLASE DOMAIN

N.N. MUSTAFAYEVA, I.N. ALIYEVA, N.M. GOJAYEV

Baku State University

Baku, Az-1145, Z.Khalilov str.,23

The low-energy conformational states of the sequence including 16 amino-acid residues, forming a part of the N-terminus regulator domain of the tyrosine hydroxylase ferment have been established by the method of the force field in the approximation of the semiempirical atom-atom potential functions. It is established, that the state with the global minimum of the conformational energy has the two α -convolutions on the segments of Pro4-Thr7 and Pro9-Lys12 amino-acid residues and a number of several reverse turns on the short segments of the peptide backbone, stabilized by the hydrogen bonds.

Introduction

The structure and the dynamic conformational properties of the sequence from 16 amino-acid residues, forming a part of the N-terminus regulator domain of the tyrosine hydroxylase ferment (TH) have been investigated by the method of the semiempirical atom-atom potential functions [1,2]. The calculations, based on the physical theory of the structural organization of the peptides and proteins, include the detail analysis of the conformational possibilities of the big number of segments and their overlapping regions are described in the refs. [3,4]. The sets of the low-energy variants of the structure of monopeptides-molecules of *N*-acetyl- α -aminoacids of metilamides, used in the calculations, are universal under the consideration of any amino-acid sequences. The low-energy conformational states of the investigated segments and the whole region Met1-Arg16 of the N-terminus regulator domain TH, obtained on the base of the results of the independent calculations, were analyzed with the use of the following parameters: a) relative conformation energy E_{rel} ; b) elements of the space structure (α -helix and β -turns), and also c) the hydrogen bonds.

Calculation method

The simulation of the segment structure was carried out by the method of the theoretical conformational analysis with taking under consideration the atom polar surrounding on the base of the parcel of the applied computer programs [5]. They rest on the quantitative calculations of the total conformational energy of the investigated segment and on the searchings of its local minimums by the conjugate gradient method. The conformational energy (E_{conf}) is represented in the form of the additive sum of contributions of the non-valency (E_{nonv}), electrostatic (E_{el}) atom interactions, torsion rotation energy around valency bonds (E_{tors}) and energy of the formation of the hydrogen bonds ($E_{h.b.}$). The semiempirical potential functions and their parametrization, used in the given paper., have been taken from the ref. [6]. The polar atom surrounding in the calculate experiment was simulated with the help of the value $\epsilon=10$ and the D parameter, describing the depth of the hydrogen bond, which is equal to 1,5 kcal/mol in the Morse potential [3,6]. The indication of the dihedral angles of the rotation was carried out according to the standard nomenclature [7].

The results ant their discussion

The theoretical conformation analysis of Met1-Arg16 segment was carried out on the base of the fragmentar

calculation according to the scheme, given on the fig.1. As the theory of the conformation analysis proceeds from the assumption about co-ordination of all types of the intramolecular interactions, the refinement scheme of the amino acid sequence on the separate segments hasn't the principal meaning and doesn't influence on the final results of the investigation.

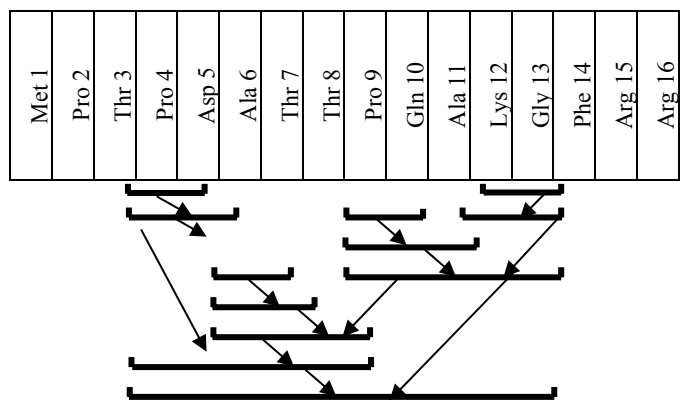


Fig.1. The scheme of the stepwise calculation of Met1-Arg16 segment of N-terminus domain from tyrosine hydroxylase.

- a) $E_{rel}=0.0$ kcal/mol.
- b) $E_{rel}=1.5$ kcal/mol.
- c) $E_{rel}=3.6$ kcal/mol.
- d) $E_{rel}=6.8$ kcal/mol.

Nonapeptid Met1-Pro2-Thr3-Pro4-Asp5-Ala6-Thr7-Thr8-Pro9

In the capacity of the initial approximation for the procedure of the minimization of the conformational energy the 684 variants, being combinations of the most profitable forms of the peptide backbone of Met1-Pro4 tetrapeptide and Pro4-Pro9 gexapeptide have been created. The low-energy conformation state contains α -helix region of the peptide chain, including the residues of Pro4-Asp5-Ala6-Thr7-Thr8. The creation of the helix structure is proved by the values of the dihedral angles of the rotation of the main chain and by the hydrogen bonds of the type 1-4, created by oxygen atoms of the carbonyl group and hydrogen atoms of the amid group of the peptide backbone $Nh(Pro4)...Oc(Thr8)$. The energy of such hydrogen bond in the different conformational states of the investigated segment varies in the limits 1,9-2,5 kcal/mol. The side chain of the threonine residuals creates the big number of the intramolecular contacts. Particularly, hydroxyl group in Thr7 and Thr8 begins to participate in the formation of the hydrogen bonds with the side chain of the aspartic. The contribution analysis of the interresidual interactions allows

us to conclude, that the dispersion interactions of the residuals in the positions 4, 8, 9 and 14 of the peptide backbone are the main factors of the stabilization of the global conformation of the nonapeptide segment. The low-energy conformation states of the segment, satisfying to the criterion $E_{rel} < 8$ kcal/mol, have been chosen for the latest calculation.

OktapeptidePro9-Gln10-Ala11-Lys12-Gly13-Phe14-Arg15-Arg16

The peptide backbone Pro9-Arg16 is divided on the simple overlapping two-, three-, and e.t.a. segments for the calculation of the Oktapeptide segment (fig.1). According to the calculation results, the global conformation of the Oktapeptide segment has the short of α -helix on the region Pro9-Gln10-Ala11-Lys12, the turn on the region Gly13-Phe14 (because of the existence conformational mobile glycine, playing the role of the knuckle residue) and the turned compact structure on the region Phe14-Arg15-Arg16. Such structure of the Oktapeptide segment is realized in 70% of the calculated conformations. The rest conformations belong either to the structures of the disorder type, or to the turned ones, among which it is possible to underline the total helix conformation ($E_{rel} < 2.7$ kcal/mol). Let's consider the peculiarities of the space construction of the conformation with the global energy minimum. It is preferred not only by the value of total energy, but on the energy of each separate type of interactions. The existence of such co-ordination between nonvalent, electrostatic and torsion interactions does the energy distribution of the conformations in respect of the parametrization of the potential functions very stable. The residues of the proline (Pro 9) and glycine (Gln 10), participating in the numerous two-, three-, tetra- and pentapeptide interactions play the significant stabilizing role in the formation of the stable segment structure.

Met1-Arg16 segment

The conformational analysis of Met1-Arg16 segment of *N*-terminus regulator domain of tyrosine hydroxylase included the minimization of the total conformational energy of the segment with taking under consideration the low-energy states of the segments, constituting it. The relative energy of the minimized structures varies in the interval of the values 0-10 kcal/mol. The results of the conformational analysis are given in the tables 1-3 and on the fig.2, where the stereoisograms of the most stable conformational states of the segment in the conditions, simulating the water surrounding are given.

According to the investigation results, the state with the global minimum of the conformation energy has two turns of α -helix on the regions Pro4-Thr7 and Pro9-Lys12 and the totally unfolded *N*- and *C*-terminus segments of Met1-Thr3 and Lys12-Arg16. It is need to note, that α -helix on the region Pro9-Lys12 saves in 72% calculated structural variants, whereas it can be subjected to the quick destabilization on the region Pro4-Thr7 in the dependence on the intermolecular interactions with the side chains of the Met1, Thr8, Lys12 and Arg16 residues. The residues of the threonine in the positions of 3 and 8 peptide chain have the maximal number of the energy profitable contacts. The sum effect from their interaction in the global conformation of the segment is 22,4 and 11,5 kcal/mol, correspondingly. The multipeptide chain creates also the several reverse β -turns on

the short regions of Thr3-Pro4-Asp5-Ala6, Asp5-ala6-Thr7-Thr8, Thr8-Pro9-Gln10-Ala11 and Gln10-Ala11-Lys12-Gly13. The general criterion, showing the existence of such turns is the distance, which is less, than 7 Å between C^{α} -atoms of the residues in the first and fourth positions of the peptide backbone (table 3). The conformations, containing the proline residues in the tops of the reverse turns are the most stable.

Table 1

The energy contributions (kcal/mol) of the different types of the interactions in the optimal conformations of Met1-Arg16 segment

Conformation	$E_{nonv.}$	E_{el}	E_{tors}	E_{conf}	E_{rel}
1	-84.4	15.4	9.3	-68.6	0.0
2	-82.1	5.9	9.0	-67.1	1.5
3	-78.2	4.3	9.0	-65.0	3.6
4	-77.2	6.6	8.8	-61.8	6.8

Table 2

The dihedral angles (grad) in the main and side chains of the amino-acid residues in the global conformation of Met1-Arg16 segment

Residual	Dihedral angles
Met1	-119, 127, 177, 185, 181, 178, 180 *
Pro2	131, 181
Thr3	-99, 153, 180, 63, 182, 179
Pro4	-41, 187
Asp5	-77, -35, 180, 59, 94
Ala6	-73, -46, 184, 185
Thr7	-74, -60, 178, 57, 180, 176
Thr8	-123, 84, 177, -54, 176, 175
Pro9	-44, 180
Gln10	-56, -38, 185, -79, 64, -107
Ala11	-75, -45, 187, 180
Lys12	-100, -70, 181, 180, 180, 179, 180, 180
Gly13	-91, 79, 180
Phe14	-118, 157, 177, 57, 85
Arg15	-106, -58, 178, 181, 178, 180, 179
Arg16	52, 63, 179, -58, 177, 183, 179

*Notice. The angles are given in the sequence $\varphi, \psi, \omega, \chi_1, \chi_2, \chi_3, \chi_4, \chi_5$ (for Pro2, Pro4 and Pro9 -in the sequence ψ, ω).

The latest segment structures on the energy ($E_{rel}=1.5$; 3.6 and 6.8 kcal/mol) include the one from the low-energy states of the nonapeptide Met1-Pro9 and save the α -helix on the region Pro9-Lys12, that allows to us to conclude about the existence of the enough close nucleation in the space structure of the segment. From the data comparison, given in the table 1 it is followed, that the nonvalent, i.e. dispersive interactions, i.e. packing density of the amino-acid sequence play the significant role in the stabilization of the low-energy conformational states of the Met1-Arg16 segment. In spite of the differences in the space packing of the polypeptide chain (fig.2), it saves the reverse turns on the regions Thr3-Ala6, Asp5-Thr8, Thr8-Ala11 and Glu10-Gly13 (table 3). Thus, despite on the conformational mobility of the polypeptide

THE THEORETICAL MODEL OF THE MET1-ARG16 SEGMENT STRUCTURE FROM N-TERMINUS OF TYROSINE HYDROXYLASE...

chain, differing by the orientation of the side chains of the separate residues, it is possible to select the character elements in its space structure. It is the existence of two

shorts of α -helices on the regions Pro4-Thr7 and Pro9-Lys12 and several β -rotations, stabilized by the hydrogen bonds between functional groups of the peptide backbone.

Table 3

The energy contributions of the interresidual interactions (kcal/mol) and the distances between C^α -atoms of the main chain (\AA) in the low-energy conformational states of Met1-Arg16 segment

Residues	1*		2		3		4	
	Distance	Energy	Distance	Energy	Distance	Energy	Distance	Energy
Met1-Pro2	3.8	-3.4	3.8	-3.2	3.8	-3.1	3.8	-3.4
Met1-Thr3	6.3	-1.2	5.5	-1.9	5.3	-2.3	6.3	-1.2
Met1-Pro4	9.6	-0.2	6.7	-2.4	6.5	-0.4	9.6	0.0
Pro2-Asp5	8.6	-3.2	9.0	-0.1	8.7	-0.1	8.6	-0.2
Pro2-Ala6	6.9	-2.5	9.4	0.0	9.1	0.0	6.9	-0.2
Thr3-Pro4	3.8	-3.1	3.8	-3.3	3.8	-3.3	3.8	-3.0
Thr3-Asp5	5.4	-3.3	5.5	-2.3	5.5	-2.0	5.4	-3.3
Thr3-Ala6	5.2	-2.1	6.7	-0.7	6.7	-0.5	5.3	-2.7
Thr3-Thr7	6.0	-1.3	8.7	-0.2	8.5	-0.2	6.7	-1.7
Thr3-Thr8	8.0	-0.4	8.1	-0.1	8.0	0.0	8.3	-0.1
Thr3-Gln10	12.3	-9.4	11.3	0.0	10.8	0.0	12.1	0.0
Thr3-Ala11	11.6	-2.7	13.0	0.0	13.0	0.0	11.0	0.0
Pro4-Thr7	5.3	-1.2	9.0	0.0	8.9	0.0	5.5	-1.8
Pro4-Thr8	5.4	-2.1	8.0	0.0	8.1	0.0	5.5	-1.1
Pro4-Phe14	11.2	-2.0	8.6	-0.1	13.5	0.0	9.7	0.0
Pro4-Arg15	14.8	-2.4	10.4	0.1	16.2	0.0	11.9	0.1
Asp5-Ala6	3.8	-1.1	3.8	-2.2	3.8	-2.1	3.8	-0.5
Asp5-Thr7	5.5	-1.0	5.7	-2.9	5.6	-2.9	5.5	-0.9
Asp5-Thr8	5.2	-1.1	5.4	-2.6	5.7	-2.9	5.5	-0.9
Asp5-Pro9	4.0	0.0	5.0	-2.1	5.1	-3.1	3.9	-2.2
Asp5-Lys12	5.4	0.0	6.9	-5.7	8.8	-11.7	5.2	-8.9
Asp5-Arg15	11.7	-0.1	11.4	-2.0	15.7	-1.7	9.5	-3.1
Asp5-Arg16	14.4	0.0	11.1	-7.9	15.6	-3.7	11.7	-5.1
Ala6-Thr7	3.8	-1.3	3.8	-1.5	3.8	-1.5	3.8	-1.4
Ala6-Thr8	5.7	-0.7	6.0	-0.5	6.2	-0.4	5.6	-0.8
Ala6-Pro9	5.6	-0.1	7.7	-0.1	7.7	-0.1	5.7	-0.9
Thr7-Thr8	3.8	-1.7	3.8	-2.9	3.8	-2.9	3.8	-1.6
Thr8-Pro9	3.8	-3.8	3.8	-3.1	3.8	-2.8	3.8	-3.7
Thr8-Gln10	5.5	-2.2	5.4	-2.3	5.6	-1.8	5.2	-3.3
Thr8-Ala11	6.0	-1.9	5.8	-2.3	5.8	-2.2	6.0	-1.4
Thr8-Lys12	6.9	-1.2	6.7	-1.5	7.2	-1.4	7.3	-0.6
Thr8-Gly13	7.8	-0.7	8.5	-0.1	8.9	0.0	7.4	-0.2
Thr8-Phe14	9.5	-1.7	8.6	0.0	10.5	0.0	10.6	0.0
Pro9-Gln10	3.8	-2.8	3.8	-0.8	3.8	-3.2	3.8	-2.1
Pro9-Lys12	5.2	-0.5	5.4	-1.6	5.3	-2.9	5.3	-1.5
Pro9-Gly13	4.4	-1.5	5.4	-1.3	5.7	-1.6	3.9	-0.9
Gln10-Gly13	5.8	-1.2	6.4	-0.3	4.8	-1.8	5.8	-0.3
Lys12-Gly13	3.8	-1.6	3.8	-1.8	3.8	-1.7	3.8	1.8
Lys12-Phe14	5.9	-3.0	6.4	-0.4	5.8	-1.4	5.9	-2.9
Gly13-Phe14	3.8	-1.0	3.8	-0.5	3.8	-0.4	3.8	-1.6
Gly13-Arg15	6.9	-0.2	5.9	-0.4	6.1	-0.3	6.3	-0.6
Gly13-Arg16	9.7	0.0	6.0	-3.3	6.5	-2.0	9.1	-0.3
Phe14-Arg15	3.8	-1.5	3.8	-3.2	3.8	-5.4	3.8	-0.2
Phe14-Arg16	6.0	-5.7	6.1	1.6	6.4	-1.0	5.5	-5.0

*Note. Conformation from table1.

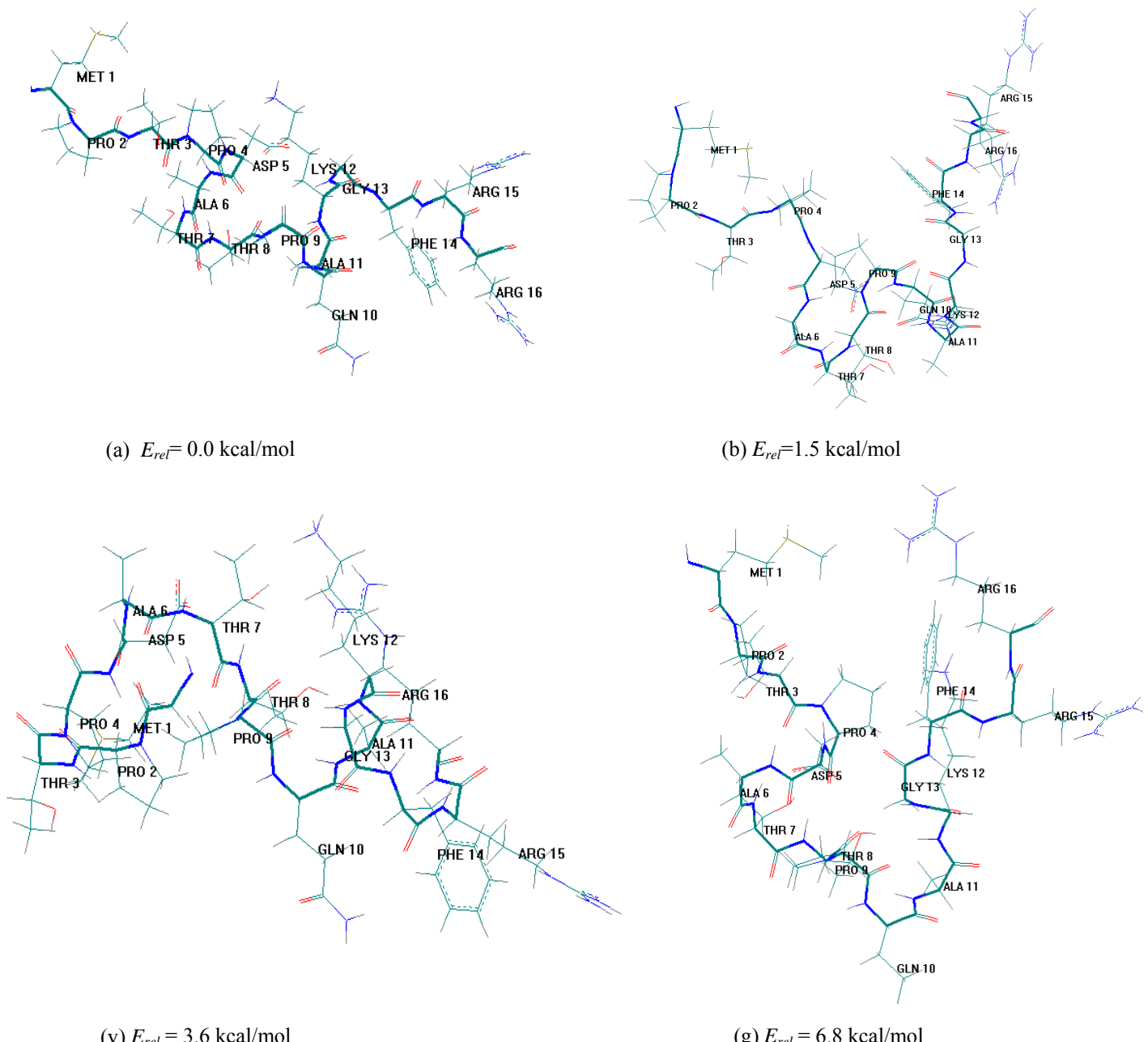


Fig.2. The low-energy conformational states of Met1-Arg16 segment from N-terminus domain of tyrosine hydroxylase.

-
- [1] E. Iseki, M. Kato, W. Mauri et al. J. Neurol. Sci., 2001, v.185(2), p.129-134.
 - [2] Nakashima, N. Hayashi, K. Mori et al. FEBS Lett., 2000, v.465, p.59-63.
 - [3] E.M. Popov. «Strukturnaya organizatsiya belkov», M., «Nauka», 1989, 352p.
 - [4] E.M. Popov. Int. J. Quant. Chem. 1979, v.16, p.707-718.
 - [5] I.S. Maksumov, L.I. Ismailova, N.M. Gojayev. J. Struk. Khimii, 1983, v.24, №4, p.147-148.
 - [6] F.A. Momany, R.F. Mc.Guire, A.W. Burgess, H.A. Scheraga. Phys. Chem. 1975, v.79, p. 2361-2381.
 - [7] IUPAC-IUB Commision on Biochemical Nomenclature Abbreviations and symbols for description of conformation of polypeptide chains. Pure Appl. Chem., 1974, v. 40, p. 291-308.

N.N. Mustafayeva, İ.N. Əliyeva, N.M. Qocayev

TİROZİNHİDROKSİLADA N-SONLU DOMENİNİN MET1-ARQ16 FRAQMENİN QURULUŞUNUN NƏZƏRİ MODELİ

Tirozinhidroksilada N-sonlu tənzimləyici domenin tərkibinə daxil olan 16 amin turşusu qaliqlarının ardıcılılığı aşağı enerjili konformasiya hallarının potensial funksiyaların yarımempirik atom-atom yaxınlaşmasında qüvvə sahəsi metodu ilə təyin edilib.

THE THEORETICAL MODEL OF THE MET1-ARG16 SEGMENT STRUCTURE FROM N-TERMINUS OF TYROSINE HYDROXYLASE...

Hidrogen rabitələrile sabitləşdirilmiş polipeptid zəncirinin qısa sahələrində yerləşən bir-neçə reversiv dönüşlər və Pro9-Lys12 və Pro4-Thr7 sahələrində α -spiral iki burulmasının olması konformasiya enerjisinin qlobal minimumlu hali təyin edilmişdir.

Н.Н. Мустафаева, И.Н. Алиева, Н.М. Годжаев

ТЕОРЕТИЧЕСКАЯ МОДЕЛЬ СТРУКТУРЫ ФРАГМЕНТА МЕТ1-АРГ16 N-КОНЦЕВОГО ДОМЕНА ТИРОЗИНГИДРОКСИЛАЗЫ

Методом силового поля в приближении полуэмпирических атом-атомных потенциальных функций установлены низкоэнергетические конформационные состояния последовательности из 16 аминокислотных остатков, входящих в состав N-концевого регуляторного домена фермента тирозингидроксилазы. Установлено, что состояние с глобальным минимумом конформационной энергии содержит два витка α -спирали на участках Pro4-Thr7 и Pro9-Lys12 и несколько реверсивных поворотов на коротких участках пептидной цепи, стабилизированных водородными связями.

Received: 28.01.05

SİNQLET-TRİPLET ANTİFERROMAQNİTLƏRDƏ İŞİĞIN SƏTH KOLLEKTİV OYANMALARI İLƏ UDULMASININ XƏTTİ NƏZƏRİYYƏSİ

A. M. SÜLEYMANOV
AMEA Fizika İnstitutu, Bakı, Az-1143, H.Cavid pr.,33

İşdə sinqlet-triplet antiferromaqnitlərdə işığın səth kollektiv modlarının oyanması ilə udulması öyrənilmişdir. Bu məqsədlə çoxzamanlı Qrin funksiyası metodundan və psevdospin formalizmindən istifadə edilmişdir. Əvvəlcə baxılan sistemin enerji spektri hesablanmışdır. Sinqlet-triplet ferromaqnitlərdən fərqli olaraq, sinqlet-triplet antiferromaqnitlərdə səth kollektiv oyanmalarının enerji spektri (w_{kr}) dörd budaqdan ibarətdir. Belə ki, iki budaq ($r=1,2$) maqnon budaqları, iki budaq ($r=3,4$) isə «maqnit eksitonu» budaqlarıdır. Sistemin dipol momenti üçün alınmış ifadədən sinqlet-triplet antiferromaqnitlərin səthində işığın səth kollektiv oyanmaları ilə udulmasını mümkün edən dörd prosesin baş vermesi aşkar olur. Bu proseslər aşağıdakılardır:

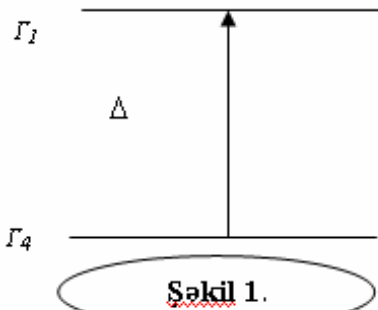
- (1) bir maqnonun $r=1$ budağından və bir maqnonun $r=2$ budağından oyanması ilə müşaiyət olunan işığın udulması
- (2) bir «eksitonu» $r=3$ budağından və bir «eksitonu» $r=4$ budağından oyanması ilə müşaiyət olunan işığın udulması
- (3) bir maqnonun $r=2$ budağından və bir «eksitonu» $r=3$ budağından oyanması ilə müşaiyət olunan işığın udulması
- (4) bir maqnonun $r=1$ budağından və bir «eksitonu» $r=4$ budağından oyanması ilə müşaiyət olunan işığın udulması.

Beləliklə, sinqlet-triplet antiferromaqnitlərin səth kollektiv modlarının spektrinin dörd budağa malik olması sinqlet-triplet ferromaqnitlərlə müqayisədə sinqlet-triplet antiferromaqnitlərin səthində işığın udulma imkanlarının daha çox olmasına səbəb olur. İşin sonunda, işığın hər bir mümkün udulma prosesine uyğun dielektrik qavrayıcılığı üçün ifadələr alınmışdır. Bu ifadələri analiz etməklə sinqlet-triplet antiferromaqnitlərdə daxili kristallik sahələr haqqında etraflı məlumat almaq olar.

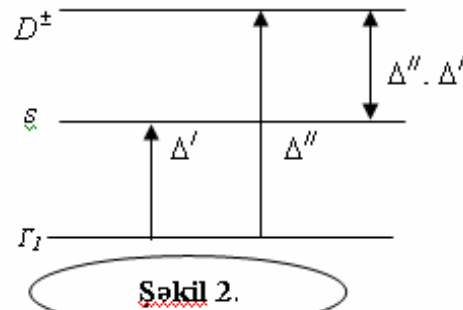
Əvvəlki işlərdə [1–4] biz sinqlet-triplet ferromaqnitlərinin səthində işığın udulması və səpilməsi məsələlərinə baxmışdıq. Təqdim olunan işdə işığın yarımsız sinqlet-triplet antiferromaqnitlərin səthində udulması məsələsinə baxılmışdır.

Konkret olaraq nadir torpaq elementi ionlarının Mendeleyev cədvəlinin V qrup anionları ilə əmələ gətirdiyi TbN, TbSb, ... tipli birləşmələrə baxılacaq və sadəlik üçün kristal sadə kubik quruluşa malik hesab ediləcəkdir. Ion səthdə yer-

ləşən hal üçün kristall sahənin potensialı ion həcmində yerləşən haldakı potensialdan fərqlənəcəkdir. Odur ki, səthdə və həcmində yerləşən ion üçün enerji səviyyələri sxemi müxtəlif olacaqdır. Belə ki, həcmində yerləşən nadir torpaq elementi ionunun əsas halı Γ_1 sinqletdən və birinci həyacanlaşmış halı Γ_4 tripletdən ibarətdirsə (şəkil 1), ion səthdə yerləşən halda Γ_4 triplet D^\pm dubletə və S sinqletə parçalanacaqdır (şəkil 2).



Həcmində yerləşən nadir torpaq elementi ionunun enerji sxemi



Səthdə yerləşən nadir torpaq elementi ionunun enerji sxemi

Yuxarıda təsvir olunan enerji səviyyələrini və eyni zamanda ionlar arasında mübadilə qarşılıqlı təsirini və anizotropiyani

nəzərə alan sistemin Hamiltonianı psevdospin formalizmində belə yazılır [5]:

$$H_0 = \sum_i [\frac{\Delta_i}{2} (S_i^+ T_i^- + S_i^- T_i^+) + \Delta'_i S_i^z T_i^z - \sum_{i,j} J(i-j) \cdot [(\alpha_i^{||} S_i^+ + \beta_i^{||} T_i^+) \cdot (\alpha_j^{||} S_j^- + \beta_j^{||} T_j^-) + (\alpha_i' S_i^z + \beta_i' T_i^z) \cdot (\alpha_j' S_j^z + \beta_j' T_j^z)] - D \left[\sum_i (\alpha_i' S_i^z + \beta_i' T_i^z)^2 + \sum_j (\alpha_j' S_j^z + \beta_j' T_j^z)^2 \right]] \quad (1)$$

Harada ki, S_i və T_i - spin $\frac{1}{2}$ -ə uyğun gələn və i -ci iona məxsus olan spin operatorlarıdır. Ion səth təbəqəsində yerləşən hal üçün $\Delta_i = \Delta$, $\Delta'_i = 2\Delta'' - \Delta'$; burada Δ' və Δ'' uyğun olaraq həyacanlaşmış sinqlet S və dublet D^\pm ilə əsas sinqlet Γ_1

arasındaki enerji məsafəsidir. $\alpha_i^{||}$, $\beta_i^{||}$, α_i' və β_i' əmsalları aşağıdakı münasibətlərdən tapılır:

$$\langle D^+ | J^+ | S \rangle = - \langle S | J^+ | D^- \rangle = \frac{\alpha'' + \beta''}{\sqrt{2}};$$

$$\begin{aligned} < D^+ | J^z | D^+ > = - < D^- | J^z | D^- > = \frac{\alpha' + \beta'}{2}; & & < \Gamma_4^+ | J^z | \Gamma_4^+ > = - < \Gamma_4^- | J^z | \Gamma_4^- > = \frac{\alpha + \beta}{2}; \\ < \Gamma_1 | J^+ | D^- > = - < D^+ | J^+ | \Gamma_1 > = \frac{\alpha'' - \beta''}{\sqrt{2}}; & & < \Gamma_1 | J^z | \Gamma_4^0 > = < \Gamma_4^0 | J^z | \Gamma_1 > = \frac{\alpha - \beta}{2}; \\ < \Gamma_1 | J^z | S > = - < S | J^z | \Gamma_1 > = \frac{\alpha' - \beta'}{2}; & & \end{aligned}$$

İon ikinci təbəqədə və ya həcmində yerləşən hal üçün $\Delta_i = \Delta'_i = \Delta$; burada $\Delta - \Gamma_1$ sinqlet və Γ_4 triplet arasındakı enerji məsafəsidir. $\alpha''_i = \alpha'_i = \alpha$, $\beta''_i = \beta'_i = \beta$, harada ki, α və β aşağıdakı münasibətlərdən təpilir:

$$\vec{p} = \sum_{i,j} \vec{\pi}_{i,j} \cdot \left[(\alpha_i^0 S_i^+ + \beta_i^0 T_i^+) \cdot (\alpha_j^0 S_j^- + \beta_j^0 T_j^-) + (\alpha_i^0 S_i^z + \beta_i^0 T_i^z) \cdot (\alpha_j^0 S_j^z + \beta_j^0 T_j^z) \right]$$

sistemin elektrik dipol momentidir, $\vec{\pi}_{i,j}$ isə yarımsuz sinqlet-triplet antiferromaqnitin elektrik polyarlaşma vektorudur. H_0 - sistemin enerji operatoru olub, (1) şəklindədir.

Holsteyn – Primakov çevrilmələrindən istifadə edərək (1) Hamiltonianını ikinci kvatlanma operatorları vasitəsilə ifadə edib (cüt və tək düyünlərə uyğun \vec{S} və \vec{T} operatorları)

$$\begin{aligned} S_i^+ &= \left(\frac{2S}{N} \right)^{1/2} \cdot \sum_{K_{//}} \left[Y_{K_{//}}(i_{\perp}) C_{K_{//}} + Z_{K_{//}}(i_{\perp}) \cdot d_{K_{//}} \right] e^{iK_{//}i_{//}}, \quad S_i^- = \left(\frac{2S}{N} \right)^{1/2} \cdot \sum_{K_{//}} \left[Y_{K_{//}}^*(i_{\perp}) C_{K_{//}}^+ + Z_{K_{//}}^*(i_{\perp}) \cdot d_{K_{//}}^+ \right] e^{-iK_{//}i_{//}} \\ S_i^z &= S - \frac{1}{N} \cdot \sum_{K_{//}, K_{//}'} \left[Y_{K_{//}}^*(i_{\perp}) C_{K_{//}} + Z_{K_{//}}^*(i_{\perp}) d_{K_{//}}^+ \right] \cdot \left[Y_{K_{//}'}(i_{\perp}) C_{K_{//}'} + Z_{K_{//}'}(i_{\perp}) d_{K_{//}'} \right] \cdot e^{i(K_{//}' - K_{//})i_{//}} \\ T_i^+ &= \left(\frac{2T}{N} \right)^{1/2} \cdot \sum_{K_{//}} \left[Y_{K_{//}}(i_{\perp}) d_{K_{//}} - Z_{K_{//}}(i_{\perp}) C_{K_{//}} \right] \cdot e^{iK_{//}i_{//}}, \quad T_i^- = \left(\frac{2T}{N} \right)^{1/2} \cdot \sum_{K_{//}} \left[Y_{K_{//}}^*(i_{\perp}) d_{K_{//}}^+ - Z_{K_{//}}^*(i_{\perp}) C_{K_{//}}^+ \right] \cdot e^{-iK_{//}i_{//}} \\ T_i^z &= T - \frac{1}{N} \cdot \sum_{K_{//}, K_{//}'} \left[Y_{K_{//}}^*(i_{\perp}) d_{K_{//}}^+ - Z_{K_{//}}^*(i_{\perp}) C_{K_{//}}^+ \right] \cdot \left[Y_{K_{//}'}(i_{\perp}) d_{K_{//}'} - Z_{K_{//}'}(i_{\perp}) C_{K_{//}'} \right] \cdot e^{i(K_{//}' - K_{//})i_{//}} \\ S_j^+ &= \left(\frac{2S}{N} \right)^{1/2} \cdot \sum_{K_{//}} \left[Q_{K_{//}}(i_{\perp}) q_{K_{//}} + F(i_{\perp}) f_{K_{//}} \right] \cdot e^{iK_{//}i_{//}}, \quad S_j^- = \left(\frac{2S}{N} \right)^{1/2} \cdot \sum_{K_{//}'} \left[Q_{K_{//}}^*(i_{\perp}) q_{K_{//}}^+ + F^*(i_{\perp}) f_{K_{//}}^+ \right] \cdot e^{-iK_{//}i_{//}} \\ S_j^z &= S - \frac{1}{N} \cdot \sum_{K_{//}, K_{//}'} \left[Q_{K_{//}}^*(i_{\perp}) q_{K_{//}}^+ + F^*(i_{\perp}) f_{K_{//}}^+ \right] \cdot \left[Q_{K_{//}'}(i_{\perp}) q_{K_{//}'} + F(i_{\perp}) f_{K_{//}'} \right] \cdot e^{i(K_{//}' - K_{//})i_{//}} \\ T_j^+ &= \left(\frac{2T}{N} \right)^{1/2} \cdot \sum_{K_{//}} \left[Q_{K_{//}}(i_{\perp}) f_{K_{//}} - F_{K_{//}}(i_{\perp}) q_{K_{//}} \right] \cdot e^{iK_{//}i_{//}}, \quad T_j^- = \left(\frac{2T}{N} \right)^{1/2} \cdot \sum_{K_{//}} \left[Q_{K_{//}}^*(i_{\perp}) f_{K_{//}}^+ - F_{K_{//}}^*(i_{\perp}) q_{K_{//}}^+ \right] \cdot e^{-iK_{//}i_{//}} \\ T_j^z &= T - \frac{1}{N} \cdot \sum_{K_{//}, K_{//}'} \left[Q_{K_{//}}^*(i_{\perp}) f_{K_{//}}^+ - F_{K_{//}}^*(i_{\perp}) q_{K_{//}}^+ \right] \cdot \left[Q_{K_{//}'}(i_{\perp}) f_{K_{//}'} - F_{K_{//}'}(i_{\perp}) q_{K_{//}'} \right] e^{i(K_{//}' - K_{//})i_{//}} \end{aligned} \quad (2)$$

harada ki, $K_{//}$ - kristalın səthinə paralel yönəlmış iki ölçülü dalğa vektorudur, $C_{K_{//}}$, $C_{K_{//}}^+$; $d_{K_{//}}$, $d_{K_{//}}^+$; $q_{K_{//}}$, $q_{K_{//}}^+$ və $f_{K_{//}}$, $f_{K_{//}}^+$ - dörd tip spin operatorlarına (S_i , S_j , T_i və T_j operatorlarına) uyğun dalğa vektoru

D - anizotropiya sabitidir.

İndi də hesab edək ki, bu yarımsuz sinqlet – triplet anti-ferromaqnetik bircins \vec{E} elektrik sahəsində yerləşir. Onda onun Hamiltomani belə olar:

$$H = H_0 - \vec{E} \cdot \vec{p}$$

burada

rinin antiferromaqnitliyini nəzərə almaqla), sonra isə impuls təsvirinə keçərək, (1) Hamiltonianını diaqonallaşdırın uyğun çevrilmələr seçmək lazımdır. Baxdigımız yarımsuz kristalda kristalın səthinə perpendikulyar istiqamətdə invariantlıq pozulub, səthə paralel istiqamətdə pozulmadığından, bu çevrilmələri aşağıdakı kimi seçmək məqsədə uyğundur:

$K_{//}$ olan səth modlarının yaranma və yoxolma operatorlarıdır, i_{\perp} və $i_{//}$ isə i -ci ionun radius – vektorunun uyğun olaraq kristalın səthinə perpendikulyar və paralel olan toplananlarıdır, N - kristalın bir təbəqəsində olan ionların sayıdır.

Diaqonallaşdırıldan sonra H_0 və \vec{p} operatorları üçün ala-

$$H_0 = \sum \left[w_1(K_{\parallel}) C_k^+ C_k + w_2(K_{\parallel}) d_K^+ d_K + w_3(K_{\parallel}) q_K^+ q_K + w_4(K_{\parallel}) f_K^+ f_k \right]$$

$$\vec{p} = \sum_{K_{\parallel}} \left[\vec{\Pi}_{K_{\parallel 1}} \cdot \vec{P}_{K_{\parallel 1}} + \vec{\Pi}_{K_{\parallel 2}} \cdot \vec{P}_{K_{\parallel 2}} + \vec{\Pi}_{K_{\parallel 3}} \cdot \vec{P}_{K_{\parallel 3}} + \vec{\Pi}_{K_{\parallel 4}} \cdot \vec{P}_{K_{\parallel 4}} \right] \quad (3)$$

burada $w_n(K_{\parallel})$ ($n=1,2,3,4$) - sinqlet – triplet antiferromaqnitin səth kollektiv modlarının (oyanmalarının) enerjilə-

ridir. $\vec{\Pi}_{K_{\parallel n}}$ ($n=1,2,3,4$) əmsalları və $P_{k_{\parallel n}}$ ($n=1,2,3,4$) operatorları aşağıdakı kimi təyin olunur:

$$\vec{\Pi}_{K_{\parallel 1}} = \vec{\Pi}_{K_{\parallel 2}} = \left[(\alpha^2 S + \beta^2 T)(Y_{K_{\parallel}} Z_{K_{\parallel}} + Q_{K_{\parallel}} F_{K_{\parallel}}) + \alpha' \beta' \sqrt{ST} \cdot (Y_{K_{\parallel}}^2 + Z_{K_{\parallel}}^2 + Q_{K_{\parallel}}^2 + F_{K_{\parallel}}^2) \right] \cdot \vec{\pi}(K_{\parallel})$$

$$\vec{\Pi}_{K_{\parallel 3}} = \left[2\alpha' p' \sqrt{ST} (Y_{K_{\parallel}} Z_{K_{\parallel}} + Q_{K_{\parallel}} F_{K_{\parallel}}) + \alpha^2 S (Z_{K_{\parallel}}^2 + Q_{K_{\parallel}}^2) + \beta^2 T (Y_{K_{\parallel}}^2 + F_{K_{\parallel}}^2) \right] \vec{\pi}(K_{\parallel})$$

$$\vec{\Pi}_{K_{\parallel 4}} = \left[2\alpha' \beta' \sqrt{ST} (Y_{K_{\parallel}} Z_{K_{\parallel}} + Q_{K_{\parallel}} F_{K_{\parallel}}) + \alpha^2 S (Y_{K_{\parallel}}^2 + F_{K_{\parallel}}^2) + \beta^2 T (Z_{K_{\parallel}}^2 + Q_{K_{\parallel}}^2) \right] \vec{\pi}(K_{\parallel})$$

$$P_{K_{\parallel 1}} = C_{K_{\parallel}} d_{-K_{\parallel}} + C_{K_{\parallel}}^+ d_{-K_{\parallel}}^+,$$

$$P_{K_{\parallel 2}} = q_{K_{\parallel}} f_{-K_{\parallel}} + q_{K_{\parallel}}^+ f_{-K_{\parallel}}^+,$$

$$P_{K_{\parallel 3}} = q_{K_{\parallel}} d_{-K_{\parallel}} + q_{K_{\parallel}}^+ d_{-K_{\parallel}}^+,$$

$$P_{K_{\parallel 4}} = C_{K_{\parallel}} f_{-K_{\parallel}} + C_{K_{\parallel}}^+ f_{-K_{\parallel}}^+$$

burada $Y_{K_{\parallel}}, Z_{K_{\parallel}}, Q_{K_{\parallel}}, F_{K_{\parallel}}$ - H_0 Hamiltonianını diaqonallaşdırıran (2) unitar çevrilmələrinin əmsallarıdır, $\vec{\pi}(K_{\parallel}) = \sum_{i \parallel, j \parallel} \vec{\pi}_j \cdot e^{-ik_{\parallel}(i_{\parallel} - j_{\parallel})}$ olub, $\vec{\pi}_{ij}$ vektorunun 2 ölçülü Furye – obrazıdır.

Beləliklə, sinqlet – triplet antiferromaqnitin səth kollektiv oyanmalarının $w_n(K_{\parallel})$ spektri 4 budaqdan – iki maqnon ($n=1,2$) və iki «maqnit eksitonu» ($n=3,4$) budaqların-dan ibarətdir [6]. Digər tərəfdən də (3) elektrik dipol momenti işığın sinqlet – triplet antiferromaqnitlərin səthində kollektiv modlarla udulmasına gətiren 4 mümkün prosesi ifadə edir:

(1) bir maqnonun $n=1$ budağından və bir maqnonun $n=2$ budağından buraxılması ilə müşayiət olunan işığın udulması

(2) bir «eksitonun» $n=3$ budağından və bir «eksitonun» $n=4$ budağından buraxılması ilə müşayiət olunan işığın udulması

(3) bir maqnonun $n=2$ budağından və bir «eksitonun» $n=3$ budağından buraxılması ilə müşayiət olunan işığın udulması

(4) bir maqnonun $n=1$ budağından və bir «eksitonun» $n=4$ budağından buraxılması ilə müşayiət olunan işığın udulması.

Beləliklə, sinqlet-triplet antiferromaqnitin səth kollektiv modlarının enerji spektrinin dörd budağa malik olması sinqlet – triplet ferromaqnitlərlə müqayisədə sinqlet-triplet antiferromaqnitlərin səthində işığın udulma imkanlarının daha çox olmasına səbəb olur.

İndi də işığın hər bir mümkün udulma prosesinə uyğun dielektrik qavrayıcılığını hesablayaqla. Qrin funksiyası texnikada \vec{p} dipol momentinin yaratdığı dielektrik qavrayıcı-

lığının ifadəsi (\vec{E} - yə görə birinci yaxınlasmada) belədir [7]:

$$\vec{\varepsilon}(w) = -i \cdot \int_{-\infty}^{\infty} dt' e^{iw(t-t')} \langle \vec{p}(t) | \vec{p}(t') \rangle \quad (4)$$

Sonrakı hesablamaları sadələşdirmək üçün aşağıdakı kimi işarələmələr daxil edək:

$$\vec{P}_{(1)} = \sum_{K_{\parallel}} \vec{\Pi}_{K_{\parallel 1}} P_{K_{\parallel 1}} \quad (5)$$

$$\vec{P}_{(2)} = \sum_{K_{\parallel}} \vec{\Pi}_{K_{\parallel 2}} P_{K_{\parallel 2}} \quad (6)$$

$$\vec{P}_{(3)} = \sum_{K_{\parallel}} \vec{\Pi}_{K_{\parallel 3}} P_{K_{\parallel 3}} \quad (7)$$

$$\vec{P}_{(4)} = \sum_{K_{\parallel}} \vec{\Pi}_{K_{\parallel 4}} P_{K_{\parallel 4}} \quad (8)$$

(5) ifadəsini (4)-də nəzərə almaqla, işığın sinqlet-triplet antiferromaqnitlərin səthində udulmasının (1) prosesinə uyğun $\leftrightarrow \mathcal{E}_{(1)}(w)$ dielektrik qavrayıcılığı üçün belə bir ifadə alarıq:

$$\overset{\leftrightarrow}{\mathcal{E}}_{(1)}(w) = 2\pi i \sum_{K_{\parallel}} \vec{\Pi}_{K_{\parallel 1}} \cdot G(P_{K_{\parallel 1}}; w) \quad (9)$$

harada ki, $G(P_{K_{\parallel 1}}; w)$

$$G(P_{K_{\parallel 1}}(\tau_1);$$

$P_{K_{\parallel 1}}(\tau_2)) = -i\theta(\tau_1 - \tau_2) \langle [P_{K_{\parallel 1}}(\tau_1), P_{K_{\parallel 1}}(\tau_2)] \rangle$ - ikizamanlı Qrin funksiyasının ikiölçülü Furye – obrazıdır.

$G(P_{K_{\parallel 1}}; w)$ Qrin funksiyası üçün hərəkət tənliyi yazıb, sonra da bu tənliyi təsadüfi fazalar yaxınlaşmasında [7] həll etsək, $G(P_{K_{\parallel 1}}; w)$ üçün alarıq:

$$G(P_{K_{//1}}; w) = \frac{(2\pi)^{-1} \cdot \Pi(K_{//}) < C_{K_{//}}^+ \vec{C}_{K_{//}} + d_{K_{//}} d_{K_{//}}^+ >}{w - [w_1(K_{//}) + w_2(K_{//})]} \quad (10)$$

(10) - u (9) - da yerinə yazımaqla, $\mathcal{E}_{(1)}(w)$ üçün belə ifadə alarıq:

$$\leftrightarrow \mathcal{E}_{(1)}(w) = -i \cdot \sum_{K_{//}} \frac{\vec{\Pi}_{K_{//1}} \vec{\Pi}_{K_{//1}} < C_{K_{//}}^+ C_{K_{//}} + d_{K_{//}} d_{K_{//}}^+ >}{w - [w_1(K_{//}) + w_2(K_{//})]} \quad (11)$$

(11) – dən göründüyü kimi, işığın singlet-triplet antiferromaqnitlərin səthində udulmasına gətirən baxdığımız prosesdə ((1) prosesində) iki səth maqnonu iştirak edir. Başqa sözlə, işığın səthdə udulması spektrin 1 budağından $w_1(K_{//})$ enerjili bir maqnonun və 2 budağından $w_2(K_{//})$ enerjili ikinci maqnonun buraxılması ilə müşaiyət olunur. İndi də (6) ifadəsini (4)-də nəzərə almaqla, işığın singlet-triplet antiferromaqnitlərin səthində udulmasının (2) prosesi-

\leftrightarrow nə uyğun $\mathcal{E}_{(2)}(w)$ dielektrik qavrayıcılığı üçün ifadə alarıq:

$$\leftrightarrow \mathcal{E}_{(2)}(w) = -2\pi i \sum_{K_{//}} \vec{\Pi}_{K_{//2}} G(P_{K_{//2}}; w) \quad (12)$$

Hərəkət tənliyini yazıb onu həll etməklə $G(P_{K_{//2}}; w)$ üçün alarıq:

$$G(P_{K_{//2}}; w) = \frac{(2\pi)^{-1} \cdot \vec{\Pi}_{K_{//2}} \cdot < q_{k_{//}}^+ q_{K_{//}} + f_{K_{//}} f_{K_{//}}^+ >}{w - [w_3(K_{//}) + w_4(K_{//})]} \quad (13)$$

(13)-ü (12) – də yerinə yazımaqla, $\mathcal{E}_{(2)}(w)$ üçün alarıq:

- [1]. Yu. M. Seidov and A. M. Suleymanov. phys. 1987,stat. sol. (b), 140, 149.
- [2]. Yu. M. Seidov and A. M. Suleymanov. phys. 1989,stat. sol. (b), 153, K 203.
- [3]. A. M. Suleymanov, M. B. Hüseynli, K. M. Sultanov. Bakı Universitetinin xəbərləri, 2003, № 2, 147.
- [4]. A. M. Suleymanov, M. B. Hüseynli, K. M. Sultanov . Bakı Universitetinin xəbərləri, 2003, № 4, 162.

$$\rightarrow \mathcal{E}_{(2)}(w) = -i \sum_{K_{//}} \frac{\vec{\Pi}_{K_{//2}} \vec{\Pi}_{K_{//2}} < q_{K_{//}}^+ q_{K_{//}} + f_{K_{//}} f_{K_{//}}^+ >}{w - [w_3(K_{//}) + w_4(K_{//})]} \quad (14)$$

(14)-dən göründüyü kimi, işığın singlet-triplet antiferromaqnitlərin səthində udulmasına gətirən baxdığımız prosesdə ((2) prosesində) iki səth «eksitonu» iştirak edir. Başqa sözlə, işığın səthdə udulması spektrin 3 budağından $w_3(K_n)$ enerjili bir «eksitonun» və 4 budağından $\omega_4(k_{\square})$ enerjisi ikinci «eksitonun» buraxılması ilə müşaiyət olunur. Analoji hesablamalarla (7) və (8)-dən istifadə etməklə, işığın singlet-triplet antiferromaqnitlərin səthində udulmasına gətirən (3) və (4) proseslərinə uyğun $\mathcal{E}_{(3)}(w)$ və $\mathcal{E}_{(4)}(w)$ dielektrik qavrayıcılıqlarının ifadələrini almaq olar:

$$\leftrightarrow \mathcal{E}_{(3)}(w) = -i \cdot \sum_{K_{//}} \frac{\vec{\Pi}_{K_{//3}} \vec{\Pi}_{K_{//3}} < d_{K_{//}}^+ d_{K_{//}} + q_{K_{//}} q_{K_{//}}^+ >}{w - [w_2(K_{//}) + w_3(K_{//})]} \quad (15)$$

$$\leftrightarrow \mathcal{E}_{(4)}(w) = -i \cdot \sum_{K_{//}} \frac{\vec{\Pi}_{K_{//4}} \vec{\Pi}_{K_{//4}} < C_{K_{//}}^+ C_{K_{//}} + f_{K_{//}} f_{K_{//}}^+ >}{w - [w_1(K_{//}) + w_4(K_{//})]} \quad (16)$$

Qeyd edək ki, dielektrik qavrayıcılıqları üçün alınmış (11), (12), (15) və (16) ifadələrini analiz etməklə, singlet-triplet antiferromaqnitlərdə daxili kristallik sahələr haqqında ətraflı məlumat almaq olar.

- [5]. Hsieh Y. Y. and Pink D. A. J. Phys. Chem. Solids, 1974, 35 № 11, p. 1481 – 1490.
- [6]. Yu. M. Seidov and A. M. Suleymanov. phys. 1985, stat. sol. (b), 131, 545.
- [7]. S. V. Təblikov. Kvantovie metodi teorii maqnetizma. – M: Nauka, 1965, 334 s.

A. M. Suleymanov

LINEAR THEORY OF THE LIGHT ABSORPTION BY THE SURFACE COLLECTIVE EXCITATIONS IN SINGLET – TRIPLET ANTIFERROMAGNETS

The light absorption by surface collective excitations in the singlet-triplet antiferromagnets has been investigated by the multi-time Green function method and the pseudospin formalism. Has been calculated the energy spectrum of the system under consideration. Unlike the singlet-triplet ferromagnets, the collective excitation spectrum (w_{kr}) of the singlet-triplet antiferromagnets consists of four branches, two of them are the maqnon branches ($r=1,2$) and the other two are the «magnetic excitons» branches ($r=3,4$). On the other hand, the electric dipole moment of the system under consideration describes the four possible absorption processes of the light by surface collective excitations on the surface of the singlet-triplet antiferromagnets. They are the following processes:

- (1) absorption of the light with simultaneous excitation of two maqnons, one from the branch $r=1$ and the other from the branch $r=2$
- (2) absorption of the light with simultaneous excitation of two «excitons», one from the branch $r=3$ and the other from the branch $r=4$
- (3) absorption of the light with simultaneous excitation of one maqnon from the branch $r=2$ and one «exciton» from the branch $r=3$
- (4) absorption of the light with simultaneous excitation of one maqnon from the branch $r=1$ and one «exciton» from the branch $r=4$.

Thus, due to the presence of four branches excitations the possibility of the light absorption on the surface of singlet-triplet antiferromagnets is larger than that on the surface of the singlet-triplet ferromagnets.

In finish, has been finded expressions for the dielectric susceptibilities corresponding to each of the four possible absorption processes of light by surface collective excitations in singlet-triplet antiferromagnets. Analysis of these expressions will provide more comprehensive information on the crystal field in the singlet-triplet antiferromagnets.

А. М. Сулейманов

ЛИНЕЙНАЯ ТЕОРИЯ ПОГЛОЩЕНИЯ СВЕТА ПОВЕРХНОСТНЫМИ КОЛЛЕКТИВНЫМИ ВОЗБУЖДЕНИЯМИ В СИНГЛЕТ-ТРИПЛЕТНЫХ АНТИФЕРРОМАГНЕТИКАХ

В работе исследовано поглощение света поверхностными коллективными возбуждениями в синглет-триплетных антиферромагнетиках. Для этой цели использован метод многовременных функций Грина и псевдоспиновый формализм. Сперва вычислен энергетический спектр рассматриваемой системы. В отличие от синглет-триплетных ферромагнетиков, спектр (w_{kr}) коллективных возбуждений синглет-триплетных антиферромагнетиков состоит из четырех ветвей – двух магнонных ($r = 1,2$) и двух «магнитных экситонных» ($r = 3,4$). С другой стороны, электрический дипольный момент данной системы описывает четыре процесса возможного поглощения света поверхностными коллективными возбуждениями на поверхности синглет-триплетных антиферромагнетиков. Эти процессы являются следующими:

- (1) поглощение света с возбуждением одного магнона ветви $r = 1$ и одного магнона ветви $r = 2$
- (2) поглощение света с возбуждением одного «экситона» ветви $r = 3$ и одного «экситона» ветви $r = 4$
- (3) поглощение света с возбуждением одного магнона ветви $r = 2$ и одного «экситона» ветви $r = 3$
- (4) поглощение света с возбуждением одного магнона ветви $r = 1$ и одного «экситона» ветви $r = 4$.

Таким образом, возможность поглощения света поверхности синглет-триплетных антиферромагнетиков богаче, чем на поверхности синглет-триплетных ферромагнетиков, из-за наличия четырех ветвей спектра поверхностных коллективных мод. В конце работы, найдены выражения для диэлектрической восприимчивости, соответствующей каждому из возможных четырех процессов поглощения света поверхностными коллективными возбуждениями в синглет-триплетных антиферромагнетиках. Анализ этих выражений дает возможность получить более подробную информацию о кристаллическом поле, существующем в синглет-триплетных антиферромагнетиках.

Received: 16.11.04

THE INFLUENCE OF THE RELAXATION TIME ON THE LIQUID HEAT CAPACITY

G.T. GASANOV, A.N. MAMEDOVA

Azerbaijan State Oil Academy, 370012, Baku, Azadlig av., 20

The nonstationary method of the simultaneous definition of the relaxation time of the temperature field and the liquid heat capacity is proposed. The proposed method rests on the solution of the inverse problem for the heat conduction equation of the relaxing temperature field. The influence of the relaxation time on the heat capacity of the liquids has been estimated.

The one of the important thermophysical liquid parameters, playing the essential role at the heat transfer, is heat capacity. The different methods were elaborated for the investigation of the heat capacity. In the work [1], the temperature dependence of the several samples of the oil is experimentally investigated. It is established, that oil heat capacity increases with the temperature increase. In the work [2], the influence of the different physical fields on the thermophysical liquid properties is investigated theoretically.

The liquid is heating under the action of the acoustic waves and goes to the nonequilibrium state. All thermophysical properties, including the heat capacity, relax, i.e. they vary depending on time. Each parameter has its own relaxation time, in the result the spectrum of the relaxation times of the thermophysical properties appears.

The investigation of the influence of the relaxation time on the liquid heat capacity presents the big interest. For the simplification of the narration let's consider, that the relaxation time is the identical and is equal to the relaxation time of the temperature field for the all thermophysical properties. The relaxing temperature field for the one-dimensional case is expressed by the differential equation (heat exchange with the environment not takes into account):

$$\begin{aligned} c\rho \left(\frac{\partial T}{\partial t} + v \frac{\partial T}{\partial x} + \tau_0 \frac{\partial^2 T}{\partial t^2} \right) &= \\ &= \lambda \frac{\partial^2 T}{\partial x^2} + 2\alpha I(t) \cdot e^{-2\alpha x} \end{aligned} \quad . \quad (1)$$

Here τ_0 is the relaxation time, α is the absorption coefficient of the acoustic waves in the liquid; I is the radiation intensity of the acoustic waves. The rest symbols are common.

Taking into consideration, that the heat transport because of the convection is more bigger, than because of the diffusion, i.e.

$$c\rho v \frac{\partial T}{\partial x} \gg \lambda \frac{\partial^2 T}{\partial x^2}$$

Equation (1) is expressed in the form:

$$c\rho \left(\frac{\partial T}{\partial t} + v \frac{\partial T}{\partial x} + \tau_0 \frac{\partial^2 T}{\partial t^2} \right) = 2\alpha I(t) \cdot e^{-2\alpha x}. \quad (2)$$

The initial and boundary conditions are expressed in the following form:

$$\begin{aligned} T(0, x) &= T_0 = \text{const}; & T(0, t) &= f(t); \\ \frac{\partial T}{\partial t}(0, x) &= 0; & T(\ell, t) &= \varphi(t). \end{aligned} \quad . \quad (3)$$

In the given work the task about the definition of the relaxation time τ_0 and its influence on the heat capacity of the liquids is solved theoretically. The given task mathematically leads to the solution of the differential equation (2) under the initial and boundary conditions (3).

The Laplace transformation is applied for the solution of this task. The equation (2) assumes the following form in images:

$$\begin{aligned} \frac{dT^*}{dx} + T^* \left(\frac{s}{v} + \frac{s^2 \tau_0}{v} \right) &= \\ &= \frac{2\alpha e^{-2\alpha x}}{c\rho v} I^* + \frac{T_0}{v} (1 + \tau_0 s) \end{aligned} \quad . \quad (4)$$

where

$$\begin{aligned} T^*(x, s) &= \int_0^\infty T(x, t) \cdot e^{-st} dt; \\ I^*(s) &= \int_0^\infty I(t) \cdot e^{-st} dt. \end{aligned}$$

Solving the equation (4) at the boundary conditions (3), we obtain the following equation:

$$\begin{aligned} \varphi^*(s) &= e^{-al} f^*(s) + \frac{b}{a} - \frac{b}{a} \cdot e^{-al} + \\ &+ \frac{2\alpha I^*(s)}{c\rho v} \frac{e^{-2\alpha l} - e^{-al}}{a - 2\alpha}, \end{aligned} \quad . \quad (5)$$

where

$$\begin{aligned} a &= \frac{s}{v} + \frac{s^2 \tau_0}{v}, & b &= \frac{T_0}{v} (1 + \tau_0 s) \\ f^*(s) &= \int_0^\infty f(t) e^{-st} dt, & \varphi^*(s) &= \int_0^\infty \varphi(t) e^{-st} dt, \end{aligned} \quad .$$

Taking into consideration, that $a < 1$ and $\alpha < 1$, we expand e^{-al} and $e^{-2\alpha l}$ into s power series. We confine ourselves

to two first members of the expansion and equation (5) assumes the following form:

$$\varphi^*(s) = (1 - a\ell)f^*(s) + b\ell + \frac{2\alpha\psi^*(s)\ell}{c\rho v}. \quad (6)$$

The method of the determinated moments is applied for the definition of the relaxation time τ_0 and heat capacity c . Expanding the functions $\varphi^*(s)$, $f^*(s)$ and $\psi^*(s)$ into series on the s power we obtain:

$$\begin{aligned} \varphi^*(s) &= \varphi_0 - s\varphi_1 + \frac{s^2}{2}\varphi_2 - \dots \\ f^*(s) &= f_0 - sf_1 + \frac{s^2}{2}f_2 - \dots \\ \psi^*(s) &= \psi_0 - s\psi_1 + \frac{s^2}{2}\psi_2 - \dots \end{aligned} \quad (7)$$

where

$$\begin{aligned} \varphi_0 &= \int_0^\infty (\varphi(t) - \varphi_\infty) dt; \quad \varphi_1 = \int_0^\infty (\varphi(t) - \varphi_\infty) t dt; \\ f_0 &= \int_0^\infty (f(t) - f_\infty) dt; \quad f_1 = \int_0^\infty (f(t) - f_\infty) t dt; \\ \psi_0 &= \int_0^\infty (\psi(t) - \psi_\infty) dt; \quad \psi_1 = \int_0^\infty (\psi(t) - \psi_\infty) t dt; \end{aligned} \quad (8)$$

Taking into account the expressions (7), for equation (6) we have:

$$\begin{aligned} \varphi_0 - s\varphi_1 + \frac{s^2}{2}\varphi_2 - \dots &= \\ = (1 - a\ell) \left(f_0 - sf_1 + \frac{s^2}{2}f_2 - \dots \right) + b\ell + . & \quad (9) \\ + \frac{2\alpha\ell}{c\rho v} \left(\psi_0 - s\psi_1 + \frac{s^2}{2}\psi_2 - \dots \right) \end{aligned}$$

Equating the coefficients having the equal s powers we obtain the following system:

$$\begin{cases} \varphi_0 = f_0 + \frac{T_0\ell}{v} + \frac{2\alpha\ell}{c\rho v}\psi_0 \\ -\varphi_1 = -f_1 - \frac{\ell}{v}f_0 + \frac{T_0\ell}{v}\tau_0 - \frac{2\alpha\ell}{c\rho v}\psi_1 \end{cases} \quad . \quad (10)$$

Solving this system we obtain the two unknown values: heat capacity c and relaxation time τ_0 :

$$c = \frac{2\alpha\ell\psi_1}{\rho v \left(\varphi_1 - f_1 - \frac{\ell}{v}f_0 + \frac{T_0\ell}{v}\tau_0 \right)} \quad (11)$$

$$\begin{aligned} \tau_0 &= \\ = \frac{v \left[\psi_1 \left(\varphi_0 - f_0 - \frac{T_0\ell}{v} \right) - \psi_0 \left(\varphi_1 - f_1 - \frac{\ell}{v}f_0 \right) \right]}{T_0\ell\psi_0} \end{aligned} \quad (12)$$

From the equation (11) it is seen, that liquid heat capacity decreases with the increase of the relaxation time.

The experiments, carried out by us, show, that liquid temperature dependences on time according to the following law:

$$\begin{aligned} f(t) &= T_0 + T_{01}(1 - e^{-k_1 t}) \\ q(t) &= T_0 + T_{02}(1 - e^{-k_2 t}). \end{aligned} \quad (13)$$

Substituting the values $f(t)$ and $q(t)$ in the equation (8) we obtain:

$$\begin{aligned} f_0 &= -\frac{T_{01}}{k_1}; \quad f_1 = -\frac{T_{01}}{k_1^2}; \\ \varphi_0 &= -\frac{T_{02}}{k_2}; \quad \varphi_1 = -\frac{T_{02}}{k_2^2}. \end{aligned} \quad (14)$$

If the system doesn't relax under the rest equal conditions, i.e. $\tau_0=0$, the equation (11) has the form:

$$c_0 = \frac{2\alpha\ell\psi_1}{\rho v \left(\varphi_1 - f_1 - \frac{\ell}{v}f_0 \right)}. \quad (15)$$

From the comparison of the formulae (11) and (15), we obtain:

$$\frac{c}{c_0} = \frac{1}{1 + \frac{T_0\ell\tau_0}{\rho v \left(\varphi_1 - f_1 - \frac{\ell}{v}f_0 \right)}}. \quad (16)$$

Substituting the formula (14) in the formula (16) we obtain:

$$\frac{c}{c_0} = \frac{1}{1 + \frac{T_0\ell\tau_0}{\rho v \left(\varphi_1 - f_1 - \frac{\ell}{v}f_0 \right)}} \quad (17)$$

where

$$\beta = \frac{T_{01}}{k_1^2} - \frac{T_{02}}{k_2^2} + \frac{\ell}{v} \frac{T_{01}}{k_1}.$$

THE INFLUENCE OF THE RELAXATION TIME ON THE LIQUID HEAT CAPACITY

It is possible to estimate the influence of the relaxation time on the heat capacity of the liquids by the formula (17).

At $\tau_0=0$, i.e. when relaxation absence and the system is in the equilibrium state, we have the ratio:

$$\frac{\psi_1}{\psi_0} = \frac{\varphi_1 - f_1 - \frac{\ell}{v} f_0}{\varphi_0 - f_0 - \frac{T_0 \ell}{v}}. \quad (18)$$

Taking into consideration the formula (14), the equation (18) is reduced to the following form:

$$\frac{\psi_1}{\psi_0} = \frac{T_{01}k_2^2(v + \ell k_1) - T_{02}vk_1^2}{k_1k_2(T_{01}k_2v - T_{02}vk_1 - T_0\ell k_1k_2)}. \quad (19)$$

From the condition (18) we find the liquid flow velocity at which the relaxation absence:

$$v = \frac{\ell \left(\frac{\psi_1}{\psi_0} T_0 - f_0 \right)}{\frac{\psi_1}{\psi_0} (\varphi_0 - f_0) - \varphi_1 + f_1}. \quad (20)$$

Therefore, we can conclude that changing the liquid flow velocity it is possible to operate of the thermodynamic state of the liquid.

- [1] G.T. Gasanov, A.A. Aliyev, L.P. Guryanova. J. «Fizika», cild 6, №1, 2000, с.41-42.
[2] Kh.G. Gasanov. Gidrodinamicheskiye issledovaniya vza-

imodeystviya akusticheskikh I lazernikh izlucheniyy s jidkostiyu. Baku, Izd.. «Açıq dünya», 2002, 384c. (in Russian).

Q.T. Həsənov, A.N. Məmmədova

RELAKSASIYA MÜDDƏTİNİN MAYELƏRİN İSTİLİK TUTUMUNA TƏSİRİ

Akustik dalğaların təsirindən maye daxilində bütün istilik fiziki parametrlər relaksasiya edirlər. Temperatur sahəsinin relaksasiya müddətini və istilik tutumunu birgə təyin etmək üçün yeni metod işlənmişdir.

Göstərilmişdir ki, temperatur sahəsinin relaksasiya müddəti ardıqca istilik tutumu azalır. Relaksasiya müddətini tənzimləmək üçün mayenin axın sürətindən istifadə olunması təklif olunur.

Г.Т. Гасанов, А.Н. Мамедова

ВЛИЯНИЕ ВРЕМЕНИ РЕЛАКСАЦИИ НА ТЕПЛОЕМКОСТЬ ЖИДКОСТЕЙ

Предлагается нестационарный метод одновременного определения времени релаксации температурного поля и коэффициента теплоемкости жидкости. Предложенный метод основан на решении обратной задачи для уравнения теплопроводности релаксирующего температурного поля. Оценено влияние времени релаксации на теплоемкость жидкостей.

Received: 15.02.05

AXIAL Ga- IMPURITY DISTRIBUTION IN Ge-Si, SOLID SOLUTIONS, GROWN BY THE MODERNIZED BRIDGMEN METHOD

L.A. GUBATOVA, G.H. AJDAROV

Institute of Physics of National Academy of Sciences of Azerbaijan, Az-1143, H. Javid av., 33

Z.M. ZEYNALOV

Ganja State University, Ganja, Azerbaijan

The problem of the distribution of the gallium impurity in the Ge-Si crystals, grown on the germanium fuse by Bridgmen method with the use of the feeding silicon rod has been solved in the Pfann approximation. It is shown, that the dependence of the impurity segregation coefficient on the composition of the solid solution Ge-Si and the change of the melt volume, connecting with its feeding influences significantly on the longitudinal concentration of the gallium in the crystal.

The work of the numerous semiconductor devices, lying in the base of the modern micro- and optoelectronics, in many cases is defined by the impurities of the different types, incalculated in the crystal. Among semiconductor materials, widely used practically, the crennium and germanium have the leading positions. Among the chemical elements, used at the doping of these semiconductors, the elements of the III and V group of the periodical system have the important places. Having the small enough ionization energy in the crystals Si and Ge, these elements define the electric properties of the matrix in the wide temperature interval [1]. Among the elements of the III group, the gallium impurity is the most frequently used for the doping of the crennium and germanium, because of the big solubility ($\sim 10^{20} \text{ cm}^{-3}$) and the small diffusion coefficient [2]. Situating in the crystal lattice points, the gallium behaves itself as the small acceptor impurity with the activation energy 72 and 10, 97 meV in the Si and Ge correspondingly.

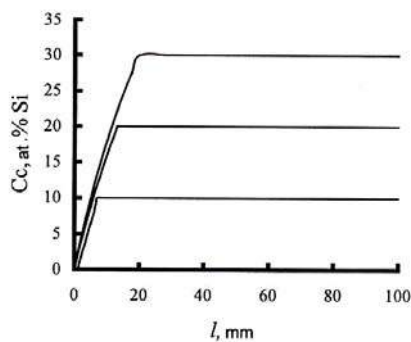


Fig.1. The calculate dependences of the crennium concentration along three ingots Ge-Si, grown in two modes for the obtaining of the crystals with the crennium concentration in the homogeneous part - 10, 20 and 30 at.%. It is accepted in calculations, that melt height in the initial position is equal to 100mm, and temperature gradient in the band of the buffer crystal corresponds 50°C/cm [5].

The one of the important questions in the investigation of the impurity centers in the semiconductors is the impurity distribution along the crystal length, connected with the segregation of the doping element. The gallium equilibrium segregation coefficient at the crystallization temperature Si and Ge is equal to $K=0,008$ and $0,087$ correspondingly [3]. Such small K values lead to the significant concentration gradient of the gallium along the crystal lengths of crennium and germanium, grown by the traditional Bridgmen method. In the present paper in the Pfann approximation and in the frameworks of the virtual crystal model for the solid solutions, the problem of the Ga - impurity distribution in the

crystals Ge-Si, grown on the germanium fuse by Bridgmen method with the use of the feeding crennium ingot has been solved [4,5]. The crystals Ge-Si, grown up by this method, in the initial region have the variable composition with the growing crennium concentration on the ingot length. Further the crystal composition stays unchangeable because of the constant balance of the melt composition by the corresponding of the velocities of its crystallization and feeding. The fig.1 shows the calculation dependences of the crennium concentration along three ingots Ge-Si, taken from [5], grown up in the modes, corresponding to the crystal obtaining with the crennium concentration in the homogeneous part - 10, 20 and 30 at.%. In the calculations it was taking under the consideration, that the melt height in the initial position was equal to 100 mm, and temperature gradient in the growth band of the buffer crystal with the flexible composition was equal to 50°C/cm. The initial part of the curves with the variable composition on the fig.1 corresponds to the first step of the crystal growth. The plateau corresponds to the second step of the crystal growth with the given homogeneous composition.

The problem of the gallium impurity distribution in the crystal, grown by this method was solved at the carrying out of the following standard conditions [2,6]: the crystallization front is plain; there is the equilibrium between solid and liquid phases on the crystallization front; the diffusion of the gallium impurity and the convention in the melt cause the homogeneous of the liquid phase on the all volume; the diffusion of Ga atoms in the solid phase is negligible small. It is need to note, that for the system Ge-Si these conditions are carried out practically at the velocities of crystal growth less, than $1 \cdot 10^{-6} \text{ m/s}$ [3,6].

Let's introduce the following denotations: V_1^0 , V_t are melt volumes in the crucible in the initial and the current moments; V_c , V_{Si} are volumes of the crystallizing melt and deliquescent crennium rod in time unit; C_1^0 , C_t are concentrations of Ga impurities in the melt in the initial and current moments; C_{Ga} is the concentration of Ga impurity in the crystal; C is the general quantity of Ga impurity in the melt; $K=C_{Ga}/C_t$ is the equilibrium segregation coefficient of Ga in the current moment; t is time.

On the first step of the growth of the buffer crystal with the flexible composition with the accepted above mentioned denotations, we have:

$$C_1 = \frac{C}{V_1} \text{ and } \frac{dC_1}{dt} = \frac{\dot{C}}{V_1} - \frac{\dot{V}_1}{V_1^2} C = \frac{\dot{C} - \dot{V}_1 C_1}{V_1} . \quad (1)$$

According to the task condition, we consider, that in the considered period V_c and V_{Si} don't depend on time. Then, taking into consideration that $C_{Gs}=C_l K$ we have:

$$V_1 = V_1^0 - (V_c - V_{Si}) t, \quad V_1 = -V_c + V_{Si} \text{ and } C = -V_c C_l K \quad (2)$$

In the limits of the model of the virtual crystal we consider, that gallium segregation coefficient depends on the crennium concentration in the crystal nonlinearly. The linear character of the change of the crennium concentration in the band of the buffer crystal with the variable composition (fig.1) means, that on this step, in the considered approximation, K will depend on t linearly. Replacing K in

$$C_{Ga} = C_l K = C_l^0 K [1 - \gamma(1 - \alpha)]^{-\frac{(1-K_0-\alpha)(1-\alpha)\gamma+(K_0-K)}{\gamma(1-\alpha)^2}} \exp\left(\frac{K_0 - K}{1 - \alpha}\right) \quad (4)$$

The equation (4) defines the dependence of the gallium impurity concentration on the length of the buffer crystal l , taking under the consideration the fact, that $\gamma = V_c t / V_1^0 = 1/L$, where L is the height of the melt in the beginning of crystallization.

On the second step of the Ge-Si crystal growth (fig.1) with the homogeneous composition the segregation coefficient of gallium impurity stays unchangeable and is equal to K for the corresponding melt composition. Changing in (4) $K_0 = K$ for this case we have:

$$C_{Ga} = C_l K = C_l^0 K [1 - \gamma(1 - \alpha)]^{-\frac{(1-K-\alpha)}{(1-\alpha)}} \quad (5)$$

The fig.2, for example, demonstrates the concentration profiles of Ga impurity along three ingots Ge-Si, grown up in the above described technological modes, data of which on the longitudinal composition are given on the fig.1. For the comparison, the dependence for the germanium, grown by the traditional Bridgmen method, is given in fig. 2 also. The following initial data are accepted in the calculations: $C_l^0 = 1 \cdot 10^{18} \text{ cm}^{-3}$; $L = 100 \text{ mm}$; $K = K_0 \cdot x(K_0 \cdot K_l)$, where K_l is the gallium segregation coefficient in the crennium; $l_B = 6.6; 13.2$ and 20 mm is the length of the buffer crystal in the ingots with the homogeneous part 10, 20 and 30 at.% Si correspondingly; $\alpha = 0.345, 0.385$ and 0.435 in the band of the buffer crystal and $0.247, 0.167$ and 0.087 in the homogeneous part of the ingots with the composition 10, 20 and 30 at.% Si correspondingly. It is need to note, that values l_B are defined by the given temperature gradient, diagram of system Ge-Si state and demanded composition in the homogeneous part of the crystal. The values of α were calculated on the data of the ref. [3,4].

As it is seen from the fig.2, the velocity of the impurity concentration growth along the crystal length significantly decreases with the increase of the crennium content in the matrix and it is caused in the final part of ingots. Such behavior from one side is explained by the decrease of the gallium segregation coefficient with the growth of the crennium concentration in the melt, and by the increase of the melt volume, caused by its crennium feeding from another side. The initial parts of two curves in the expanded

(2) by $K = K_0 \cdot A \cdot t$ (K_0 is the segregation coefficient of the impurity in the pure germanium, A is the constant factor) and substituting it in (1) after the simple transformations and integration we have:

$$\ln \frac{C_l}{C_l^0} \left[\frac{V_1^0 - (V_c - V_{Si}) t}{V_1^0} \right]^{\frac{(V_c - V_c K_0 - V_{Si})(V_c - V_{Si}) + AV_c V_1^0}{(V_c - V_{Si})^2}} = -\frac{AV_c t}{V_c - V_{Si}} \quad (3)$$

Introducing following denotes: $V_{Si}/V_c = \alpha$; $V_c/V_1^0 = \beta$; $V_c t/V_1^0 = \gamma$ from (3) after some transformations we have:

$$C_{Ga} = C_l K = C_l^0 K [1 - \gamma(1 - \alpha)]^{-\frac{(1-K_0-\alpha)(1-\alpha)\gamma+(K_0-K)}{\gamma(1-\alpha)^2}} \exp\left(\frac{K_0 - K}{1 - \alpha}\right) \quad (4)$$

scale (fig.2), corresponding to Ge and $\text{Ge}_{0.7}\text{Si}_{0.3}$ are given for the visual demonstration of the roles of the given factors on the gallium concentration in the crystals (fig.3).

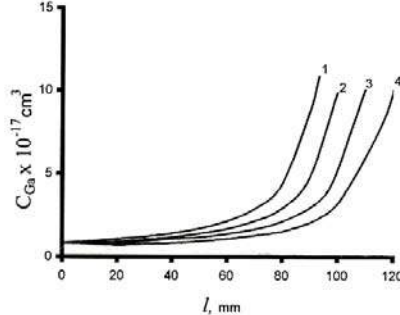


Fig.2. The concentration profiles of Ga impurity along Ga crystal, grown by traditional Bridgmen method (curve 1) and three ingots Ge-Si, the data on the longitudinal composition of which are given on the fig.1. In the calculations it is accepted for all crystals, that $C_l^0 = 1 \cdot 10^{18} \text{ cm}^{-3}$ and $L = 100 \text{ mm}$. The curves 2,3 and 4 refer to the crystals with the homogeneous part 10, 20 and 30 at.% Si correspondingly.

The data on the germanium crystal, grown up in the same conditions of the feeding (curve 2), as the $\text{Ge}_{0.7}\text{Si}_{0.3}$ (curve 3) are given for the separation of the contribution of the change of the melt volume, connected with its feeding on the concentration profile of the gallium impurity. The relative weak change of the longitudinal impurity concentration in the germanium crystal, grown with the use of the feeding (curve 2), in the comparison with the same, grown up by the traditional Bridgmen method (curve 1), connects with the partial compensation of the melt volume by feeding. In the case $\text{Ge}_{0.7}\text{Si}_{0.3}$ (curve 3), in the band of the buffer crystal, given in the fig.3, the reversible course of the dependence of the gallium impurity concentration along the ingot length takes place. Such course is defined by the essential decrease of the impurity segregation coefficient with the increase of the longitudinal crennium concentration in the crystal, which is dominant influence on C_{Ga} in the comparison with the influence factor of the decrease of the melt volume.

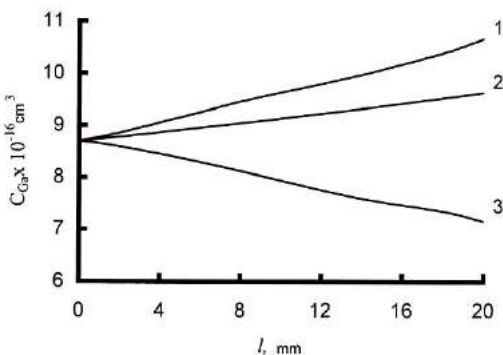


Fig.3. The axial concentration profile of gallium impurity in the initial region of Ge crystals (curves 1,2) and Ge_{0.7}Si_{0.3} (curve 3). The curve 1 corresponds to germanium crystals growth by the traditional Bridgmen method.

On the base of the above mentioned data, it is possible to make the conclusion. In the crystals of the solid solutions, grown up by the modernized Bridgmen method with the use of the germanium fuse and feeding crennium rod, the dependence of the impurity segregation coefficient on the composition Ge-Si and the change of the melt volume, connected with its feeding essentially influences on the velocity of the concentration change of the gallium impurity along the crystallization axis. Taking under consideration these facts is the important condition at the solution of the problems, connected with the growing of the crystals with the given concentration profile of the gallium impurity in the crystals of Ge-Si system.

- [1] B.I. Shklovskiy, A.L. Efros. Elektronniye svoystva legirovannikh poluprovodnikov. M. Nauka, 1979, 416. (in Russian).
- [2] V.M. Glazov, V.S. Zemskov. Fiziko-khimicheskiye osnovi legirovaniya poluprovodnikov. M. Nauka, 1967, 371. (in Russian).
- [3] A. Barz, P. Dold, U. Kerat, S. Recha, and K.W. Benz, Journal of Vac. Sci. Technol. B 16(3) (1998) 1627.
- [4] G.Kh. Adzhdarov. Izvestiya BUZov Rossii. Materiali elektronnoy tekhniki, 2004, 2, 47. (in Russian).
- [5] G.Kh. Adzhdarov, R.Z. Kyazimzade. Tezisi dok. Nacionalnoy konferencii po rostu kristallov. Moskva, 2004, s. 109. (in Russian).
- [6] G.Kh. Azhdarov, T. Kucukomerogly, A. Varilci, M. Altunbas, A. Kobya, P. G. Azhdarov. Journal of Crystal Growth, 226 (2001) 437.

L.Ә. Qubatova, Z.M. Zeynalov, H.X. Әjdərov

MODERNİZƏ EDİLMİŞ BRİDJMEN ÜSULU İLƏ ALINAN Ge-Si BƏRK MƏHLULLARINDA GALLIUM AŞQARININ KRİSTALLAŞMA OXU BOYUNCA PAYLANMASI

Pfann yaxınlaşması çərçivəsində modernizə edilmiş Bridjmen üsulu ilə ərintini Si ilə qidalandırma rejimində alınan Ge-Si kristallarında Ga aşqarının paylanması məsəlesi həll edilib. Aşqarın seqregasiya əmsalının Ge-Si kristalının tərkibindən asılılığı və ərintinin qidalandırma nəticəsində dəyişilən həcmi Ga aşqarının kristallaşma oxu boyunca konsentrasiyasına əhəmiyyətli təsiri göstərilib.

Л.А. Губатова, З.М. Зейналов, Г.Х. Аждаров

РАСПРЕДЕЛЕНИЕ ПРИМЕСИ ГАЛЛИЯ ВДОЛЬ ОСИ КРИСТАЛЛИЗАЦИИ ТВЁРДЫХ РАСТВОРОВ Ge-Si, ВЫРАЩЕННЫХ МОДЕРНИЗИРОВАННЫМ МЕТОДОМ БРИДЖМЕНА

В пфанновском приближении решена задача распределения примеси галлия в кристаллах Ge-Si, выращенных на германиевой затравке методом Бриджмена с использованием подпитывающего стержня кремния. Показано, что на продольную концентрацию галлия в кристалле существенное влияние оказывают зависимость коэффициента сегрегации примеси от состава твёрдого раствора Ge-Si и изменение объёма расплава, связанное с его подпиткой.

Received: 16.03.2005

THE NONLINEAR THEORY OF GUN'S EFFECT

E.R. GASANOV, R.K. GASIMOVA

*Baku State University,
Baku, Az-1145, Z.Halilov str.,23*

The nonlinear theory of Gun's effect has been constructed. The amplitude and the frequency of the current oscillation in the second approximation by the method of Bogolubov-Mitropolski have been found. The amplitude and frequency of the current oscillation in the GaAs have been calculated for the typical experiment. The amplitude of the current oscillation as the function of the electric field has been calculated in the first approximation.

The phenomena of the current instability, which firstly was observed in the compounds GaAs and InP [1] are called Gun's effect. The frequency of the current installation mainly lies in the ultrahigh frequency range (UHF) and differs from the low-frequency oscillation [2]. The mechanism of Gun's effect was supposed in the refs. [3,4,5]. The authors of these works show, that in the materials GaAs, InP, probably, the number of the carriers with the low energy decreases at the increase of the external electric field strength. Moreover, the electrons transit to the superincumbent energetical bands or in the case of the low-frequency ranges they transit on the ionized traps in the forbidden band.

The mobility of the electrons decreases strongly with the comparison of the mobility in the lower trough at the electron transfer in the upper energetical bands. When transfer of the current carriers is higher, than the definite value, the material conductivity decreases and the negative differential conductance appears:

$$\frac{dI}{dE} = \sigma_d < 0 \quad (1)$$

At the values $\sigma_d < 0$ the electric field E in the crystal becomes nonhomogeneous and the acute regions of the electric field, i.e. "domains" creat. The theoretical investigations are strong nonlinear because of the domains and the amplitude of the current oscillation in the crystal depends on the time.

Moreover, at $\sigma_d < 0$ the redistribution of the space charge begins and this process leads to the UHF radiation. The small-signal theory (i.e. near the threshold $\sigma_d \approx 0$) of this phenomenon have been constructed in the ref. [6]. However, the dependence of the amplitude on the time and on the frequency of the oscillations hadn't been investigated theoretical.

In our paper we will declare the nonlinear theory of the amplitude and frequency of the current oscillation, based on the model of Gun's effect at the existence of the external constant electric field. We will consider, that transport time in the low-mobile states is negligible small and the carrier concentration in the main vale decreases inversely of the some degree of the electric field. Besides it, we will suppose, that the number of the ionized donors doesn't almost change and the current oscillations are only because of the electron transition in the upper energetical states. As it is shown in the ref. [6], the mobility in the upper energetical state in GaAs is more less, than in the central vale, D is the electron diffusion coefficient in the lower trough for GaAs 130 cm/sec.. The

total carrier concentration $N=n+n'$, the carrier mobility μ and μ' correspondingly, diffusion coefficients D and D' satisfy to the following relations:

$$D \gg D', \quad \mu \gg \mu', \quad n \gg n' . \quad (2)$$

The number of the carriers in the lower (central) vale will be equal to the some part of f of the total number of the carriers:

$$n = f N = f(E)N \quad (3)$$

parameter $f(E) = (m-1) \left[m-1 + \left(\frac{E}{E_a} \right)^m \right]^{-1}$ [7].

Here E_a is the electric field, at which the current oscillation begins. The parameter m is calculated experimentally as the ratio of the ohmic current to the real current in the point $E_0 = E_a$ (at $\sigma_d = 0$).

The static current is

$$I_0 = \sigma_0 E_a f_0 x_0, \quad x_0 = \frac{E_0}{E_a}, \quad (4)$$

where σ_0 is the sample conductivity in the weak field. We will follow on the experiment [7] in calculations. The ration of the dynamic conductivity σ to the conductivity in the weak field σ_0 has the form:

$$S_0 = \frac{\sigma}{\sigma_0} = \frac{1}{\sigma_0 E_a} \frac{dI_0}{dx_a} = (f_0 + x_0 \frac{df_0}{dx_a}) \quad (5)$$

$$S_0 = f_0 [1 - m(1 - f_0)]$$

The value S_0 is the ratio of the tangent of inclination angle of the VAC curve at $E = E_0$ (work point) to the tangent of inclination angle at the weak fields. At $E_0 > E_a$ it is negative. In the point of the zero inclination $x_0=1$ and $f_0 = -\frac{df_0}{dx_0}$. The statistic current in this point is:

$$I_p = \frac{m-1}{m} \sigma_0 E_a \quad \text{and} \quad m = \frac{1}{1 - \frac{I_p}{\sigma_0 E_a}} .$$

The dynamics of the current transition through the sample is characterized by the following equations:

$$\begin{aligned} I &= e f N \mu E + D e \frac{\partial(f N)}{\partial z} \\ \frac{\partial I}{\partial z} &= e \frac{\partial N}{\partial t} \\ I_1 + \varepsilon \frac{\partial E_1}{\partial t} &= 0; \quad \nu_0 = -\mu E_0. \end{aligned} \quad (6)$$

The equation system (6) is enough for our goals, i.e. they connect between themselves the three unknown values I, E, N .

In the frameworks of “small-signal” theory, by method [7] for the solution of these equations it was supposed:

$$\begin{aligned} I_0 &= I_0 + I_1 = I_0 + I_1(0) e^{i \omega t}, \quad I_1 \ll I_0 \\ E &= E_0 + E_1 = E = E_0 + E_1(0) e^{i \omega t}, \quad E_1 \ll E_0 \\ N &= N_0 + N_1 = N_0 + N_1(0) e^{i \omega t}, \quad N_1 \ll N_0 \end{aligned} \quad (7)$$

For the finding of the amplitude values E, N, I the condition (7) isn't enough and it is need to find the solutions (6) at the any values E_1, N_1 and I_1 , i.e.

$$\begin{aligned} I &= I_0 + I_1, \quad I_1 < I_0, \quad I_1 > I_0, \quad N = N_0 + N_1, \quad N_1 < N_0, \quad N_1 > N_0, \\ E &= E_0 + E_1, \quad E_1 < E_0, \quad E_1 > E_0 \end{aligned} \quad (8)$$

We will find the solutions of the equation systems (6) at the conditions (8) by the Bogolubov- Mitropolski method [7].

Substituting (8) into (6) and denoting $x = \frac{I_1}{\sigma_0 E_0}$ we obtain:

$$\begin{aligned} x = & \left(f_0 \frac{E_1}{E_0} + f_0 \frac{N_1}{N_0} + f_0 \frac{N_1}{N_0} \cdot \frac{E_1}{E_0} + f_1 + f_1 \frac{E_1}{E_0} + f_1 \frac{N_1}{N_0} + f_1 \frac{N_1 E_1}{N_0 E_0} \right) + \\ & + \frac{D}{\nu_0} \frac{\nu}{\partial z} \left(f_0 \frac{N_1}{N_0} + f_1 + f_1 \frac{N_1}{N_0} \right) \\ I_1 &= -\varepsilon \frac{\partial E_1}{\partial t}; \quad \frac{\partial I_1}{\partial z} = e \frac{\partial N_1}{\partial t}; \quad f_1 = (S_0 - f_0) \frac{E_1}{E_0} \end{aligned} \quad (9)$$

We will express the change of the electric field through the change of the current carriers for the reducing the equation (9) to one nonlinear equation by the following way:

$$E_1 = \frac{E_0}{N_0 k \nu_0} \frac{\partial N_1}{\partial t} \quad \text{and then} \quad I_1 = -\frac{\varepsilon}{N_0 k \mu} \frac{\partial^2 N_1}{\partial t^2} \quad (10),$$

where k is the wave vector, propagating on Z axis. If we denote $y = \frac{N_1}{N_0}$, so taking into consideration (10) from (9), we will obtain the following nonlinear equation for y for finding:

$$\begin{aligned} \frac{\partial^2 y}{\partial t^2} + \omega_0^2 y &= \frac{\sigma_0 f_0}{\varepsilon} \left[-\frac{\partial y}{\partial t} - y \frac{\partial y}{\partial t} + m(1-f_0) \frac{1}{k \nu_0} \left(\frac{\partial y}{\partial n} \right)^2 + m(1-f_0) y \frac{\partial y}{\partial n} + \right. \\ &\quad \left. + m(1-f_0) y \frac{1}{k \nu_0} \left(\frac{\partial y}{\partial n} \right)^2 \right] + f_0 \frac{m(1-f_0) \sigma_0 D k}{\nu_0} \left(\frac{\partial y}{\partial t} + y \frac{\partial y}{\partial t} \right) \end{aligned} \quad (11)$$

$$\text{Here } \omega_0^2 = \frac{\sigma_0 f_0}{\varepsilon} (k \nu_0 + D k^2).$$

The nonlinear equation (11) respect of y can be reduced to the equation of Van-der-Pole one. For this we denote $\tau = \omega_0 t$ and $r = \frac{\sigma_0 f_0}{\varepsilon \omega_0}$ and reduce the equation (11) to the dimensionless equation. Then the Van-der-Pole equation assumes the following form:

$$\frac{\partial^2 y}{\partial \tau^2} + y = r F \left(\frac{dy}{d\tau}, y \right), \quad (12)$$

where $r = \frac{\sigma_0 f_0}{\varepsilon \omega_0}$ is the small parameter for the typical crystal GaAs, $D = 130 \frac{\text{cm}^2}{\text{sec}}$, $\nu_0 \approx 10^7 \frac{\text{cm}}{\text{sec}}$, $\omega_c \approx \frac{\sigma_0}{\varepsilon} \approx 10^{12} \text{ sec}^{-1}$, $r \ll 1$.

THE NONLINEAR THEORY OF GUN'S EFFECT

The solution of the equation (12) is as follows

$$y = a \cos(\tau + \theta) = a \cos(\omega t + \theta) = a \cos \psi \text{ at } r=0. \quad (13)$$

We will use Bogolubov-Mitropolski method [7] for the finding of the solution (12) at $r \neq 0$ by the following way:

wher

$$\begin{aligned} A_1(a) &= -\frac{\omega_0}{2\pi} \int_0^{2\pi} F\left(y, \frac{dy}{d\tau}\right) \sin \psi d\psi ; \quad B_1(a) = -\frac{\omega_0}{2\pi a} \int_0^{2\pi} F\left(y, \frac{dy}{d\tau}\right) \cos \psi d\psi \\ A_2(a) &= -\frac{\omega_0}{2} \left(2A_1 B_1 + A_2 \frac{dB_1}{da} a \right) - \frac{\omega_0}{2\pi} \int_0^{2\pi} \left[u_1 \frac{dF}{dY} + \left(A_1 \cos \psi - aB_1 \sin \psi + \omega_0 \frac{du_1}{d\psi} \right) \frac{dF}{dy'} \right] \sin \psi d\psi \\ B_2(a) &= -\frac{\omega_0}{2} \left(B_1^2 - \frac{A_1}{a} \frac{dA_1}{da} \right) - \frac{\omega_0}{2\pi a} \int_0^{2\pi} \left[u_1 \frac{dF}{dy} + \left(A_1 \cos \psi - aB_1 \sin \psi + \omega_0 \frac{du_1}{d\psi} \right) \frac{dF}{dy'} \right] \cos \psi d\psi \\ u_1 &= g_0 - \sum_{n=2}^{\infty} \frac{g_n \cos n\psi + h_n \sin n\psi}{n^2 - 1} ; \quad g_n = \frac{1}{\pi} \int_0^{2\pi} F\left(y, \frac{dy}{d\tau}\right) \cos n\psi d\psi \\ h_n &= \frac{1}{\pi} \int_0^{2\pi} F\left(y, \frac{dy}{d\tau}\right) \sin n\psi d\psi \end{aligned} . \quad (15)$$

We confine ourselves only by the second approximation. Firstly, we will find the amplitude in the first approximation from equation (14):

$$\frac{da_1}{d\tau} = rA_1(a) . \quad (16)$$

Substituting the equation (13) in the equation (15) after the integration, we will obtain

$$\frac{da_1}{dt} = \frac{r\omega_0}{2} \left[\frac{m(1-f_0)Dk\epsilon}{v_0} - 1 \right] a :$$

Solving above mentioned equation we find:

$$a_1 = a_0 e^{\frac{r}{2} \left[\frac{m(1-f_0)Dk\epsilon}{v_0} - 1 \right] t \omega_0} ; \quad Y = a_1 \cos \psi . \quad (17)$$

From the equation (17) it is seen, that the amplitude of the current oscillation increases exponentially for the crystal GaAs:

$$\begin{aligned} \frac{da}{d\tau} &= rA_1(a) + r^2 A_2(a) + r^3 A_3(a) + \dots \\ \frac{d\psi}{d\tau} &= \omega_0 + rB_1(a) + r^2 B_2(a) + r^3 B_3(a) + \dots \end{aligned} \quad (14)$$

$$\frac{mDk\epsilon}{v_0} (1 - f_0) > 1 \quad (18)$$

As $f_0 < 1$, so we obtain the values of the change interval of the constant electric field:

$$E_0 > E_a \left(\frac{2v_0}{3Dk\epsilon} \right)^{1/3} \quad (19),$$

at which the current oscillates with the frequency ω_0 . Indeed, it is clearly seen from the equation (15), that $B_1(a) = 0$ and that's why the frequency is ω_0 . As it is seen from the equation (17) the amplitude a_1 tends to the initial value a_0 , ($a_1 \rightarrow a_0$) at $t \rightarrow 0$.

It is need to calculate the u_1 , $\frac{\partial \psi_1}{\partial \psi}$, g_0 in the second

approximation for the finding of the amplitude a_2 and the frequency of the current oscillation ω_2 .

After the simple calculation we find:

$$\begin{aligned} u_1 &= 3R \left(\frac{\cos 2\psi}{6} - \frac{Dk^2 \epsilon}{6\omega_0} \sin 2\psi - 1 \right); \quad \frac{du_1}{d\psi} = -R \left(\frac{Dk^2 \epsilon}{\omega_0} \cos 2\psi + \sin 2\psi \right) \\ R &= \frac{m(1-f_0)}{3kv_0\omega_0} a^2 ; \quad g_0 = -\frac{m(1-f_0)\omega_0}{kv_0} a^2 \end{aligned} \quad (20)$$

Substituting the equation (20) in the equation (15), we obtain the following values for $A_2(a)$ and $B_2(a)$ after the integration:

$$\begin{aligned}
 A_2(a) &= -\frac{\omega_0 a^3}{8} \left[\frac{Dk^2 \varepsilon}{V_0} \left(\frac{m Dk \varepsilon}{V_0} + m \right) \frac{m \omega_0}{6k V_0} + \frac{2m \omega_0}{6k V_0} \right] = -La^3. \\
 B_2(a) &= \frac{\omega_0}{8} \left[\left(\frac{m Dk \varepsilon}{V_0} \right)^2 - 26 \left(\frac{m Dk \varepsilon}{V_0} + m \right) \frac{\omega_0 m a^2}{6k V_0} - \right. \\
 &\quad \left. - 4Dk^2 \varepsilon \frac{m a^2}{6k V_0} \left(\frac{2m \omega_0}{k V_0} + m + \frac{m Dk \varepsilon}{V_0} \right) \right] = B_2(0) + B'_2 a^2
 \end{aligned} \tag{21}$$

Substituting the equation (21) in the equation (14), we obtain the equations for the finding of the oscillation frequency in the second approximation:

$$\frac{da}{dt} = rA_1(0)a + r^2 La^3 \omega_0 \tag{22}$$

$$\frac{d\psi}{dt} = \omega_{\parallel} = \omega_0 + r^2 B_2(0) + B'_2 r^2 a^2 \tag{23}$$

$$\frac{da}{dt} = \omega_0 [rA_1(0)a + r^2 La^3] \tag{24}$$

$$\frac{d\psi}{dt} = \omega_2 = \omega_0 [1 + r^2 B_2(0) + B'_2 r^2 a^2] \tag{25}$$

$$\text{where } A_1(0) = \frac{m(1-f_0)Dk\varepsilon}{V_0} - 1 ; B_2(0) = \frac{1}{8} \left(\frac{m Dk \varepsilon}{V_0} \right)^2$$

$$\begin{aligned}
 B'_2 &= \frac{13m\omega_0}{24kV_0} \left(1 - m - \frac{m Dk \varepsilon}{V_0} \right) - \frac{4Dk^1}{12V_0} m^2 \left(\frac{2\omega_0}{kV_0} + \frac{Dk\varepsilon}{V_0} \right) \\
 L &= \frac{m\omega_0}{48kV_0} \frac{Dk\varepsilon}{V_0} \left(1 - m - \frac{m Dk \varepsilon}{V_0} \right) - \frac{m\omega_0}{24kV_0}
 \end{aligned}$$

After the integration we obtain from the equation (22):

$$a_2 = \frac{a_0}{\left[a_0^2 \frac{L}{A_1(0)} \left(e^{-\frac{rA_1(0)}{2}\omega_0 t} - 1 \right) + e^{-\frac{rA_1(0)}{2}\omega_0 t} \right]^{1/2}} = \frac{a_0}{\Phi^{1/2}} ; \quad Y = a_2 \cos \psi \tag{26}$$

$$\text{As } f_0 < 1, \text{ so for the typical GaAs, } A_1(0) = \frac{m Dk \varepsilon}{V_0}$$

and

$$\begin{aligned}
 L &= -\frac{m^2 \omega_0}{48kV_0} \left(\frac{Dk\varepsilon}{V_0} \right)^2 - \frac{m\omega_0}{2kV_0} \approx -\frac{m^2 \omega_0}{48kV_0} \left(\frac{Dk\varepsilon}{V_0} \right)^2 \\
 \frac{L}{A_1(0)} &= -\frac{m\omega_0}{48kV_0} \frac{Dk\varepsilon}{V_0} \ll 1
 \end{aligned} \tag{27}$$

$$\omega_0 \frac{rA_1(0)}{2} \approx \frac{m Dk}{2V_0} \frac{\sigma_0 f_0}{\varepsilon \omega_0} \omega_0 \approx \frac{m}{2} \frac{Dk}{V_0} \sigma_0 f_0 t \gg 1$$

Taking into consideration the experiment conditions [7] and (27), which has been proved in the experiment for the typical GaAs from the equation (26), we obtain:

$$\begin{aligned}
 a_2^2 &= \frac{a_0^2}{e^{-\frac{rA_1(0)}{2}\omega_0 t} - \frac{a_0^2 L}{A_1(0)}} \quad \text{or} \\
 a_2 &= \frac{a_0}{\left[e^{-\frac{m Dk \sigma_0 f_0 t}{2V_0}} + \frac{m\omega_0}{48kV_0} \frac{Dk\varepsilon}{V_0} a_0^2 \right]^{1/2}}
 \end{aligned} \tag{28}$$

It is easy seen from the equation (28), that amplitude in the second approximation decreases and tends to the constant limit (i.e. to the value, not depending on time).

$$a_2 \rightarrow \left(\frac{48kV_0}{m\omega_0} \frac{V_0}{Dk\varepsilon} \right)^{1/2} \tag{29}$$

The frequency of the current oscillation is defined by the expression (23), i.e. $\frac{d\psi}{dt} = \omega_2$ and the expression phase low is $\psi = \omega_2 t$. It is possible to find the amplitudes of the current oscillation on the formula (10), substituting a from

$$\begin{aligned} J_1 &= \sigma_o E_o f_o (1 + \nu_o) e^{\beta \omega_o t} [2\beta \sin \psi - (\beta^2 - 1) \cos \psi] \\ x &= \frac{J_1}{\sigma_o E_o} = f_o \left(1 + \frac{Dk}{\nu_o} \right) [2\beta \sin \psi - (\beta^2 - 1) \cos \psi] e^{\beta \omega_o t} \end{aligned} \quad (30)$$

From the equation (30) it is seen, that oscillations of the current amplitude x have the oscillating form as the functions $\sin \psi$ and $\cos \psi$ in dependence on time. Using the equation (30) it is possible to find the experimental values x (i.e. $\frac{\partial x}{\partial t} = 0$) with the time and the maximum conditions

for x i.e. $\frac{\partial^2 x}{\partial t^2} < 0$. However, for the finding \bar{J}_1 it is need to

the equations (17) and (26) in the equation (10) serially in the first and second approximations. We will calculate the current amplitudes only in the first approximation because of the striving of the amplitude of the current oscillation to the constant limit in the second approximation (29). After the simple calculation we obtain:

find \bar{J}_1^2 , since the harmonic functions $\sin \psi$ and $\cos \psi$ are in the equation (30), and further it is need to find the values $\bar{J}_1 = \bar{J}_{1\min}$ and $\bar{J}_1 = \bar{J}_{1\max}$, which define the minimal and maximal values of the amplitude of the current oscillation.

-
- | | |
|--|---|
| [1] <i>J.B.Gunn</i> . Proc.Int.Phys.Semicond Kyoto, 1966, p.505.
[2] <i>D.C. Northrop, P.R.Thornton, K.E. Trezise</i> . Solid State Electronics, 7,17,1964.
[3] <i>A.Barrand</i> . Compt. Rend. 256,3632,1963.
[4] <i>B.K. Ridley, T.B. Watkins</i> . Proc. Phys. Soc. 78, 293, 1961. | [5] <i>B.K. Ridley</i> . Proc. Phys. Soc. 82, 954, 1963.
[6] <i>R.W.H.Engelmann, G.F.Quate</i> IEEE Trans, ED.13, 14, 1966.
[7] <i>N.N. Bogolyubov, Yu.A. Mitropol'skiy</i> . «Asimptoticheskie metodi v teorii nelineynikh kolebaniy», Moskva, 1963, p. 36-94. |
|--|---|

E.R. Нәсәнов, Р.К. Qasimova

QANN EFFEKTİNİN QEYRİ-XƏTTİ NƏZƏRİYYƏSİ

Boqolyubov-Mitropolski riyazi metodu ilə GaAs kristalında cərəyan rəqslerinin amplitudu və tezliyi nəzəri olaraq hesablanmışdır. Birinci yaxınlaşmada cərəyan rəqslerinin amplitudu elektrik sahəsindən asılı olaraq hesablanmışdır.

Э.Р. Гасанов, Р.К. Гасымова

НЕЛИНЕЙНАЯ ТЕОРИЯ ЭФФЕКТА ГАННА

Построена нелинейная теория эффекта Ганна. Найдены амплитуда и частота колебания тока во втором приближении методом Боголюбова-Митропольского. Для типичного эксперимента в кристалле GaAs вычислены частота и амплитуда колебания тока. Вычислена в первом приближении амплитуда колебания тока как функция электрического поля.

Received: 18.01.05

THE INTERLAYER ENERGY BARRIER IN THE ANISOTROPIC TIB^{III}C₂^{VI} MONOCRYSTALS

S.N. MUSTAFAEVA

*Institute of Physics of National Academy of Sciences of Azerbaijan,
Az-1143, H. Javid av., 33*

The temperature dependence of the anisotropy degree of the conductivity of the TlInS₂, TlGaS₂ and TlGaSe₂ layered monocrystals has been investigated. It is established, that TlGaSe₂ monocrystals have the most anisotropy degree, and TlInS₂ has the less anisotropy degree. The values of the interlayer energy barrier $\Delta\varphi$, eV in the TlInS₂ (0.04), TlGaS₂ (0.17) and TlGaSe₂ (0.3) crystals are obtained.

The TlGaSe₂, TlGaS₂ and TlInS₂ monocrystals are representatives of the layered materials of the group T1B^{III}C₂^{VI}. They are characterized by the strong anisotropic physical properties, caused mainly by the fact, that charge carriers can move freely inside the layers in them, and between the layers its movement is limited because of the interaction of the layers by the Van der Waals type and the small overlapping of the wave functions of the neighboring layers. The important parameter of the layered compounds is anisotropy of the electric conduction:

$$N = \sigma_{\perp C} / \sigma_{|| C} , \quad (1)$$

where $\sigma_{|| C}$ and $\sigma_{\perp C}$ is the electric conduction in the parallel and perpendicular directions of the crystallographic crystal C axis (C axis is perpendicular to the plane of the crystal layers) correspondingly.

It is need to note, that anisotropy degree of the layer crystals can be increased because of their intercalation, i.e. because of the introducing of the foreign ions, atoms or the molecules in the interlayer Van der Waals spaces. So, in the ref. [1] it was shown, that the anisotropy degree of the conductivity increased in 2-2,5 times because of the decrease in the similar times of the conductivity transversally to the layers at the intercalation of T1B^{III}C₂^{VI} crystals by the lithium ions, whereas the crystal conduction was almost changeless along the layers.

The aim of the present paper is the investigation of the anisotropy degree of the conductivity of the layer semiconductors TlInS₂, TlGaS₂ and TlGaSe₂ in the dependence on the temperature and the finding of the energy barrier value between the layers.

The results of the conductivity investigation of the given layer monocrystals in the constant electric field are given below. The indium was used in the capacity of the contact material, which was melted in the monocrystals and it creates the ohmic contacts. The samples for the measurements have the thickness about 80÷130 mkm and were prepared as in the planar-, so in the sandwich-variant. For the samples in the planar variant, the indium contacts were carried on the lateral terminate edges so, that the electric current was directed along the natural layers of the monocrystal, i.e. perpendicularly to monocrystal C axis ($\sigma_{\perp C}$). In the samples, prepared in the sandwich-variant, the electric current was directed transversally to the natural layers, i.e. along the monocrystal C axis ($\sigma_{|| C}$). The amplitude of the constant electric field, applied to the samples ($F=10^2 \div 10^3$ V/cm) corresponded to the ohmic region of VAC. During the

measurements the samples were established in the cryostat of the "Utrex" mark with the system of the temperature stabilization (the accuracy of the stabilization was 0,02 K).

The measurement results of the temperature dependence of the anisotropy electric conduction for the TlInS₂ monocrystals (curve 1), TlGaS₂ (curve 2) and TlGaSe₂ (3) in the temperature region, at which the jump conductivity takes place in these crystals are given on the fig.1 [2,3]. From the fig.1 it is seen, that $\lg N$ increases for all three crystals with the temperature decrease.

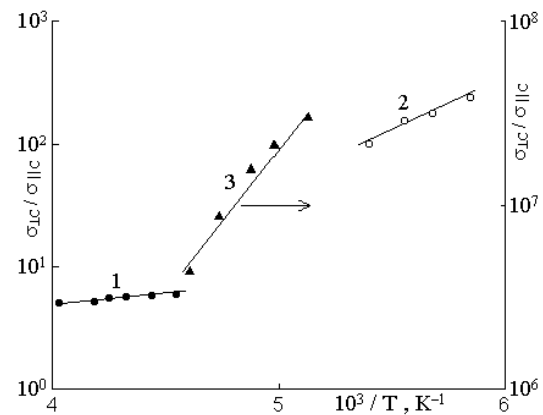


Fig.1. The temperature dependences of the anisotropy degree of the electric conduction of TlInS₂, TlGaS₂ and TlGaSe₂ monocrystals in the region of the low temperatures.

The energy barrier $\Delta\varphi$ between the layers can be valued because of the jump conductivity in the given crystals along C axis by the relation:

$$\sigma_{\perp C} / \sigma_{|| C} \sim \exp(\Delta\varphi / kT). \quad (2)$$

From all three investigated crystals, the TlGaSe₂ monocrystals had the most energy barrier between the layers: $\Delta\varphi=0.30$ eV. In the TlGaS₂ $\Delta\varphi=0.17$ eV, and in TlInS₂ the value $\Delta\varphi$ was the less: 0.04eV.

According to these $\Delta\varphi$ values, the most anisotropy degree of the conductivity was in the TlGaSe₂ monocrystals, and the less one in the TlInS₂.

The dependence of the anisotropy degree of conductivity at the fixed temperature ($T=232K$) on the value of the interlayer energy barrier in the crystals TlInS₂, TlGaS₂ and TlGaSe₂ is given for the comparison on the fig.2. As it is seen from the fig.2, the experimentally obtained dependence $\lg N$ on $\Delta\varphi$ is linear that is in the agreement with the formula (2).

THE INTERLAYER ENERGY BARRIER IN THE ANISOTROPIC $TlB^{III}C_2^{VI}$ MONOCRYSTALS

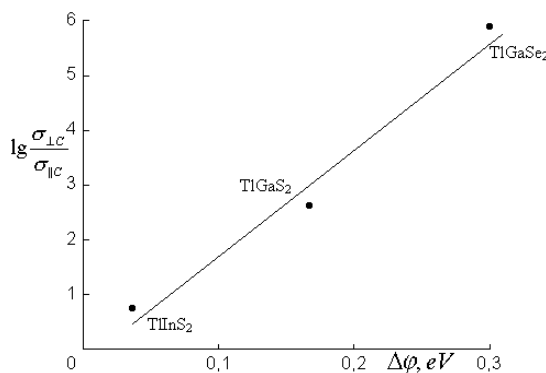


Fig.2. The dependence of the anisotropy degree of the conductivity on the value of the interlayer energy barrier in TlInS₂, TlGaS₂ and TlGaSe₂ monocrystals.

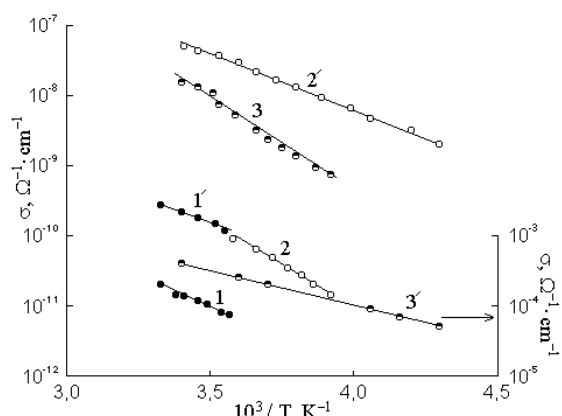


Fig.3. The temperature dependences of the conductivity of TlInS₂ (curve 1; 1'), TlGaS₂ (2; 2') and TlGaSe₂ (3; 3') monocrystals transversally and along to the layers near 300 K.

[1] S.N. Mustafaeva, V.A. Ramazanzade, M.M. Asadov. Materials Chemistry and Physics. 1995, v.40, n.2, p. 142–145.

The value of the interlayer energy barrier can be estimated also by the difference of the activation energies of the conductivity transversally and along the layers, i.e. as follows:

$$\Delta E = E_{\sigma\parallel c} - E_{\sigma\perp c}. \quad (3)$$

The temperature dependences of the conductivity of TlInS₂ (curve 1; 1'), TlGaS₂ (2; 2') and TlGaSe₂ (3; 3') monocrystals in the temperature interval near 300 K along and transversally to layers are given on the fig.3.

The obtained values of the activation energies of the conductivity from the fig.3 are given in the table, where the values $\Delta\varphi$ and ΔE are given for comparison also.

Table.

The electrical parameters of TlInS₂, TlGaS₂ and TlGaSe₂ monocrystals.

Monocrystal	$\Delta\varphi, eV$	$E_{\sigma\parallel c}, eV$	$E_{\sigma\perp c}, eV$	$\Delta E, eV$
TlInS ₂	0.04	0.39	0.34	0.05
TlGaS ₂	0.17	0.50	0.31	0.19
TlGaSe ₂	0.30	0.54	0.20	0.34

As it is seen from the table, the $\Delta\varphi$ and ΔE values well agree with each other in the limits of the experiment fault for all investigated monocrystals. Moreover, the ΔE value was a little bit bigger, than $\Delta\varphi$ in all three cases.

Thus, the values of the interlayer energy barrier, well-agreed with each other, in the TlInS₂, TlGaS₂ and TlGaSe₂ monocrystals are obtained by two independent methods.

- [2] S.N. Mustafaeva, V.A. Aliev, M.M. Asadov. FTT, 1998, t.40, n1, s. 48–51. (in Russian).
[3] S.N. Mustafaeva, V.A. Aliev, M.M. Asadov. FTT, 1998, t.40, n4. s. 612–615. (in Russian).

S.N. Mustafayeva

TlB^{III}C₂^{VI} ANİZOTROP MONOKRİSTALLARINDA LAYLAR ARASINDAKI ENERJİ MANEƏLƏRİNİN TƏYİNİ

TlInS₂, TlGaS₂, TlGaSe₂ laylı monokristallarda keçiriciliyin anizotropiya dərəcəsinin temperaturdan asılılığı tədqiq edilmiş və müəyyən olunmuşdur ki, TlGaSe₂ ən çox, TlInS₂ isə ən az anizotropiya dərəcəsinə malikdir. TlB¹¹¹C₂^{V1} monokristallarında laylararası enerji maneələrinin qiymətləri təpilmişdir ($\Delta\varphi, eV$): 0,04 (TlInS₂), 0,17 (TlGaS₂) və 0,3 (TlGaSe₂).

С.Н. Мустафаева

ОПРЕДЕЛЕНИЕ МЕЖСЛОЕВОГО ЭНЕРГЕТИЧЕСКОГО БАРЬЕРА В АНИЗОТРОПНЫХ МОНОКРИСТАЛЛАХ TlB^{III}C₂^{VI}

Изучена температурная зависимость степени анизотропии проводимости слоистых монокристаллов TlInS₂, TlGaS₂ и TlGaSe₂. Установлено, что наибольшую степень анизотропии имеют монокристаллы TlGaSe₂, а наименьшую – TlInS₂. Определены величины межслоевого энергетического барьера $\Delta\varphi$, эВ в кристаллах: TlInS₂(0.04), TlGaS₂(0.17) и TlGaSe₂(0.3).

Received: 09.02.05

THERMAL CONDUCTIVITY OF $\text{In}_{1-x}\text{Ga}_x\text{As}$ SOLID SOLUTION

R.N. RAHIMOV

*Institute of Physics of National Academy of Sciences of Azerbaijan,
Az-1143, H. Javid av., 33*

The thermal conductivity of $\text{In}_{1-x}\text{Ga}_x\text{As}$ (with $0 \leq x \leq 0.08$) solid solutions has been investigated in the 80–300K range. The thermal conductivity as a function of temperature and the alloy composition has been analyzed on the basis of the theory taking into account boundary phonon scattering, three – phonon normal and three – phonon Umklapp process, phonon resonance scattering and also phonon scattering on point defects with regard to the local change of density and elastic properties of crystals. The revealed dip in the temperature dependence of the thermal conductivity is explained by the phonon resonance scattering on various complexes.

1. Introduction

$\text{In}_{1-x}\text{Ga}_x\text{As}$ solid solutions are perspective materials for solid-state devices and studies of their thermal properties may be used at computations necessary on designing. Besides experimentally investigating the phonon thermal conductivity of the solid solutions versus the content in the wide range of temperatures enables one to study the influence of distortion of the crystal lattice periodicity (lattice imperfections) and the phonon scattering and to estimate applicability of available theories of the phonon scattering on various defects. The thermal conductivity of this system was investigated in a number of works [1–7]. Abrahams, Braunstein, and Rossi [1] investigated the thermal conductivity of the $\text{In}_{1-x}\text{Ga}_x\text{As}$ system except regions near initial components. Ohmer et al. [2] measured the thermal conductivity of GaAs-InAs alloys for the alloy concentration less than 1%. In a paper of Szmulowicz et all. [3] on a basis of theories of Klemens and Callaway gave a theoretical estimation for the Ohmer's and et al. experimental result. Their calculation considers both normal interactions and Umklapp anharmonic ones, as well as mass differences and size distortions for the scattering by point defects. The results indicate that it is the size-distortion scattering, which leads to a very abrupt decrease in the thermal conductivity for dilute alloys. In a work of Adachi [4] the lattice thermal resistivity of $\text{Ga}_{1-x}\text{In}_x\text{As}$ alloys was analyzed with a theoretical prediction based on a simplified model of the alloy-disorder scattering. It was shown a quite good agreement with experimental data on various III-V ternary compounds.

It should be noted that in all above-mentioned works the thermal conductivity dependence on the indium and gallium contents is analyzed at room temperature.

Arasly et al.[5] investigated the thermal conductivity of the $\text{In}_{1-x}\text{Ga}_x\text{As}$ solid solutions at high temperatures by the light flash method.

In the present work as a continuation of our earlier conducted investigations, the thermal conductivity of the $\text{In}_{1-x}\text{Ga}_x\text{As}$ alloys near the InAs initial components in the range of 80 to 300K has been investigated.

2. Experimental

The investigated samples, which grown by the Czochralski method, had the identical charge carriers concentration of $2.4 \cdot 10^{17} \text{ cm}^{-3}$ and the dislocation density 10^3 to 10^4 cm^{-2} . The thermal conductivity was measured by the

absolute stationary method and flash light method between 80 and 300K.

The thermal conductivity of the initial InAs and $\text{In}_{1-x}\text{Ga}_x\text{As}$ solid solution (with $0 \leq x \leq 0.08$) as function of temperature is plotted in fig. I. As it is seen, with increasing the GaAs content the value of the thermal conductivity decreases and its temperature dependence is weaken that is typical for alloys. In the temperature dependence of the thermal conductivity is observed the obvious dip within the narrow interval of 90 to 120K.

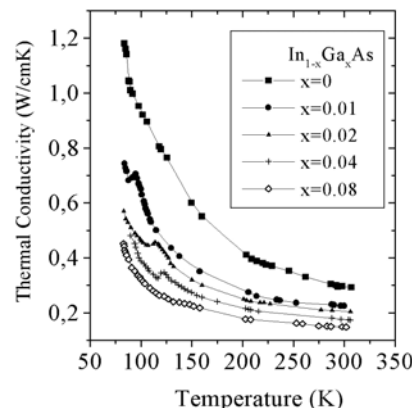


Fig.1. Thermal conductivity of $\text{In}_{1-x}\text{Ga}_x\text{As}$ alloys versus temperature.

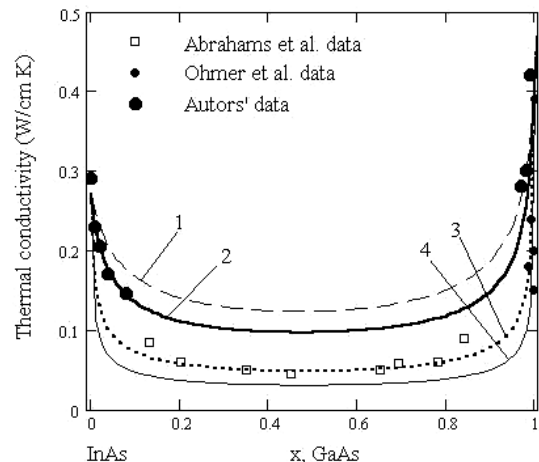


Fig.2. Thermal conductivity of $\text{In}_{1-x}\text{Ga}_x\text{As}$ alloys as a function of the alloy concentration (x). The theoretical curves 1–4 have been calculated with formulas (1)–(4); (5)–(4); (5)–(6) with the value of $G=1$; and (5)–(6) with $G=2$, respectively.

The thermal conductivity for In_{1-x}Ga_xAs at room temperature versus the alloy composition and data of Abrahams et al. [1] and Ohmer et al. [2] are presented in fig.2.

3. Discussion

The electron share of the thermal conductivity (K_e), determined in accordance with the Widemann-Franz formula, is insignificant and the observed change in the thermal conductivity is related with phonon processes.

The lattice thermal conductivity are analyzed in the framework of the well-known Callaway-Klemens model.

Despite that in the Callaway's model [8] it does not take into account the nonlinearity of the phonon spectrum dispersion and also makes no differences for longitudinal and transverse phonons in phonon-phonon interactions, in the literature widely use this model for the thermal conductivity analysis.

For a quantitative estimation of the phonon scattering on point defects in In_{1-x}Ga_xAs at 300K first was computed the thermal conductivity taking into account U-processes and the phonon scattering on point defects by the given formula [9]:

$$K_p = K_0 \left(\frac{\omega_0}{\omega_D} \right) \arctan \left(\frac{\omega_D}{\omega_0} \right) \quad (1)$$

where

$$\left(\frac{\omega_0}{\omega_D} \right)^2 = \frac{\hbar}{2\pi^2 v K_0 \theta A} \quad (2)$$

$$A = \frac{\Gamma \cdot V}{4\pi v^3} \quad (3)$$

$$\Gamma = x(1-x) \left[\left(\frac{\Delta M}{M} \right)^2 + \epsilon \left(\frac{\Delta \delta}{\delta} \right)^2 \right] \quad (4)$$

Here K_0 is the lattice thermal conductivity in the absence of defects, v is the speed of sound, V is the primitive cell volume, θ is Debye temperature, Γ is the disorder parameter including local changes of the density and elastic properties of the alloy when one atom is replaced with another, ω_D is the phonon frequency maximum in the Debye model, and ω_0 is the frequency at which the value of relaxation times, due to

the phonon scattering on point defects $\tau_D^{-1} = A\omega^4$ and Umklapp prosesses $\tau_U^{-1} = B_U\omega^2 T$, are equal.

In the case of the A³B⁵ semiconductor compound, parameter ϵ is determined from the relation between elastic constants and the atomic volume. As for the In_{1-x}Ga_xAs solid solution the Vegard's law remains in force, the change of the lattice constant, in accordance with Ref.6, has been considered as a measure of the local change of material elastic properties. The parameters, which are necessary for the computation, have been taken from the work [3] and they have been linearly extrapolated for the solid solutions. It should be noted that in the In_{1-x}Ga_xAs solid solution, the term connected with the local change of the elastic properties of medium makes its significant contribution to the disorder parameter, Γ .

As it is seen from fig.2, experimental data laid beneath the computed curve 1. It may be supposed that the significant quantitative divergence between the computation and the experimental data is connected with that the three-phonon normal process is not taking into consideration.

It is known that three-normal phonon processes themselves directly do not result in the thermal resistivity. At the same time the N -processes can determine the structure of the stationary nonequilibrium phonon distribution. As a result, their role turns out to be rather essential and they render the important influence on the thermal conductivity magnitude.

At high temperatures in solid solutions the high frequency phonons strongly scatter on point defects, and interaction between longitudinal phonons with conservation of the quasi-impulse, may influence on the lattice thermal conductivity.

The influence of N -processes on the thermal conductivity at $T > \theta$ in alloys is considered in Ref. 6, 10. Abeles [6] has proposed a phenomenological approach to a lattice thermal conductivity of disordered semiconductor alloys at high temperatures. His theory is based on the model presented by Klemens and Callaway and successfully used for alloys. Assuming that the temperature and frequency dependences of the relaxation time for three-phonon N - and U -processes, are the same, namely, $\tau_N^{-1} = B_N \omega^2 T$ and $\tau_U^{-1} = B_U \omega^2 T$, and for the scattering on point defects $\tau_i^{-1} = V \omega^4 \Gamma / 4\pi v^3$, in [6] it was obtained the following formula for the lattice thermal conductivity:

$$K = K_0 \left(\frac{1}{1 + \frac{5C}{9}} \right) \left[\frac{\arctan Y}{Y} + \frac{\left(1 - \frac{\arctan Y}{Y} \right)}{\left(\frac{1+C}{C} \right) \frac{Y^4}{5} - \frac{Y^2}{3} + 1 - \frac{\arctan Y}{Y}} \right] \quad (5)$$

where $Y^2 = \frac{(\omega_D / \omega_0)^2}{1 + 5C / 9}$, $C = B_N / B_U$

C is the adjustable parameter indicating in how many times the N -processes are stronger than the U -processes.

At computations the parameter of disorder, Γ , is calculated with the formula (4), where the local change both the density and elastic properties of the alloy is taken into account. The curve 2 in fig.2, calculated by the formula (5) with the adjustable parameter value of $C=2$, well fits our

experimental data. It shows the essential role of the N processes in the phonon scattering in the $\text{In}_{1-x}\text{Ga}_x\text{As}$ solid solution.

In Ref.3 the role of the N processes in the thermal

conductivity in the GaAs-InAs alloy for the dilute alloy (with the InAs concentrations less than 1%) is appreciated and the disordered parameter Γ is expressed as:

$$\Gamma = \sum_i f_i \left[\frac{M_i - M}{M} + 2G \frac{V_i - V}{V} \frac{1 + (4\mu / 3E)}{1 + (4\mu / 3E_i)} \right]^2 \quad (6)$$

where the sum is over the two alloy components; f_i is the alloy fraction for each constituent, M_i its molecular mass, V_i its molecular volume, E_i its bulk modulus; G is the Gruneisen constant, M, V , and E are averages of mass, volume, and bulk modulus; the μ is averages shear modulus.

The computed curves by the formula (5) and (6) for $C=2$ and $G=2$ (curve 3), $G=1$ (curve 4) are presented in Fig. 2 As it is seen, the curve 3 well fits Ohmer et al. (for dilutely alloyed) experimental data [2], but does not fit Abrahams and et al. [1] and our experimental data.

Thus our experimental data on the In-rich and Ga-rich $\text{In}_{1-x}\text{Ga}_x\text{As}$ solid solutions well follow the Abeles expression (5).

The dips observed for various GaAs concentrations in the temperature dependence of the thermal conductivity in the of 90 to 120K (Fig.1) are of great interest. The observed dips evidently indicate the resonance phonon scattering realization. The $K(T)$ behavior like this was also observed for pure A^3B^5 compounds at temperature lower 50K [11-14] and it is related, in the authors' opinion, with the resonance phonon scattering. However, the nature of the resonance phonon scattering center is not clear as yet. The resonance

phonons scattering is observed at comparatively "high" temperatures in the range of 90 to 120 K in A^3B^5 alloys, in contrast with binary compounds.

The analysis of the temperature dependence of the thermal conductivity is carried out by the following formula:

$$K = \frac{k}{2\pi V} \left(\frac{2\pi k}{\hbar} \right)^3 T^3 \int_0^{\theta/T} \frac{\tau_c z^4 e^z}{(e^z - 1)^2} dz \quad (7)$$

$$\text{where, } z = \frac{\hbar\omega}{kT}.$$

The combined relaxation time (τ_c) includes all probable phonon scattering processes, the crystal boundary scattering, three -phonon normal process, three -phonon *Umklapp* process, Rayleigh scattering on point defects, phonon resonance scattering

$$\tau_c^{-1} = v/L + A\omega^4 + (B_N + B_U)\omega^2 T^3 + R \frac{\omega^2 T}{(\omega^2 - \omega_R^2)^2}, \quad (8)$$

where L is the length of a sample, ω_R is the resonance frequency. For comparison of calculated data with experiments we have used the method of least squares.

In a fig.3 the experimental data and computed by formula (7) curves for two of $\text{In}_{1-x}\text{Ga}_x\text{As}$ alloys (with $x=0,01$ and $x=0,04$) are plotted. Values of the approximation coefficients are given in table 1. As it is seen from fig.3, including in the combined relaxation time also the relaxation time of the resonance phonon scattering, it is possible to quantitatively circumscribe the dips observed in the temperature dependence of the thermal conductivity.

It should be noted that the adjustable parameter, A , is considerably differs from the computed parameter of the alloy-disorder scattering, determined by formula (3). Probably, it is connected with the presence of the other defects. It is possible that in solid solutions compositions of various atoms turn out to be in an environment of the "impurity" center owing to the chaotic distribution of components of the atoms in the crystal lattice. The nonequivalence of the nearest environment of the same atom can result in formation of various complexes, the presence of which brings about features of the phonon scattering. Such complexes can be also impurity – vacancy complexes

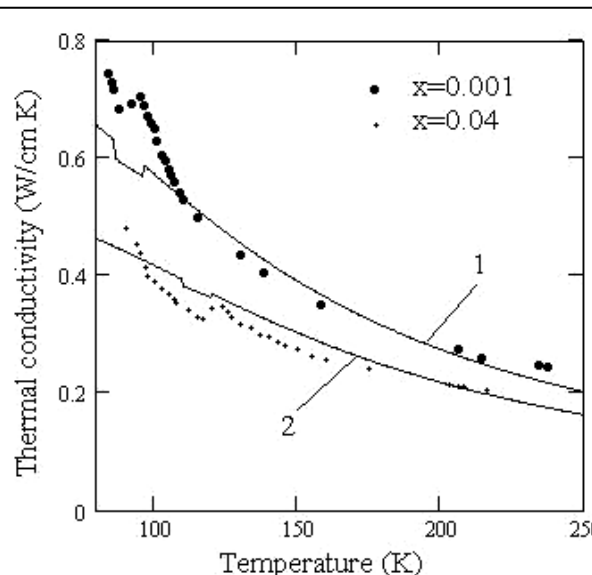


Fig.3. Thermal conductivity of $\text{In}_{1-x}\text{Ga}_x\text{As}$ for $x=0.01$, $x=0.04$ alloys as a function of temperature The curves 1,2 have been calculated with Formulas (7),(8).

Table 1.

Parameters used at computation of the phonon thermal conductivity of In_{1-x}Ga_xAs with x=0,01; 0,04.

	InAs	GaAs	In _{0.99} Ga _{0.01} As	In _{0.96} Ga _{0.04} As
θ (K)	280	370	281	283
v (cm/s)	3.09 x 10 ⁵	3.8x10 ⁵	3.1 x 10 ⁵	3.12 x 10 ⁵
V, cm ³	5.56 x 10 ⁻²³	4.52x10 ⁻²³	5.55 x 10 ⁻²³	5.52 x 10 ⁻²³
μ (dyn/cm ²)	1.9 x 10 ¹¹	3.26x10 ¹¹	1.91 x 10 ¹¹	1.95 x 10 ¹¹
E (dyn/cm ²)	5.79 x 10 ¹¹	7.55x10 ¹¹	5.81 x 10 ¹¹	5.86 x 10 ¹¹
A _{exp} (s ³)			3.988 x 10 ⁻⁴²	7.507 x 10 ⁻⁴²
A _{cal} (s ³)			0.78 x 10 ⁻⁴³	3.01 x 10 ⁻⁴³
B _U (s K ⁻³)			0.718 x 10 ⁻²⁵	0.637 x 10 ⁻²⁵
B _N /B _U			2	2
ω _R (s ⁻¹)			1.327 x 10 ¹³	1.54 x 10 ¹³
v/L (s ⁻¹)			6.2 x 10 ⁵	6.5 x 10 ⁵
R (s ⁻³ K ⁻²)			1.73 x 10 ⁻²⁸	1.796 x 10 ⁻²⁶

4. Summary

The investigation of the thermal conductivity of the In_{1-x}Ga_xAs alloys at temperature between 80 and 300K has been shown that with increasing the Ga content the value of the thermal conductivity decreases and its temperature dependence is weaken. It has been established that for the solid solution in the phonon scattering on point defects together with *Umklapp* processes the normal processes also play essential role. The best good agreement with the theory is obtained with the quadratic frequency dependence for the relaxation time of the *N*-processes. In the temperature dependence of the thermal conductivity is revealed the obvious dips within the narrow interval of 90 to 120K. The analysis of the thermal conductivity temperature dependence has displayed that in the combined relaxation time of the phonon scattering,

including also the relaxation time of the resonance phonon scattering in the Klemens-Callaway formula, it is possible to quantitatively describe the dip observed in the temperature dependence of the thermal conductivity. It is assumed that in the solid solutions resonance phonon scattering centers can be complexes related with the nonequivalence of the nearest environment of the same atom in the crystal lattice.

Acknowledgment

The author would like to thank members of the National Academy of Sciences of Azerbaijan, prof. M.I.Aliyev and prof. F.M.Hashimzade and prof.D.H.Arasy for helpful discussions.

-
- [1] M.S. Abrahams, R.Braunstein, F.D.Rossi J.Phys. Chem. Solids, 1959,10, 204-210.
 - [2] C.Ohmer, W.C.Mitchel, G.A.Graves, D.T.Holmes, H.Kuwamoto and P.W.Yu, J.Appl. Phys. 1988, 64, 2775-2777.
 - [3] F.Szmulowicz, F.L.Madarasz, P.G.Klemens, J.Diller, J. Appl. Phys. 1989, 66, 252-255.
 - [4] S.Adachi J.Appl.Phys. 1983, 54, 1844-1848
 - [5] M.I.Aliyev, D.H.Arasy, R.E Huseynov Fizika i Tekhnika Poluprovodnikov (Semiconductors), 1973, 7, 1846-1848.
 - [6] B.Abeles Phys.Rev. 1963, 131, 1906-1911.
 - [7] W.Nakwaski J.Appl.Phys. 1988, 64, 159-166.
 - [8] J.Callaway, Phys.Rev. 1959, 113, 1046-1051.
 - [9] J.Wu, N.P.Padture, P.G.Klemens, M.Gell, E.Garcia, P.Miranzo, M.I.Osendi, J.Mater.Res. 2002, 17, 3193-3200.
 - [10] J.E.Parrot Proc.Phys.Soc. 1963, 81, 726-735.
 - [11] N.K.S.Gaur, C.M.Bhandari, G.S.Verma Physica, 1966, 32, 1048-1049.
 - [12] A.I.Ivanov, A.N.Lukyanov, Fizika Nizkikh Temperatur 2002, 28, 648-652.
 - [13] K.Guckelsbergert., A.Briggst J.Phys.C: Solid State Phys., 1975, 8, L195-198.
 - [14] S.K.Pal, A.Kumar. Phys.stat.sol. (b) 1985, 128, K15-19.

R.N. Rəhimov

In_{1-x}Ga_xAs BƏRK MƏHLULLARININ İSTİLİK XASSƏLƏRİ

In_{1-x}Ga_xAs bərk məhlullarının istilik keçiriciliyi 80-300K temperatur bölümündə tədqiq olunmuşdur. Kristalların tərkibindən və temperaturdan asılılığı olaraq istilik keçiriciliyinin dəyişməsi fononların müxtəlif mexanizmlərdən - üç-fononlu *N* və *U*-prosesleri, fononların rezonans səpilməsi, kristalın sərhədindən, sixlığın və elastiki xassələrin dəyişməsini nəzərə alan nöqtəvi defektlərdən səpilməsini nəzərə alan nəzeriyə əsasında araşdırılmışdır. İstilik keçiriciliyin temperatur asılılığında müşahidə olunan çuxurlar fononların müxtəlif mərkəzlərdən-komplekslərdən rezonansla səpilməsi ilə izah edilir.

P.H. Rəhimov

ТЕПЛОПРОВОДНОСТЬ ТВЕРДЫХ РАСТВОРОВ In_{1-x}Ga_xAs

Исследование теплопроводности твердых растворов In_{1-x}Ga_xAs проведено в области 80-300К. Теплопроводность сплавов как функция от температуры и состава анализирована на основе теорий, учитывающих рассеяние фононов на границах, трехфононные *N* и *U* - процессы, резонансное рассеяние фононов, рассеяние фононов на точечных дефектах с учетом локального изменения плотности и упругих свойств кристалла. Обнаруженное углубление в температурной зависимости теплопроводности объясняется резонансным рассеянием фононов на различных центрах- комплексах.

Received:12.01.05

INVERSE CHAOS SYNCHRONIZATION IN THE MULTI-FEEDBACK IKEDA MODEL

E.M. SHAHVERDIEV, R.A. NURIEV, E.M. HUSEYNOVA, L.H. HASHIMOVA

*Institute of Physics of National Academy of Sciences of Azerbaijan,
Az-1143, H. Javid av., 33*

R.H.HASHIMOV

Azerbaijan Technical University, 370073 Baku, Azerbaijan

We investigate inverse synchronization between two uni-directionally coupled chaotic multi-feedback Ikeda systems and find both the existence and stability conditions for anticipating, lag, and complete synchronizations.

Keywords: Time-delayed systems, chaos synchronization, multi-feedback systems

1. INTRODUCTION

Recently chaos synchronization [1] in coupled systems have been extensively studied in the context of laser dynamics, electronic circuits, chemical and biological systems, etc. [2]. This phenomenon can be applicable in secure communication, optimization of nonlinear system performance, pattern recognition phenomena, species population control, etc., see e.g. [2] and references there in.

Finite signal transmission times, memory effects make systems with a single and multiple delays ubiquitous in nature and technology [3]. Dynamics of multi-feedback systems are representative examples of the multi-delay systems. Therefore, the study of synchronization phenomena in time-delayed systems is of high practical importance. Prominent examples of such dynamics can be found in biological and biomedical systems, laser physics, integrated communications [3]. In laser physics such a situation arises in lasers subject to two or more optical or electro-optical feedback. Second optical feedback could be useful to stabilize laser intensity [4]. Chaotic behavior of laser systems with two optical feedback mechanisms is studied in recent works [5]. Chaos synchronization between the uni-directionally coupled continuous multi-feedback systems is investigated in [6].

Recently in [7] we reported a type of synchronization: inverse anticipating synchronization, where a time-delayed chaotic system x drives another system y in such a way that a driven system anticipates the driver by synchronizing to its inverse future state: $x(t)=-y_i=y(t-\tau)$ or equivalently $y(t)=-x(t+\tau)$ with $\tau>0$. In [7] we focused our attention on cases when a driving system contains a single delay time.

In this paper for the first time we investigate inverse synchronization between two uni-directionally coupled chaotic multi-feedback Ikeda systems and find both the existence and stability conditions for different synchronization regimes (retarded, complete, and anticipating).

2. SYNCHRONIZATION BETWEEN THE MULTI-FEEDBACK IKEDA SYSTEMS

Consider inverse synchronization between the multi-feedback Ikeda systems,

$$\frac{dx}{dt} = -\alpha x + m_1 \sin x_{\tau_1} + m_2 \sin x_{\tau_2}, \quad (1)$$

$$\frac{dy}{dt} = -\alpha + m_3 \sin y_{\tau_1} + m_4 \sin y_{\tau_2} + K \sin x_{\tau_3} \quad (2)$$

with positive $\alpha_{1,2}$ and $-m_{1,2,3,4}$.

This investigation is of considerable practical importance, as the equations of the class B lasers with feedback (typical representatives of class B are solid-state, semiconductor, and low pressure CO₂ lasers [8]) can be reduced to an equation of the Ikeda type [9].

The Ikeda model was introduced to describe the dynamics of an optical bi-stable resonator, plays an important role in electronics and physiological studies and is well-known for delay-induced chaotic behavior [10-11], see also e.g. [12]. Physically x is the phase lag of the electric field across the resonator; α is the relaxation coefficient for the driving x and driven y dynamical variables; $m_{1,2}$ and $m_{3,4}$ are the laser intensities injected into the driving and driven systems, respectively. $\tau_{1,2}$ are the feedback delay times in the coupled systems; τ_3 is the coupling delay time between systems x and y ; K is the coupling rate between the driver x and the response system y .

We find that systems (1) and (2) can be synchronized on the synchronization manifold

$$y = -x_{\tau_3 - \tau_1} \quad (3)$$

as the error signal $\Delta = -x_{\tau_3 - \tau_1} + y$ for small Δ under the condition

$$m_1 + K = m_3, \quad m_2 = m_4 \quad (4)$$

obey the following dynamics

$$\frac{d\Delta}{dt} = -\alpha\Delta + m_3 \Delta_{\tau_1} \cos x_{\tau_3} + m_2 \Delta_{\tau_2} \cos x_{\tau_2 + \tau_3 - \tau_1} \quad (5)$$

It is obvious that $\Delta=0$ is a solution of system (5). We notice that for $\tau_3 > \tau_1$, $\tau_3 = \tau_1$, and $\tau_3 <$

τ_1 (3) is the inverse retarded, complete and anticipating synchronization manifold [12], respectively. To study the stability of the synchronization manifold $y = -x_{\tau_3 - \tau_1}$ one can use the Krasovskii-Lyapunov functional approach. According to [3], the sufficient stability condition for the trivial solution $\Delta=0$ of time-delayed equation

$$\frac{d\Delta}{dt} = -r(t)\Delta + s_1(t)\Delta_{\tau_1} + s_2(t)\Delta_{\tau_2}$$

is: $r(t) > |s_1(t)| + |s_2(t)|$.

Thus, we obtain that the sufficient stability condition for the synchronization manifold $y = -x_{\tau_3-\tau_1}$ (3) can be written as:

$$\alpha > |m_3| + |m_4|. \quad (6)$$

As Eq.(5) is valid for small Δ stability condition (6) found above holds locally. Conditions (4) are the existence conditions for the synchronization manifold (3) between unidirectionally coupled multi-feedback systems (1) and (2).

$$\frac{dy}{dt} = -\alpha y + m_{1y} \sin y_{\tau_1} + m_{2y} \sin y_{\tau_2} + \dots + m_{ny} \sin y_{\tau_n} + k \sin x_{\tau_k}, \quad (8)$$

we find that the existence and sufficient stability conditions e.g. for the synchronization manifold $y = -x_{\tau_k-\tau_1}$ are: $m_{1x} + k = m_{1y}$, $m_{nx} = m_{ny}$ and $\alpha > |m_{1y}| + |m_{2y}| + \dots + |m_{ny}|$, respectively. For the synchronization manifold $y = -x_{\tau_k-\tau_2}$, $m_{2x} + k = m_{2y}$ and $m_{nx} = m_{ny}$ are the existence conditions, and $\alpha > |m_{1y}| + |m_{2y}| + \dots + |m_{ny}|$ is the sufficient stability condition.

3. CONCLUSIONS

For the first time we have investigated inverse synchronization between two uni-directionally coupled chaotic multi-feedback Ikeda systems and find both the

Analogously we find that $y = -x_{\tau_3-\tau_2}$ is the synchronization manifold between systems (1) and (2) with the existence $m_2 + K = m_4$ and $m_1 = m_3$ and stability conditions $\alpha > |m_3| + |m_4|$.

We notice that in the case of drivers with several feedback mechanisms synchronization manifold's stability condition requires larger value for the relaxation coefficient in comparison with the case of single feedback.

One can generalize the previous results to n -tuple feedback Ikeda systems. Applying the error dynamics approach to synchronization between the following Ikeda models

$$\frac{dx}{dt} = -\alpha x + m_{1x} \sin x_{\tau_1} + m_{2x} \sin x_{\tau_2} + \dots + m_{nx} \sin x_{\tau_n} \quad (7)$$

existence and stability conditions for inverse anticipating, lag, and complete synchronization regimes. We established that in general compared to the case of driver systems with a single feedback system additional feedback channels requires larger values for the relaxation coefficient.

Having in mind different application possibilities of chaos synchronization, synchronization in multi-feedback systems can provide more flexibility e.g. in obtaining different anticipating time scales, etc. and opportunities in practical applications.

It is well known that laser arrays hold great promise for space communication applications, which require compact sources with high optical intensities. The most efficient result can be achieved when the array elements are synchronized. Additional feedback channels could be useful to stabilize nonlinear system's output, e.g. laser intensity.

- [1] L. M. Pecora and T. L. Carroll, Phys. Rev. Lett. 1990, 64, 821; E.Ott, C.Grebogi and J.A.Yorke . Phys. Rev. Lett., 1990, 64, 1196.
- [2] A.Pikovsky, M.Rosenblum, and J.Kurths, Synchronization: A universal Concept in Nonlinear Sciences (Cambridge University Press, Cambridge, 2001). CHAOS, Special issue on chaos synchronization 7, N4 (1997) edited by W.L.Ditto and K.Showalter; G.Chen and X.Dong, From Chaos to Order. Methodologies, Perspectives and Applications (World Scientific, Singapore,1998); Handbook of Chaos Control, Ed. H.G.Schuster (Wiley-VCH, Weinheim, 1999); R.Dilao, T.Domingos, and E.M.Shahverdiev, Mathematical Biosciences 2004, 189, 141; E.M.Shahverdiev, R.A.Nuriev, R.H.Hashimov, and K.A.Shore, Chaos, Solitons and fractals, in press, 2004; E.M.Shahverdiev and K.A.Shore, Phys.Rev.E 2005, 71, 016201. G.Hu, Y.Zhang, H.A.Cerdeira, and S.Chen, Phys.Rev.Lett. 2000, 85, 3377.
- [3] J.K.Hale and S.M.V.Lunel, Introduction to Functional Differential Equations (Springer, New York, 1993).
- [4] Y.Liu and J.Ohtsubo, IEEE J.Quantum Electron. 1997, 33, 1163.
- [5] I.Fischer, O.Hess, W.Elsaber, and E.Gobel, Phys.Rev.Lett.1994, 73, 2188; F.Rogister, P.Megret, and M.Blondel, Phys.Rev.E 67 2003, 67, 027203; F.Rogister, D.W.Sukow, A.Gavrielides, P.Megret, O.Deparis, and M.Blondel, Optics letters 2000, 25, 808; F.Rogister, P.Megret, O.Deparis, M.Blondel, and T.Erneux, Optics letters 1999, 24, 1218.
- [6] E.M.Shahverdiev, Phys.Rev.E 2004, 70, 067202.
- [7] E.M.Shahverdiev, S.Sivaprakasam, and K.A.Shore, Phys.Rev.E 2002, 66, 017204; E.M.Shahverdiev, R.A.Nuriev, and R.H.Hashimov, Int.J. Modern Physics B 2004, 18, 1911.
- [8] Ya.I.Khanin, Chaos 1996, 6, 373.
- [9] F.T.Arecchi, G.Giacomelli, A.Lapucci, and R.Meucci, Phys.Rev.A 1994, 43, 4997.
- [10] H.U.Voss, Phys.Rev.E 61 2000, 61, 5115.
- [11] C.Masoller, Phys.Rev.Lett. 2001, 86, 2782 ; C.Masoller and D.H.Zanette, Physica A 2001, 300, 359.
- [12] E.M.Shahverdiev, S.Sivaprakasam, and K.A.Shore, SPIE Proceedings: Physics and Simulations of Optoelectronic Devices; Eds: P.Blood, M.Osinski, and Y.Arakawa 2002, 4646, 653.

E.M. Şahverdiyev, R.A. Nuriyev, E.M. Hüseynova, L.H. Həşimovab R.H. Həşimov

ƏKS RABİTƏLƏRLİ İKEDA MODELİNĐƏ İNVERSİON XAOC SİNXRONLAŞMASI

Bir istiqamətdə əlaqələndirilmiş bir neçə eks rabitəli хаотик Ikeda modelinin inversion sinxronlaşması öyrənilib. Müxtəlif sinxronlaşma rejimləri üçün zəruri və stabillik şərtləri tapılıb.

Э.М. Шахвердиев, Р.А. Нуриев, Е.М. Гусейнова, Л.Г. Гашимова, Р.Г. Гашимов

ИНВЕРСИОННАЯ ХАОТИЧЕСКАЯ СИНХРОНИЗАЦИЯ В МОДЕЛИ ИКЕДЫ С НЕСКОЛЬКИМИ ОБРАТНЫМИ СВЯЗЯМИ

На примере популярной модели Икеды инверсионная хаотическая синхронизация анализирована в системах с несколькими обратными связями. Найдены условия существования и стабильности различных синхронизационных режимов.

Received:23.03.2005

EFFECT OF NON-REFLECTIVE ABSORPTION OF MICROWAVE RADIATION IN SOLUTIONS OF ACETYL ACETONE IN N-HEPTANES

M.I. VALIYEV, R.M. KASIMOV, Ch.O. KADJAR

*Institute of Physics of National Academy of Sciences of Azerbaijan,
Az-1143, H. Javid av., 33*

The dielectric properties of solutions of acetyl acetone in n-heptanes were researched in a range of microwaves. The existence of a spectrum of concentrations and thicknesses of the solutions layer at which resonant non-reflective absorption of radiation in these solutions occurs has been established.

Preparation and research of the materials absorbing electromagnetic radiation without its appreciable reflection on the basis of solutions of polar substance in non-polar solvent is of scientific and practical interest. Such materials can be applied as composite materials for reception of non-reflective absorbing coverings.

On the basis of the analysis of the results represented in works [1,2] it has been shown that under certain conditions in polar dielectric possessing wave dispersion and placed on a metal substrate, can take place full (non-reflective) absorption of the electromagnetic radiation passing through it and reflected from a conducting surface. As experimental detection of the given effect in pure dielectric liquid is complicated because of necessity of application of more complex technical equipment, solutions of polar substances in non-polar solvent have been used as an object of research. The effect of non-reflective absorption in this case is reached by variation of the structure of solution and its thickness.

According to carried out experimental studies and taking into account that dispersive area of acetyl acetone occurs in the microwave range, non-reflective absorption of electromagnetic radiation has been investigated in solutions of acetyl acetone in n-heptanes at wavelengths $\lambda=4,28; 10,0$ and $20,0$ mm and at temperature $T=293$ K. Measurements of reflective characteristics of the given solutions were carried out with use of panoramic measuring instruments for the standing wave factor P2-66, P2-67 and P2-69 and connected with them short-circuited on the end measuring wave guide cells which, in turn, were equipped by the device of fine regulation of solution layer thickness. From the experimentally obtained dependences of the module of wave reflection factor ρ on thickness l of the solution layer in a cell the minimal values of wave reflection factor ρ_{min} were determined and their dependence on concentration of a polar component in a solution was obtained. At the same time the quantitative estimation of dielectric properties of studied solutions was carried out with application of the measurement method described in [3] based on determination of dielectric permittivity ϵ' and dielectric losses ϵ'' of a solution on the base of experimental measurement of standing wave factor η and thickness l of a solution layer in extreme points of dependence $\eta(l)$.

Results of measurements of ϵ' and ϵ'' for solutions of acetyl acetone in *n*-heptanes are given in Table 1.

Dielectric properties of pure acetyl acetone are sufficiently good described in the field of a dispersion by Debye's equation. The average concentrations of polar component in the studied solutions are best described by Debye-Cole's equation [4].

Table 1
Dielectric permittivity ϵ' and dielectric losses ϵ'' of
solutions of acetyl acetone in n-heptanes at wavelengths
 $\lambda=4,28; 10,0$ и $20,0$ mm and at temperature $T=293$ K.

$\varphi, \%$	$\lambda=4,28$ mm		$\lambda=10,0$ mm		$\lambda=20,0$ mm	
	ϵ'	ϵ''	ϵ'	ϵ''	ϵ'	ϵ''
100	5,62	4,65	7,32	8,13	13,04	12,64
90	5,21	3,93	6,84	6,56	11,73	10,17
80	4,87	3,40	6,40	5,51	10,49	8,00
60	4,20	2,32	5,54	3,92	8,06	4,95
50	3,89	1,95	5,06	3,18	6,80	3,76
40	3,52	1,55	4,65	2,49	5,70	2,72
20	2,92	0,81	3,65	1,08	3,75	1,04
10	2,68	0,52	3,09	0,55	2,83	0,56
5	2,59	0,41	2,79	0,31	-	-

Found experimental concentration dependences of ϵ' and ϵ'' at $\lambda=4,28; 10,0$ and $20,0$ mm and temperature 293 K have been used for calculation of conditions at which in studied solutions probably the effect of non-reflective absorption of electromagnetic radiation occurs. According to [2], this effect could be realized in points of minima of dependence of the module of reflection factor ρ_{min} on thickness l of the substance layer while fulfilling the following conditions:

$$(1 + y^2) \frac{\lambda_b}{\lambda_g} = \operatorname{th}\left(\frac{2\pi y l_0}{\lambda_g}\right) - y \operatorname{tg}\left(\frac{2\pi l_0}{\lambda_g}\right) \quad (1)$$

$$y \operatorname{sh}\left(\frac{4\pi y l_0}{\lambda_g}\right) + \sin\left(\frac{4\pi l_0}{\lambda_g}\right) = 0$$

where

$$y = \operatorname{tg} \frac{\Delta}{2}, \quad \Delta = \operatorname{arctg} \frac{\epsilon''}{\epsilon' - p}; \quad (2)$$

$$p = \left(\frac{\lambda}{\lambda_k}\right)^2, \quad \lambda_b = \frac{\lambda}{\sqrt{1-p}};$$

λ_b, λ_g – lengths of waves in empty and filled by researched substance direct system correspondingly; λ_k – critical wavelength of direct system; l_0 – thickness of a layer of substance at which reflection of a wave is absent.

The value l_0 , included in (1) is close to $(2n-1)\lambda_g/4$ and differs from it by the small size dependent on properties of substance and number n of a minimum of $\rho(l)$ dependence. In reduced coordinates $\varepsilon_1 = (\epsilon' - p)/(1-p)$; $\varepsilon_2 = \epsilon''/(1-p)$ the equations (1) are transformed to family of lines for set

numbers of minima of dependences ρ on l at which condition $\rho=0$ (curve B, fig.1) is realized. It is typical that with increase in number n these lines come nearer to X axis. Last circumstance specifies an opportunity of non-reflective absorption of electromagnetic radiation by substance, even

with very small value of dielectric losses that as follows from fig.1, is realized at significant thickness of substance layer.

Put on a coordinate plane $[\varepsilon', \varepsilon'']$ experimental data of various concentration solutions determine a behavior of experimental dependence ε'' from ε' of studied solution of acetyl acetone in n-heptanes (curve A, fig.1).

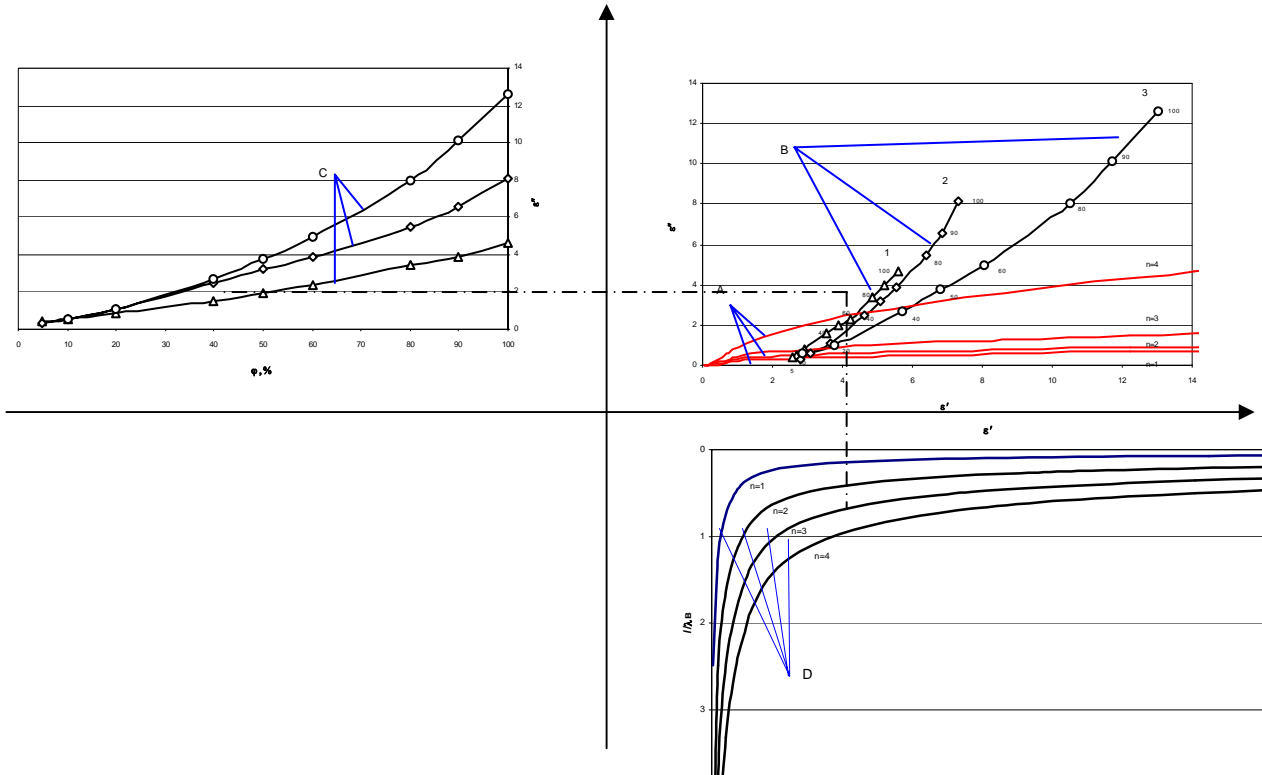


Fig.1. Graph-analytical method of determination of selective concentration and thickness of solutions of acetyl acetone in n-heptanes at which in them take place non-reflective absorption of electromagnetic radiation.

- A – theoretically estimated dependences ε'' from ε' corresponding to conditions of non-reflective absorption of electromagnetic radiation in polar dielectrics.
- B – experimental dependences of ε'' from ε' in solutions of acetyl acetone in n-heptanes at wavelengths $\lambda=4,28$ (1); $10,0$ (2) and $20,0$ (3) mm and at temperature $T=293$ K. Signatures to points designate values of weight concentration of a solution in percents (%). n - number of a minimum.
- C – experimentally found dependence of ε'' of the solutions on concentration at $\lambda=20,0$ (1); $10,0$ (2) and $4,28$ (1) mm.
- D – theoretically estimated dependences of ε' from l_0/λ_0 corresponding to conditions of non-reflective absorption of electromagnetic radiation in polar dielectrics.

As $\varepsilon'' \approx 0$ for n-heptanes, with the growth of concentration of acetyl acetone in a solution the curve of the dependence of ε'' from ε' in solutions of acetyl acetone in n-heptanes begins from a point laying on an X axis, and comes to an end in the top part of a plane $[\varepsilon', \varepsilon'']$ at point with the coordinates corresponding to the pure acetyl acetone. At the movement to this coordinate point the curve will cross family of lines of resonant non-reflective absorption of radiation of the solutions described by the equation (1). Taking into account the specified character of an arrangement of lines of resonant values ε' and ε'' , it is necessary to expect existence of infinite lines of concentration of acetyl acetone in non-polar n-heptanes and a thickness of a reflecting layer of a solution at

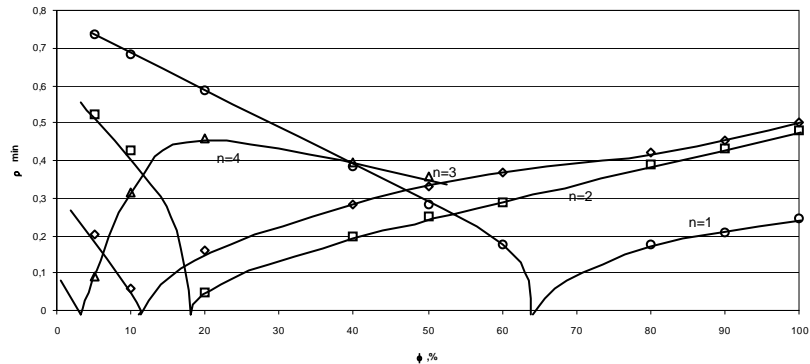
which an effect of full absorption of the reflected radiation occurs. Unfortunately, behavior of ε' and ε'' in binary solutions with change of their structure is difficult to express analytically. Therefore, for calculation of resonant concentrations φ_0 of acetyl acetone in solutions and corresponding resonant values ε'_0 and ε''_0 graph-analytical method has been applied for the solution of the equations (1) with use of experimentally obtained data from measurements of ε' and ε'' in solutions of acetyl acetone in n-heptanes at various concentrations. Results of these calculations for several first zero minima ρ_{min} are given in Table 2.

EFFECT OF NON-REFLECTIVE ABSORPTION OF MICROWAVE RADIATION IN SOLUTIONS OF ACETYL ACETONE IN N-HEPTANES

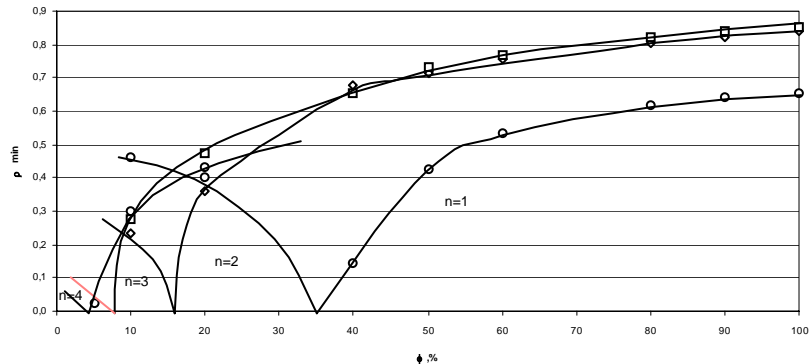
Table 2

Dielectric permittivity ϵ'_0 , dielectric losses ϵ''_0 , thickness of a layer l_0 and concentration of acetyl acetone φ_0 in its solutions with n-heptanes in points of zero minima of the module of reflection factor ρ_{min} at wavelengths $\lambda=4,28; 10,0$ and $20,0$ mm and temperature $T=293$ K.

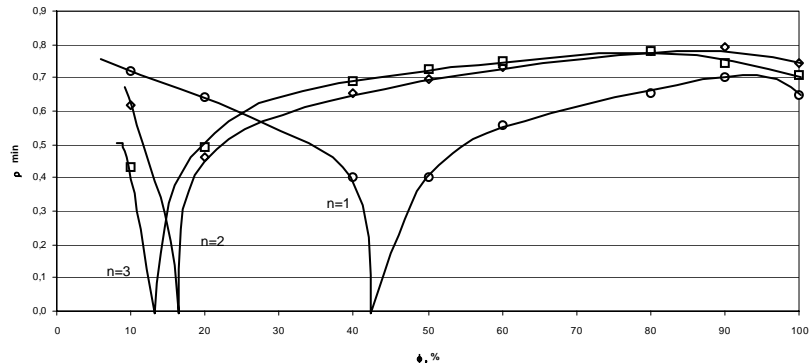
n	$\lambda=4.28$ mm					$\lambda=10,0$ mm					$\lambda=20,0$ mm				
	ϵ'_0	ϵ''_0	l_0/λ	φ_0	φ_m	ϵ'_0	ϵ''_0	l_0/λ	φ_0	φ_m	ϵ'_0	ϵ''_0	l_0/λ	φ_0	φ_m
1	4,31	2,47	0,552	63,6	63,4	4,75	2,60	1,23	42,0	42,0	5,97	2,95	2,24	42,7	42,5
2	2,86	0,76	1,939	18,6	18,3	3,42	0,83	4,13	17,1	18,6	3,44	0,83	8,22	16,6	16,8
3	2,66	0,50	3,321	9,3	10,4	3,04	0,50	7,24	9,0	7,9	2,76	0,76	15,16	14,7	13,5
4	2,54	0,33	4,704	2,4	3,2	2,83	0,33	10,48	5,4	4,6	-	-	-	-	-



a)



b)



c)

Fig. 2. Dependence of the module of reflection factor ρ of an electromagnetic wave on concentration φ of acetyl acetone in solution with n-heptanes for first minima ρ_{min} of lines for different thickness of solution layer at wavelengths $\lambda=4,28$ (a); $10,0$ (b) and $20,0$ mm (c) and temperature $T=293$ K.

- [1] I.Preissner. NTZ Arch.4, 1989, 175.
[2] R.M. Kasimov. Izmeritel'naya tekhnika. 10, (1970), 48.
[3] R.M. Kasimov. Metrology. 7, 1987, 45
[4] J.Y. Akhakov. Dielectric parameters of pure liquids. M.;
izd. MAI, 1999, 854.
(in Russian).

M.İ. Vəliyev, R.M. Qasimov, Ç.O. Qacar

**ASETİLASETONUN N-HEPTANDAKI MƏHLULLARINDA İFRAT YÜKSƏK TEZLİKLİ ŞÜALANMA
ZAMANI ƏKSOLUNMAYAN UDULMA EFFEKTİ**

Asetilasetonun *n*-heptandakı məhlulullarının dielektrik xassələri mikrodalğa diapazonunda tədqiq olunmuşdur. Məhlulun müxtəlif qalınlıqlı ləylərində və konsentrasiyalarında şüalanmanın əksolunmadan rezonansla udulmasının yaradığı müəyyənləşdirilmişdir.

М.И.Велиев, Р.М.Касимов, Ч.О.Каджар

**ЭФФЕКТ БЕЗОТРАЖАТЕЛЬНОГО ПОГЛОЩЕНИЯ СВЕРХВЫСОКОЧАСТОТНОГО ИЗЛУЧЕНИЯ
В РАСТВОРАХ АЦЕТИЛАЦЕТОНА В Н-ГЕПТАНЕ**

Исследованы диэлектрические свойства растворов ацетилацетон-гептан в диапазоне микроволн. Установлено существование в этих растворах спектра концентраций и толщин слоя раствора, при которых возникает резонансное безотражательное поглощение электромагнитного излучения.

Received: 08.12.2004

PLAZMALI İON MƏNBƏYİNƏ MALİK KÜTLƏ SPEKTROMETRLƏRİNDE İKİNCİ NÖV İONLARIN NİSBİ HƏSSASLIĞININ TƏYİNİ

K.Z. NURİYEV
Azərbaycan Milli Aerokosmik Agentliyi

İşdə bərk maddələrin etalonsuz tədqiqatı zamanı müxtəlif tip plazmali ion mənbələrinə (çığlcımlı və seyriyən boşalmalı, lazer şüası, ikinci ion emissiyası) malik kütlə spektrometrlərində yaranan ionların nisbi çıxışını əvvəlcədən hesablamaya üçün alqoritm təklif olunmuşdur. Alqoritm ion əmələ gəlmə prosesinin müxtəlif mexanizmlərinin toqquşma təbiəti ümumiləşmiş modeli əsasında nisbi çıxışın analitik ifadəsini almağa imkan verir. Təklif olunan alqoritm kinetik yaxınlaşmanın köməyi ilə plazma zərrəciklərinin sıxlığının zaman – məkan dəyişmələrini araşdırmağa və kvant mexanikası çərçivəsində və toqquşma ilə ionlaşma prosesinin kəsiyinin hesablanmasına imkan verir.

İonları ion mənbəyində plazma üsulu ilə alınan (plazmali ion mənbələri) kütlə spektrometrləri son vaxtlar maye və bərk maddələrin element (izotop) tərkibini yüksək dəqiqliklə öyrənmək üçün geniş miqyasda tətbiq olunur. Buna səbəb istər qılgılcımlı və seyriyən boşalma, istər induktiv əlaqəli plazma, istərsə də lazer şüası ilə ionlaşmaya malik kütlə spektrometrlərində praktik olaraq hətta tek – tek ionlara da qeyd etməyin mümkünüyündür [1]. Məhz plahmalı ion kamerasında (bu sıraya ikinci növ ion emissiyasını da daxil etmək olar), yaranan ionların neytral atomalara nisbətini artırmağa, və deməli ion mənbəyinin effektivliyini artırmağa real şərait yaratmışdır. Doğrudan da, lazer şüası ilə ionlaşma kütlə spetrometrinin mütləq həssaslığı $1 \cdot 10^{-19} \text{ q}$ [2], induktiv əlaqəli plazma və seyriyən boşalmalı plazmanın köməyi ilə nisbi həssaslığın aşağı həddi $10^{-7} \div 10^{-11}$ (atom %), xəta isə 0,01 % aşırı.

Ümumiyyətlə, kütlə spektrometrik sistemlərin istənilən obyektlərin tədqiqində dövrü sistemə daxil olan demək olar ki, bütün elementlərini qeyd etmək üstünlüyü onları maddələrin element tərkibini tədqiq edə bilən bütün üsullardan ən önemlisi, bəzən isə yeganəlik səviyyəsinə qaldırı.

Başqa anilitik üsullarda olduğu kimi kütlə spektrometrik üsulda da tədqiqat zamanı məlum tərkibə malik nümunədən istifadə olunur. Bu zaman etalon (tərkibi əvvəlcədən məlum olan) nümunəni analiz etməklə müxtəlif naməlum tərkibli nümunələrin element (və ya izotop) tərkibini təyin etmək olar. Qeyd etmək lazımdır ki, bu üsul sadalanan üstünlükleri ilə yanaşı bəzən bir sıra problemlərlə dül üzləşir. Məsələn, bir çox hallarda xüsusi təmiz maddələrin və ya ətraf mühitin obyektlərinin analizi zamanı öyrənilən obyektə adekvat olan və ya təyin olunacaq elementlərin tərkibini xarakterize edən standart nümunə tapmaq praktiki olaraq mümkün olmur. Belə hallarda mütxəssislər tədqiqatın etalonsuz analiz, başqa sözlə standart nümunələrdən istifadə etmədən analiz aparmaq məcburiyyətində qalır. Bu isə o deməkdir ki, bütün elementlər üçün nisbi həssaslıq əmsali (NH_3) vahidə bərabər qəbul edilir ki, bu da 300 % - lik sistematik xətalara gətirir.

Araşdırımlar göstərir ki, kütlə spektrometrik üsuldan istifadə edən kimyaçı tədqiqatçılar etalonsuz kəmiyyət analizi aparmaq üçün külli miqdarda tədqiqatlar əsasında adekvat standart nümunələr kataloqu yaratmalıdır, bu isə yaxın gələcəkdə mümkün olan iş deyil. Bu problemi həll etmək üçün nisbətən real yol təyin ediləcək elementlərin əsas parametrləri, matrisanın fiziki – kimyəvi xüsusiyyətlərini və eksperimentin aparılma şəraitini də nəzərə almaqla NH_3 – ni əvvəlcədən hesablamaq məqsədi ilə onun riyazi ifadəsini ionların yaranmasının məlum mexanizmləri əsasında dəqiqləşdirməkdir.

Bu baxımdan NH_3 – nə (u_i) plazmaya daxil olan və ionların orada gedən fiziki proseslərdə iştirakının müxtəlifliyini (ε_i – fiziki amil) və onların kütlə analizatorunun daxilində kütləyə və yük tərkibinə görə diskriminasiyasını (cihaz amili – β_i) nəzərə alan integral xarakteristikası kimi baxmaq olar:

$$u_i = \varepsilon_i \cdot \beta_i. \quad (1)$$

Qeyd edək ki, ionların analizatorda diskriminasiyanı onun ion – optik sistemini yüksək dəqiqliklə dərəcələməklə nəzərə almaq olar. Lakin ionların plazmadakı diskriminasiyasını (fiziki amili) nəzərə almaq olduqca çətindir. Məhz bu səbəbdən plazmali ion mənbəyində ionların yaranma prosesinin tədqiqi həm nəzəriyyəçi, həm də eksperimentator mütxəssislərin daim diqqət mərkəzində olub, müxtəlif müəlliflər [3, 4] plazmada ionların yaranma mexanizmini izah etmək üçün orada gedən bəzi fiziki proseslərin eyni ehtimalla olmasına qəbul edən bir sıra nəzəriyyələr irəli sürürlər. Bəziləri isə, əksinə sübut etməyə çalışırlar ki, nə yüksək temperaturlu (qılgılcımlı boşalma və lazer şüalanması [5]), nə də alçaq temperaturlu (induktiv əlaqəli plazma və seyriyən boşalma [6] plazmalarda gedən proseslərin bərabər ehtimalli olmasından söhbət gedə bilməz. Qeyri – bərabər statik çəkiyə malik proseslərin araşdırılması isə həm fiziki, həm də riyazi nöqtəyi – nəzərdən olduqca mürəkkəbdir.

Hazırda mövcud olan ion mənbələrini təyinatına görə iki impulslu (lazer və qılgılcımlı boşalma) hissəyə ayırmak olar. İmpulslu ion mənbələri zərrəciklərinin sıxlığı $10^{15} \div 10^{21} \text{ sm}^{-3}$, temperaturu isə 1 eV olan zərrəciklər işləyən 2 hissəyə ayırmak olar [7]. Alçaq temperaturlu plazma ilə işləyən mütxəssislər belə hesab edirlər ki, yüksək temperaturlu plazmada (yəni impulslu ion mənbələrində) zərrəciklər yüksək sıxlığa və yüksək toqquşma ehtimalına malik olduqlarına görə müxtəlif ion yüksək ionların nisbətini Sax – Eqqert [8] düsturu ilə hesablamak olar. Eyni zamanda enerjisi 1 eV, sıxlığı 10^3 sm^{-3} olan yüksək temperaturlu plazma mütxəssisləri hesab edirlər ki, plazmanın parametrlərini hesablamak üçün ideal qaz statistikasını (Bolsman, Fermi – Dirak və i.a. [9]) tətbiq etmək olar.

Beləliklə, hazırda plazmanın parametrlərinin və orada baş verən proseslərin müxtəlif elementlərin nisbi çıxışına təsirinin tədqiqat metodologiyası demək olar ki, yox dərəcəsindədir. Ona görə belə güman edirik ki, bu metodologiya bütün plazmali ion mənbələri üçün ümumiləşmiş olmalıdır. Ən azı ona görə ki, ion əmələ gətirən bütün fiziki proseslərin bazasında təbiətcə eyni olan toqquşma prosesləri durur.

Təqdim olunan işdə məqsəd nəticə etibarı ilə etalonşuz ölçmələr zamanı sistematik xətaları azaltmaq naminə plazma mənbəli kütłə spektrometrlərdə gedən proseslərin öyrənilməsi üçün vahid metodologiyanın işlənməsi və əsaslandırılması cəhdidir.

Plazmalı ion mənbələrində ionların əmələ gəlmə mexanizmini dərk etmək üçün hesablama üsulu qəbul edilmiş modeldən asılı olaraq NHƏ tapılmasıdır. Bu mənada təklif olunan modelləri 4 qrupa bölmək olar:

1. Səthdən qopan atomların elektron mübadiləsi hesabına ionlaşma ehtimalının kvant mexanikasına əsaslanmış hesablanması. Yeri gölmişkən, bu model yalnız təmiz metal və sadə xəlitələrin səthindən qopan ionlara tətbiq oluna bilər.

2. İkinci növ ionların yarımemprik yaxınlaşmaya əsaslanan nisbi çıxışının intensivliyini təyin etməyə imkan verən «analitik» yaxınlaşma.

3. Plazmadakı ionların konsentrasiyasının real dəyişmə dinamikasına əsaslanan və plazma kimyası [10] çərçivəsində təkamül tapmış kinetik yaxınlaşma.

4. Plazma proseslərinin tədqiqində geniş istifadə olunan plazma fizikası metodlarına əsaslanan «təmiz plazma» yaxınlaşması.

Hazırda ədəbiyyatda ionların yaranmasının kvant mexanikasına söykənən və riyazi baxımdan müxtəlif dərəcəli mürəkkəb modelləri verilmişdir. Nisbətən geniş tədqiqatçı sinfinin reğbətini qazanmış modellərdən atomların səthdə həyəcalanması [10], hiddətlənməsi [11], səthi ionların metalla əlaqəsinin pozulması [12] modellərini qeyd etmək olar. Bu ionlaşma modellərinin əsasını təşkil edən və atomların elektron mübadiləsinə bəraət qazandıran əsas amil həyəcanlanmış atomların relaksasiya müddəti onların metaldan çıxmə müddətindən çox – çox kiçik olmalıdır. Digər tərfdən qarşılıqlı təsir oblastının ölçüləri atomun ölçüləri ilə müqayisə oluna bildiyindən bu oblastda maddənin fiziki – kimyəvi xassələri onun həcmi orta göstəricilərindən fərqlənə bilər [10]. Bu modellərə əsasən plazmanın ionlaşma dərəcəsinə atomların ionlaşma potensialından, atomun hərəkət sürətindən, onun səthdən çıxış işi və analizi elektron quruluşundan ibarətdir. Qeyd edək ki, sonuncu iki amil səthdən qopan ionların metalin sərbəst elektronları hesabına neytrallaşmasını və deməli, ionların nisbi çıxışını təyin edir.

Fenomenoloji modellər ionların yaranma mexanizminin fundamental tədqiqinə əsaslanmamığını baxmayaraq NHƏ empirik və yarımemprik ifadələrin köməyi ilə səthdən qopan ionların nisbi sayına müəyyən dəqiqliklə hesablamaya imkan verir.

Bəzi müəlliflərin fikrincə [13, 14] səthdən qopan ionların tərkibinin formallaşmasında molekullararası elektron mübadiləsinə əsaslanan kimyəvi ionlaşma durur. Bu zaman belə qəbul olunur ki, birinci növ ionların (və ya lazer şüasının) təsiri ilə nümunənin səthində «kvaziserbəst», böyük sıxlığa malik nazik (1-2 mm) plazma təbəqəsi yaranır [13]. Qeyd etmək lazımdır ki, dəfələrlə edilən cəhdlərə baxmayaraq adı çəkilən plazma təbəqəsi eksperimental müşahidə olunmamışdır. Yeri gölmişkən ikinci növ ionların nisbi çıxış əmsalının plazmada gedən proseslərlə bilavasitə əlaqəsi [15]-də tənqid olunmuşdur.

Beləliklə, deyilənlərdən məlum olur ki, kvant mexanikasına əsaslanmış modellər, yalnız sade sistemlərə – təmiz metallara və sadə xəlitələrə tətbiq etmək mümkün olursa, fenomenoloji modelləri keyfiyyət analizlərində tətbiqi heç mümkün deyil.

İstənilən halda, təklif olunan nəzəri modellərin nəticələri ilə təcrübənin (xətasını) hər modelin öz riyazi aparatı

daxilində qiymətləndirmək üçün bu prosesləri bir qədər ətraflı araşdırıq. Kvant mexanikasına əsasanan yaxınlaşmada əsas məsələ zərrəciklər arasında elementar qarşılıqlı təsirin araşdırılması Şredinger tənliyinin həllinə (ən sadə halda zərrəciklərin mərkəzi – simmetrik sahədə səpilməsinə) gətirilir [16]

$$\Delta u + 2m/h^2 [E - U(r)]u = 0, \quad (2)$$

burada u - dalğa funksiyası, m - zərrəciyin kütləsi, h - Plank sabiti, E - sistemin məxsusi enerjisi, $U(r)$ - bir birindən r - məsafəsində yerləşən zərrəciklərin qarşılıqlı təsir enerjisidir. Dalğa funksiyası u -nın (2) tənliyini ödəyən qiymətləri səpilmə amplitudası adlanan hər hansı $f(u)$ funksiyası ilə mütənasibdir

$$u = f(u) \exp(i k r)/r, \quad (3)$$

burada θ - səpələnmə bucağı, k - dalğa vektorudur. $|f(u)|^2$ qiymətcə bir zərrəciyin digərindən $d\varPi$ cisim bucağı daxilində səpilməsinin dy differensial kəsidir [16]

$$dy = |f(u)|^2 d\varPi. \quad (4)$$

Onda elektronun atomdan qeyri – elastik səpilməsi (elektron zərbəsi ilə ionlaşma) aşağıdakı kimi təyin olunur [16]

$$dy_w = 8p(e^2/hV_e) dq \cdot \left| \left\langle w \left| \sum_b \exp(-iqr_b) \right| 0 \right\rangle \right|^2 d\varPi, \quad (5)$$

burada q - gətirilmiş dalğa vektoru, V_e - elektronun sürəti, e - elektronun yükü, w - zərrəciyin statik halıdır.

(5)-dən, təcrübədə istifadə edilə biləcək real analitik ifadə yalnız Kulon – Born yaxılaşması daxilində, yəni toqquşan zərrəciklərin birinin enerjisinin o birisindən qat – qat çox olduqda qəbul oluna bilər [17]. Əksər hallard bu yaxınlaşmanın enerjisi bir neçə keV olan zərrəciklərin sükunətdə olan zərrəcikləri bombardman olunması halında tətbiq etmək olar (ikinci növ ion emissiyası).

Ümumiyyətlə qeyd etmək lazımdır ki, bir – biri ilə möhkəm əlaqəli zərrəciklər kimi baxılan plazma proseslərinin tədqiqində kvant mexanikası yaxınlaşmasından istifadə etmək praktiki nöqtəyi – nəzərdən bir o qədər də təqdirə layiq deyil. Plazma proseslərinin tədqiqi plazma fizikasında tətbiq olunan üsulların köməyi ilə öyrənmək daha məqsədə uyğun sayılır.

İkinci növ ionların yaranma mexanizminin tədqiqi kvant mexanikası yaxınlaşmasından fərqli olaraq «təmiz plazma» yaxınlaşmasına əsaslanan enerjinin, impulsun və momentin saxlanılması qanunlarından, həm de daşınma tənliyindən alınan aşağıdakı tənliklər sisteminin həlli üzərində qurulub [18]

$$\begin{aligned} & (\partial c / \partial t) + \nabla(c x) = \nabla(D v c), \\ & c(\partial v / \partial t) + c(v \nabla)v = -\nabla p + \nabla(m \nabla v) + g[\vec{S} \times \vec{B}] \\ & c(\partial v / \partial t) + c(v \nabla)u = -c \nabla u + \nabla(z \nabla u) + g S^2 - R + \Lambda, \\ & \partial f_j(x, E) / \partial x = z_j [d\varPi(x) / dx] \cdot [\partial f_j(x, E) / \partial E] - \\ & - f_j(x, E) / \Lambda_j + \partial(E) / \Lambda_j \end{aligned} \quad (6)$$

burada t - zaman, x - koordinat, p və u - təzyiq və plazmanın daxili enerjisi, ρ - plazmanın sıxlığı, \vec{S} və \vec{B} - xarici elektrik sahəsinin intensivliyi və maqnit induksiyası, E - zərrəciklərin kinetik enerjisi, D - ambipolyar diffuziya əmsali, μ - elektronların yüruklüyü, R - plazmanın şüalanma itkisi, A - plazmaya verilən enerji, $f_j(x, E) - E$ enerjili j -tip zərrəciyin x nöqtəsində olmasının ehtimalı, z_j - j -tip zərrəciyin yükü, λ - sərbəst qaçış yoluñun uzunluğu.

(6) tənliklər sistemini sadələşdirmək məqsədi ilə [19] - da qəbul edilmiş bir və ya iki komponentli sistemlər üçün aldiqları həllər plazmanın müxtəlif parametrləri üçün bir - birini təkzib edən müxtəlif qiymətlərə gətirdi. Bu cür sadələşdirmələr xatirinə plazma parametrlərinin ideallaşdırılması ionların yaranma effektivliyinin real qiymətləndirməsini qeyri - mümkün edir ki, bu da «təmiz plazma» yaxınlaşmasının əsas çatışmayan cəhəti sayılır.

Kimyəvi plazma çərçivəsində inkişaf tapmış kinetik yaxınlaşma metodu [20] plazmada təmərküzləşmiş yüksü zərrəciklər toplusunun faza xarakteristikalarını nəzərə almadan hər hansı j - tipli zərrəciklərin n_j konsentrasiyasının zamana görə dəyişməsin aşağıdakı tənliklər sistemi vasitəsilə ifadə edir

$$dn_j/dt = \sum_{b=1}^N n_j \cdot n_y \delta(b), \quad (7)$$

burada $\delta(b)$ - j və y tipli zərrəciklərin qarşılıqlı təsir prosesinin sürətidir. Burada ən əsas çətinlik müxtəlif toqquşma proseslərinin $\delta(b)$ sürətinin təyin olunmasıdır. Məsələn, elektron zərbəsi ilə ionlaşma prosesləri üçün

$$\delta(b) = \langle y, V_e \rangle = \int_{\varphi}^{\infty} V_e(T_e) y(E_a) F(E_a) dE_a, \quad (8)$$

burada φ - uyğun elementin atomunun birqat ionlaşma potensialı, V_e - $T_e F(E_a)$ - elektronun sürəti, temperaturu və paylanma funksiyasıdır.

Hər şeydən əvvəl qeyd etmək lazımdır ki, plazmanın yaranmasında aparıcı rol oynayan proseslər eyni statistik çəkiyə malik olmadıqdan orada əmələ gəlməmiş yüksü zərrəciklərin (əsasən elektronların) enerjiyə görə paylanma funksiyasının dayanıqlığı (zamana görə) haqqında danışmağa dəyməz. Digər tərəfdən $F(E_e)$ paylanma funksiyası kimi Maksvel, Bolsman və ya başqa funksiyalardan alınan nəticələr eksperimentlə uzaqlaşır. Bu o deməkdir ki, plazma özünün yaranma mərhələlərində zaman və məkana görə dəyişən paylanma funksiyalarına malik zərrəciklərdən ibarət olur. Belə olan halda nəzəriyyə ilə eksperimenti uzaqlaşdırmaq üçün yeganə çıxış yolu $\delta(b)$ -nın $F(E_e)$ - dən təcrübə yolu ilə alınmış yarımempirik asılılığından istifadə etməkdir.

Doğrudan [3, 4] işlərində müəlliflər ionların nisbi çıxışını hesablamaq üçün yarımempirik xarakterli «analitik» yaxınlaşmadan istifadə etmişlər. Bunun üçün onlar lazer şüası ilə tədqiq olunan səth arasında gedən fiziki proseslərin eyni statistik çəkili qəbul edərək bir neçə uzaqlaşdırıcı parametrlərin köməyi ilə ionların nisbi çıxışı haqqında mülahizə yürüdürlər. Bu yaxınlaşmanın ən parlaq təzahürü ionların yaranmasının lokal termodinamik tarazlıq [21] və kvazitarazlıq [22] modelləridir. Bu modellər çərçivəsində elektronun temperaturunu elə seçmək olar ki, qəbul olunmuş

fərziyələr daxilində γ_i^+ -ni 30 % xəta ilə hesablamaga imkan verir. γ_i^+ təcrubi və nəzəri qiymətlərini daha yaxınlığını əldə etmək üçün hesablama düstürlərinə çoxlu sayda uzaqlaşdırıcı parametrlər daxil olunmalıdır.

Uxarıda göstərilən səbəblər üzündə plazmalı ion mənbələrində plazmanın yaranmasını və qərarlaşmasını tədqiq etmək üçün adları çəkilən yaxınlaşmala praktikada ayrı - ayrı tətbiq edirlər. Təbiidir ki, bu səbəblərə görə həmin ion mənbələrində yaranan çoxkomponentli plazmadan çıxan ionların nisbi çıxışının hesablanması sistematik xətalara əhəmiyyətli dərəcədə azaltmaq mümkün olmur. Elə həmin səbəblərdəndir ki, bərk cisimlərin (xüsusən metal və xəlitələrin) etalonsuz kəmiyyət analizinin nəticələri həqiqətə lazımi qədər yaxın olmur.

Uxarıda aparılan analiz və plazmalı ion mənbələrində ionların yaranma proseslərinin tədqiqi üsullarının sistemləşdirilməsi göstərdi ki, həmin mənbələr kimi çoxkomponentli sistemlərdən çıxan ionların nisbi çıxışını tədqiq etmək üçün (7) kinetik tənliklər sistemi həll olunmalı və hökmən aydınlaşdırılmalıdır ki:

- plazma kütləsində gedən toqquşma proseslərinin hansı xəlitəyə daxil olan elementlərin nisbi çıxışını təyin edir;
- plazma kütləsinin hansı makroparametrləri (atom və elektronların sıxlığı) həyacanlandırıcı amil kimi nümunəyə dəha çox təsir edir;
- plazmada gedən proseslərin hansının sürəti onun formalamaşmasında və ionların yaranmasında daha böyük rol oynayır.

Aparılan tədqiqat işlərinin nəticələrinin emalı zənnimizə aşağıdakı alqoritm götürülməlidir.

Hər şeydən əvvəl ionların nisbi çıxışının (γ_i^+) plazmanın yaranmasında iştirak edən atomların fiziki - kimyəvi xassələrindən və onların sistemə (plazmaya) təsirinin tip və parametrlərindən asılılığı müəyyənləşdirilməlidir. Bunun üçün böyük həcmədə eksperimental məlumatlar bazası yaranmalıdır. Hər her şeydən əvvəl ionların nisbi çıxışının γ_i^+ yuxarıda göstərilən parametrlərlə korreksiyanı tapmaq üçün təklif olunan hər hansı modelini (məsələn, kvazitarazlıq) mexanizmi riyazi operatorundan istifadə etmək kifayətdir.

$$\gamma_i^+ = A \exp\left(-\frac{\varphi_a^x - \varphi_a^e}{kT_a}\right) \exp\left(-\frac{\varphi_i^x - \varphi_i^e}{kT_e}\right), \quad (9)$$

burada φ_a^x və φ_i^e - uyğun olaraq elementin əlaqə (atomlaşma) və birqat ionlaşma potensialları, T_a və T_e isə atomlaşma və ionlaşma temperaturları, k - Bolsman sabitidir.

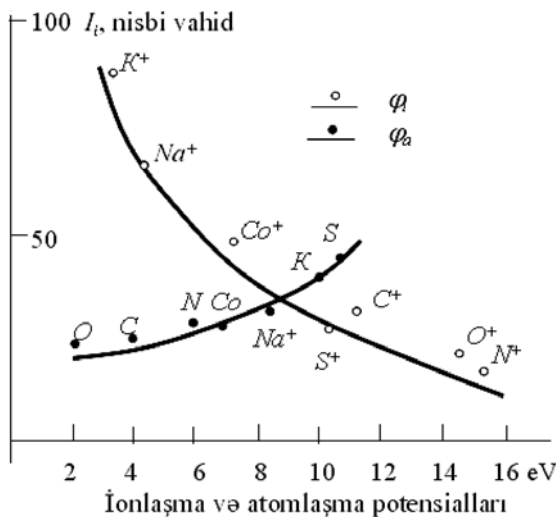
(9) - dək γ_i^+ -nın φ_a^x və φ_i^x arasındaki korrelyasiyasıya əyrisi şək. 1 [23] - də verilmişdir. Hər üç ionlaşma üsulu (induktiv əlaqəli plazma, lazer şüası və seyriyən boşalma üçün) $\gamma_i^+(\varphi_i)$ asılılığı kvadratik azalan, $\gamma_i^+(\varphi_a)$ isə təqribən monoton artan asılılıqdır. $\gamma_i^+(\varphi_i)$ asılılığı yaranmış plazmada elektron toqquşması tipli ionlaşmanın üstünlüyünü, $\gamma_i^+(\varphi_a)$ asılılığı isə ionlaşmaya əlaqə enerjisinin və ionlaşmanın sürətinin təsirinin olduğunu göstərir.

Növbəti mərhələdə qarşılıqlı təsirdə olan zərrəciklər sistemində yaranmış plazmanın zaman - məkan tekamülünün fiziki və riyazi təsviri araşdırılmalıdır. Bunun üçün hər hansı

bir yaxınlaşma (məsələn, kvazitarazlıq) metodundan istifadə edirək plazma kütlesinə daxil olan zərrəciklərin sürətə və enerjiyə görə paylanma funksiyasının ifadəsi tapılmalıdır.

Sonrakı mərhələ (7) kinetik tənliklər sisteminin həllidir. Bunun üçün əsas toqqusma proseslərinin (σ) bilmək vacibdir. Hər növ elementin toqqusma kəsiyini hesablamaq üçün kvant mexanikası yaxınlaşmasında (5) tənliyində zərrəciklərin xarakteristik enerjilərinin nəzərə almaqla (məlum təcrübə neticələrə əsasən) istifadə etmək olar. Nəhayət «təmiz plazma» yaxınlaşmasının köməyi ilə plazma kütlesinin makroparametrləri olan atom, ion və elektronların sıxlığını bilib müəyyən növ zərrəcisinin (elementin) sıxlığının zamana görə dəyişməsinin (6) köməyi ilə analitik ifadəsini almaq olar. Başqa sözlə, çoxkomponentli sistem olan plazmadan çıxan ionların nisbi çıxışını əvvəlcədən hesablamaq üçün ifadə almaq olar.

Yuxarıda təklif olunan alqoritm lazer plazmasında yaranan ionların nisbi çıxışını hesablamaq üçün konkret misal üzərində tətbiq edək.



Şəkil 1.

- [1] Yu. A. Bikovskiy, V.N. Nevolin. Lazernaya mass – spektrometriya. M. Enerqatomizdat, 1985, 128 s.
- [2] I.D. Kovalyov, N.V. Larin, A.I. Suçkov. Jurn. analit. ximii, 1985, t. 40, s. 1971 – 1983.
- [3] J.F. Eloy. Scanning Electron Microscopy. 1986. No. 4, p. 1243 – 1250.
- [4] Yu.B. Afanasyev, N.Q. Basov. Vzaimodeystvie moshnoqo lazernoqo izlučeniya s plazmoy. M., Radiotexnika, 1978, t.17.
- [5] Yu.A. Bikovskiy, S.M. Silnov. Fizika plazmi. 1987, t. 15, s. 731.
- [6] J. Abril. Comp. Phys Comm. 1988, v. 51, p. 413.
- [7] S.A. Verie, R. Gilbels, F. Adams. Mass - spectrometry Reviews. 1990, v. 9, p. 71 – 77.
- [8] J.R.W. Smithwick, D.M. Lynch, J.C. Franklin. Journ. Amer. Soe. Mass – spectromenty. 1993, No. 4, p. 278 – 285.
- [9] P. Williams. Appl. surt. sci. 1982, v. 13, No. 1-2, p. 241.
- [10] G. Blaise, A. Nourtier. Surt. Sci. 1979, v. 90, No. 2, p. 495.
- [11] M.L. Ju, K. Mann. Phys. Rev. Lett. 1986, v. 57. No. 2, p. 1476.
- [12] V.Q. Litovčenko Vtoričnaya ionnaya ionno – fotonay emissiya. Xarkov: XQU, 1980, s. 17.
- [13] V.Q. Litovčenko, R.I. Marčenko, V.P. Melnik, B.N. Romanyuk. Vtoričnaya ionnaya i ionno – fotonaya emissiya. Xarkov, XQU, 1988, s. 40.
- [14] O.S.T. Tsong. Surt. Sci. 1978, v. 75, v. 1, p. 1591.
- [15] L.D. Landau, E.M. Lifšits. Kvantovaya mexanika (perelyatevistkaya teoriya). M., Nauka, 1974.
- [16] Fizika ionno – ionníx i elektronno – ionníx stolknoveniy. / Per. s anql. pod red. Firsova O.B., M., Mir, 1986, 248 s.
- [17] A.V. Nedospasov, V.D. Xaim. Osnovı fiziki protsessov v ustroystvax s nizko temperaturnoy plazmoy. M., Enerqatomizdat. 1991, 224 s.
- [18] A. Veries, P. Juhase, De Wolf, M. Gilbels K. Scanning Microscopy. 1988, v. 2, p. 1853.
- [19] S.L. Pojarov, P.K. Xabibullaev. Diaqnostika ionnoqo sostava plazmi. Taşkent, FAN, 1987, s. 15.
- [20] C.A. Andersen. Nat. Bur. Stand. Spec. Publ. 1975. No. 427, p. 79.
- [21] V.S. Fayberq, Q.İ. Ramendik. Jurn. analit. ximii. 1991, № 2, s. 241 – 252.
- [22] Z.K. Nurubeyli. Trudi pyatoy mejd. konferentsii SİGT, q. Odessa, 2004.
- [23] M.J. Seaton. Proc. Phys. Sci. 1962, v. 79, p. 1105 – 1117.

Şək. 1-dən göründüyü kimi $\gamma_i^+ (\varphi_i)$ əyrisi kvadratik xarakter daşıyır. Bu o deməkdir ki, ionların elektron zərbəsi ilə yaranma prosesinin kəsiyi Siton düsturu [24] ilə ifadə oluna bilər

$$a_e = A \left(T_e^{1/2} / \varphi_i^2 \right) \exp(i\varphi_i/T_e), \quad (10)$$

burada A - sabit, T_e plazma elektronlarının temperaturu, φ_i - elementin ionlaşma potensialıdır. (7) kinetik tənliyini 3 zərrəcikdən ibarət sistem üçün ifadəsi aşağıdakı kimi olar

$$d n_i / d t = n_a \cdot n_e \cdot \alpha_e, \quad (11)$$

burada n_i, n_a, n_e - ion, atom və elektronların sıxlıqları, α_e - atomların elektron zərbəsi ilə ionlaşma kəsiyidir.

Məlumdur ki, bir (məsələn, x) elementin ionlarının başqa (məsələn, y) elementinin ionlarına nisbətən çıxış əmsali həmin elementlərin atomlarının uyğun ionlaşma sürətlərinin nisbəti ilə təyin olunur

$$\gamma_y^x = \frac{a_{ex}}{a_{ey}}. \quad (12)$$

(12) – də (10) – u nəzərə alsaq

$$\gamma_y^x = \left(\frac{\varphi_y^2}{\varphi_x^2} \right) \exp \left[-(\varphi_x - \varphi_y)/T_e \right] \quad (13)$$

alariq. [25] verilən lazer şüasının enerji sıxlığı Q (Vt / sm²) ilə T_e arasında empirik əlaqəni nəzərə alsaq ($T_e = 2 \cdot 10^{-5} Q^{2/3}$), (13) – ün köməyi ilə γ_y^x tapmaq olar.

Beləliklə, təklif olunan alqoritm lazer şüası ilə ionlaşma mənbələrinə məxsus kütłə spektrometrindrə etalonsuz analiz zamanı ionların nisbi həssaslığını nisbətən kiçik xətalarla hesablamaga imkan verir.

- [24] Yu.A. Bikovskiy, K.Q. Oksenoyd, Q.İ. Ramendik, S.M. Silnov, E.A. Sotniçenko. Rol protsessov ionizatsii primesnix atomov, uskoreniya i rekombinatsii ionov v lazerno – plazmennom mass – spektrometrii. Preprint MİFİ, Moskva, 1980, № 003 – 89, 24 s.

K.Z. Нуриев

**МЕТОД РАСЧЕТА ОТНОСИТЕЛЬНОЙ ИНТЕНСИВНОСТИ ВТОРИЧНЫХ ИОНОВ
В МАСС – СПЕКТРОМЕТРАХ С ПЛАЗМЕННЫМИ ИСТОЧНИКАМИ ИОНОВ**

В работе проведено исследование процессов ионообразования в различных плазменных источниках масс – спектрометров на основе анализа литературных данных. Дан алгоритм для расчета относительной интенсивности вторичных ионов на основе единой ударной природы ионообразования.

K.Z. Nuriyev

**THE METHOD FOR CALCULATION OF RELATIVE INTENSITY OF THE SECONDARY
IONS IN MASS – SPECTROMETERS WITH PLASMA TYPE IONS SOURCE**

The research of processes of ions formation in various plasma type sources of mass – spectrometers carried out on the basis of analysis of referneed data sources is described in the article.

The algorithm for calculation of relative intensity of the secondary ions on the basis of single impact nature of ion formation is given.

Received: 18.01.05

FeGaInS₄ - DƏ TERMO-E.H.Q. VƏ XOLL EFFEKTİ

N.N. NİFTİYEV

Azərbaycan Dövlət Pedaqoji Universiteti, AZ1000, Bakı, Ü.Hacıbəyov, 34

O.B. TAĞIYEV

AMEA Fizika institutu, Az.1143, Bakı, H.Cavid, 33

F.M. MƏMMƏDOV

AMEA Kimya problemləri institutu

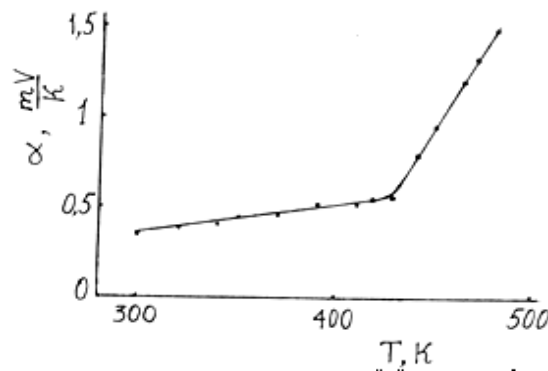
FeGaInS₄ yarımkəcicicisində müxtəlif temperaturlarda termo – e.h.q. və Xoll effekti tədqiq edilmişdir. Müəyyən edilmişdir ki, FeGaInS₄ p-tip keçiriciliyə malikdir. Termo – e.h.q. əmsali, yüksəkçiyyicilərin konsentrasiyası və Xoll yüyürklüyü təyin edilmişdir.

Son zamanlar d və f təbəqələri tamamilə dolmayan elementlər daxil olan yarımkəcicici birləşmələr yarımkəcicici və maqnit xassələrini özündə cəmləşdirən qeyri-adi xüsusiyyətləri sayesində intensiv tədqiqatların obyektinə çevrilmişlər. Bu cür perspektivli yarımkəcicici birləşmələrə son illər yarımkəcicilər fizikası və texnikasında az öyrənilmiş maqnit yarımkəciciləri aiddir. Bu planda AB₂X₄ (burada A – Mn, Fe, Co, Ni; B – Ga, In; X – S, Se, Te) tipli birləşmələr böyük maraq kəsb edir [1-6]. Bu birləşmələr optielektronikada tətbiq edilə bilən maqnit sahəsi ilə idarə oluna bilən lazerlər, modulyatorlar, fotodektorlar və s. funksional qurğular yaratmaq üçün perspektividir. [7]-də şpiel quruluşlu CoIn₂S₄ (fəza qrupu Fd3m) və tetraqonal quruluşlu CoGa₂S₄ (fəza qrupu I4)-ün 1:1 münasibətindən yeni CoGaInS₄ tərkibli laylı yarımmaqnit yarımkəcicici alınmış və onların quruluşu, maqnit xassələri tədqiq edilmişdir. Maqnit yarımkəcicici birləşmələrin qarşılıqlı təsirindən laylı birləşmələrin əmələ gəlməsi faktı bizi başqa kecid elementləri əsasında laylı yarımmaqnit yarımkəcicici birləşmələr almağı cəhd etməyə vadar etdi. Bizim tərifimizdən [7]-yə oxşar olaraq MnGaInS₄ tərkibli yeni laylı yarımmaqnit yarımkəcicici alındı və onun elektrin, optik və fotokeçicilik xassələri tədqiq edildi [8-10]. FeGa₂S₄-FeIn₂S₄ sisteminin hal dioqramının öyrənilməsi nəticəsində bizim tərifimizdən ilk dəfə olaraq FeGaInS₄ laylı birləşməsi aşkarla çıxarıldı və [11] işində bəzi elektrik xassələri öyrənildi.

Hal hazırkı işdə FeGaIn₄ kristalında termo – e.h.q. və Xoll effektinin tədqiqinin nəticələri verilmişdir.

FeGaInS₄ stexiometrik miqdarda, yüksək təmizlikli (99,999%) elementlərin birbaşa ərintisində alınmışdır. Rentqeneqrafik tədqiqatlar göstərdi ki, FeGaInS₄ qəfə sabitləri $a=3,81$; $c=12,17\text{ \AA}$; $z=1$, fəza qrupu p3m1 olan ZnIn₂S₄ birləşməsi yarım tip quruluşuna kristallaşır [7]. Nümunelər mexaniki cıtalama yolu ilə orta ölçüsü $3\times6\times8\text{ mm}^3$ olan paralelopiped formasında hazırlanmışdır. Ölçmələr FeGaInS₄ nümunələrində sabit maqnit sahəsində və sabit cərəyannda aparılmışdır.

Şəkil 1-də FeGaInS₄ kristalı üçün termo – e.h.q. əmsalının temperatur asılılığı əyrisi verilmişdir. Termo – e.h.q.-nin işarəsinə görə müəyyən edilmişdir ki, tədqiq edilən temperatur intervalında FeGaInS₄ p tip keçiriciliyə malik olur.

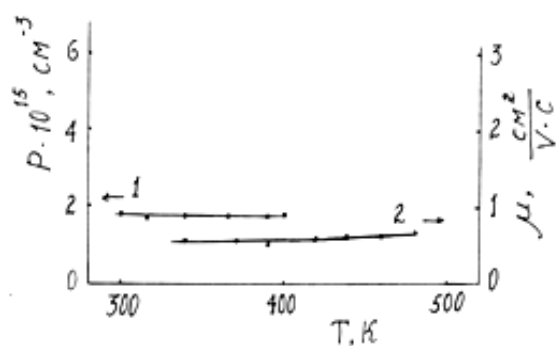


Şəkil 1. FeGaInS₄ kristalı üçün termo – e.h.q. əmsalının temperaturundan asılılığı.

Şəkildən görünür ki, termo – e.h.q. əmsali 300-400K temperatur intervalında zəif artır. Sonra temperatur artıqca termo – e.h.q.-nin qüvvəti artımı müşahidə olunur və onun qiyməti 1,5 mV/K-nə çatır. Burada α termo-e.h.q. əmsali temperaturla $\ln(T)^{\frac{3}{2}}$ kimi mütənasib olaraq artır. Bu da

$$\alpha = \frac{k}{e} \left(\ln \frac{N_v}{P_0} + r + 2 \right)$$

ifadəsinə uyğundur [12]. (Effektiv hal sıxlığı $N_v \sim T^{\frac{3}{2}}$).



Şəkil 2. FeGaInS₄ kristalı üçün yüksəkçiyyicilərin konsentrasiyası (1 əyrisi) və yüyürklüğünün (2 əyrisi) temperaturundan asılılığı

Şəkil 2-də FeGaInS₄ kristalı üçün Xoll effekti ölçülməsindən təyin edilən yüksəkçiyyicilərin konsentrasiya

siyasi və Xoll yüyürüklüğünün temperaturdan asılılığı göstərilmişdir. Buradan görünür ki, 300ç400K temperaturlarda yükdaşıyıcıların konsentrasiyası (1 əyrisi) sabit qalır və $p=1,8 \cdot 10^{15} \text{ sm}^{-3}$. Yükdaşıyıcıların yüyürüklüyü də təyin olunan temperatur intervalında demək olar ki, sabit qalır və $\mu = 0,6 \frac{\text{sm}^2}{V \cdot \text{san}}$ - yə

bərabər olur.

Bələliklə, FeGaInS₄ kristalında müxtəlif temperaturlarda termo – e.h.q. və Xoll effekti təyin edilmişdir. Keçiriciliyin tipi müəyyənəşdirilmiş, yükdaşıyıcıların konsentrasiyası və Xoll yüyürüklüyü təyin edilmişdir.

-
- [1] T. Kanomata, H. Ido, T. Kaneko. J.Phys. Japan, 1973. v.34. №2, p.554.
 - [2] B.K. Babayeva. V sb. Troyne poluprovodniki i ix primenenie. Kişinev. Ştiintsa, t.1976. s.96.
 - [3] R.N. Bekimbetov, Q.A. Medvedkin, V.D. Proçuxan i dr. Pisma v CTF. 1987, t.13, V17, s. 1040-1043.
 - [4] G.A. Medvedkin, Yu.B. Rud, M.V. Tairov. Phys. Status solidi (a) 1989, V.3, p.289.
 - [5] Q.K.Averkieva, R.N. Bekimbetov, N.N. Konstantinova i dr. Neorganičeskie materiali, 1988, t.24, №4, s.591-594.
 - [6] N.N. Niftiev, M.A. Alidcanov, O.B.Taqiev, M.B.Muradov. FTP, 2003, T.37, V.2, s.173-175.
 - [7] C. Battistioni, Gastaldi L., Mattagno et al. Sol. St. Commun. 1987, v.61, №1, p.43-46.
 - [8] N.N. Niftiev, A.Q. Rustamov, O.B.Taqiev i dr. Optika i spektroskopiya. 1993, T.75, V2., s.351-354.
 - [9] N.N. Niftiev, O.B. Taqiev, Q.M. Niftiev Neorganičeskie materiali. 1996, t.32, №3, s.291-293.
 - [10] N.N. Niftiev, O.B. Taqiev. Pisma v CTF. 2003, t.29, V10, s.49-53.
 - [11] N.N. Niftiyev. FTP, 2004, t.38, v.5, s.522-524.
 - [12] A..İ.Anselm. Vvedenie v teoriyu poluprovodnikov, M.,Nauka, 1978, s.420

N.N. Niftiyev, O.B. Tagiyev, F.M. Mamedov

THERMOELECTROMOTIVE FORCE AND HALL EFFECT IN FeGaInS₄

Thermoelectromotive force and Hall effect at the different temperatures are investigated in FeGaInS₄ semiconductors. It is established, that FeGaInS₄ has p-type conductivity. The thermoelectromotive force coefficient, concentration and Hall mobility of current carriers are obtained.

Н.Н. Нифтиев, О.Б. Тагиев, Ф.М. Мамедов

ТЕРМО – Э.Д.С. И ЭФФЕКТ ХОЛЛА В FeGaInS₄

В полупроводниках FeGaInS₄ исследованы термо-э.д.с. и эффект Холла при различных температурах. Установлено, что FeGaInS₄ обладает р-тиром проводимости. Определены коэффициент термо – э.д.с., концентрации и холловская подвижность носителей тока.

Received: 18.03.05

MULTI DATA MODE METHOD IN THE SCANNING PROBE MICROSCOPY

S.P. MOLCHANOV, I.A. CHERNOVA-KHARAEVA

Technology research and development Institute CRC, Moscow, Russia

S.H. ABDULLAYEVA, S.D. ALEKPEROV

Institute of Physics of National Academy of Sciences of Azerbaijan,

Az-1143, H. Javid av., 33

Scanning probe microscope "ForceMaster-402MD" (Russia) combines structurally and functionally two devices with different principle of operation – scanning tunneling microscope and atomic-force microscope. All these facts allows surface of any substances with any degree of conductivity, and also surfaces of any dielectrics to be investigated in detail. This device provided with the unique so-called multiparameter method (this method covered by patent) which ensures possibility to obtain distribution map of some parameters of objects with the surface topographer (conductivity, polarization, thickness of adsorbent layer and etc.).

Scanning probe microscopy (SPM) is a well known powerful tool for surface topography investigations [1-2]. However, in most cases the image of topography does not answers all questions of the researchers. For complete information we frequently need the data on various physic-chemical, electrical, magnetic and other properties of the explored surface which would allow to distinguish or even identify the objects of various nature on a surface.

To solve this problem it has developed and permanently improves the new mode of probe microscopy – Multi Data Mode (MDM) (the patented method [3]). This mode has unique facilities to provide single-scan exploration of the surface to get the whole data set available in SPM. This ability is obvious and essential advantage over other SPM methods where as a rule we gain limited number of parameters using one device.

In probe microscopy, piezo elements of various kinds are used for precise surface scanning and a number of modulation techniques have been developed to eliminate viscous friction when moving a probe over the surface. In fact, a probe is not to be constantly in contact with the surface in any SPM. A reliable method would be the one that allows to bring a probe down to the surface, to make all the necessary measurements, to withdraw the probe into the region free of interaction, and then to move the probe to another point (Multi Data Mode method). In "ForceMaster-402MD" we used a beam deflection registrations scheme. Tips on the end of a DI rectangular silicon cantilever and a home-made rectangular tungsten cantilever served as probes (fig. 1).

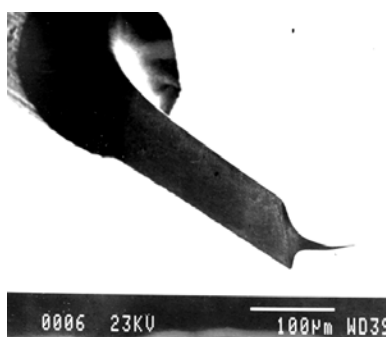


Fig.1.

To explain the principle of the operation of device, let us consider the behavior of a needle-probe on an elastic console near the surface under study [4]. Figure 2 (a) shows a typical dependence of the force $F(z)$ acting on the tip upon the

distance from the surface. Let us begin with the simplest case of pure solid surface. Assume the cantilever stiffness k is less than the maximum of function dF/dz . If the cantilever holder is positioned in point z_1 , the force of attraction would bend the cantilever and the tip would be in point A which is the intersection of the curve $F(z)$ and the straight line from point z_1 , with the slope $\tan \alpha = -k$, according to the conditions of force equilibrium

$$F(z) = k \times dx(z_1) \text{ with } dx(z_1) = z_2 - z_1$$

Now construct the plot of $dx(z)$ versus the holder position (fig. 2 (b)) for decreasing z . In point B, where $dF/dz = k$ upon force equilibrium law, the condition of stable equilibrium is violated because $dF/dz > k$ to the left of the point, which situation forces the tip move to point C. The plot $dx(z)$ would exhibit a jump. As z decreases, the function $dx(z)$ is virtually a straight line with a slope of unity because of strong dependence of $F(z)$ asymptotically approaching the Y axis. In point D, the sign change of $dx(z)$ occurs, and this point can be termed the point of surface contact the point of surface touching. A set of these points describe the surface from the viewpoint of touching S_{tch} . By measuring the parameters of the $dx(z)$ function, say, in an $N \times N$ square of point on the surface under study, we can reconstruct the relief S_{tch} , and create a map of heights of the constant gradient S_{tap} . If any other measurement X is made on the $N \times N$ points, this would give an additional map of the surface S_x by the parameter X . The property measured can be either the conductivity in the point C or the surface hardness as the slope of the function $dx(z)$ in the region of repulsion ($z < 0$).

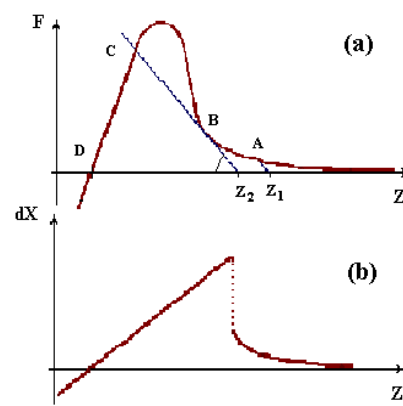


Fig.2.

MDM has peculiar abilities to explore surfaces with complex topography and large differences of heights. Moreover, it allows to exclude uncontrollable interaction of probe with sample, and artifacts caused by scanning process. In study of soft delicate objects the MD-mode can combine gentle action of tapping mode and non-contact mode with minuteness and high resolution of contact mode. The MDM image of the surface gives simultaneous and independent information about various surface layers including adsorbed layers and substrate. MDM solves problems associated with contamination and impurities. It opens the broad opportunities to study electrical, magnetic and polarization properties of surface and layers (including opportunities similar to Electric Force microscopy, Magnetic Force microscopy, Lift mode, Polarization mode, Scanning Tunneling microscopy and Scanning Tunneling Spectroscopy) together with adhesive forces and mechanical properties measurements (including opportunities similar to Phase Imaging mode, Force Modulation mode, Lateral Force mode).

Below we present obvious example to demonstrate the potentialities of the method MDM. Research being held at the SPM-spectroscope "ForceMaster-402MD" (Russia) and electro conductive probe has also been used. A fragment of the matrix of golden islands on the surface of GaAs is presented in fig. 3 (a). The gold was based into the semiconductor to obtain an ohmic contact. The corresponding map of conductivity is shown in fig. 3 (b), which was measured on the sample at +0,3 V. The MD-mode image of the map of conductivity demonstrates that only golden islands have electrical conduction, and electric current isn't leak across of substrate of the GaAs.

The physical ground of the MDM provides the capability to register and build map of any kind of information the scanning probe microscopy does. Moreover, MDM enables to register the data inaccessible for other modes.

In MD-mode extraction of the surface topography and its properties, quantity of surface layers, their thickness, configuration and properties are not separated in time [5]. All measurements are carried out in the current point of surface simultaneously. It makes measured quantities comparable allowing to correct one using or relative the others, to divide the information on the surface object properties and the substrate surface, to build the distribution maps associated with and relative to the surface topography.

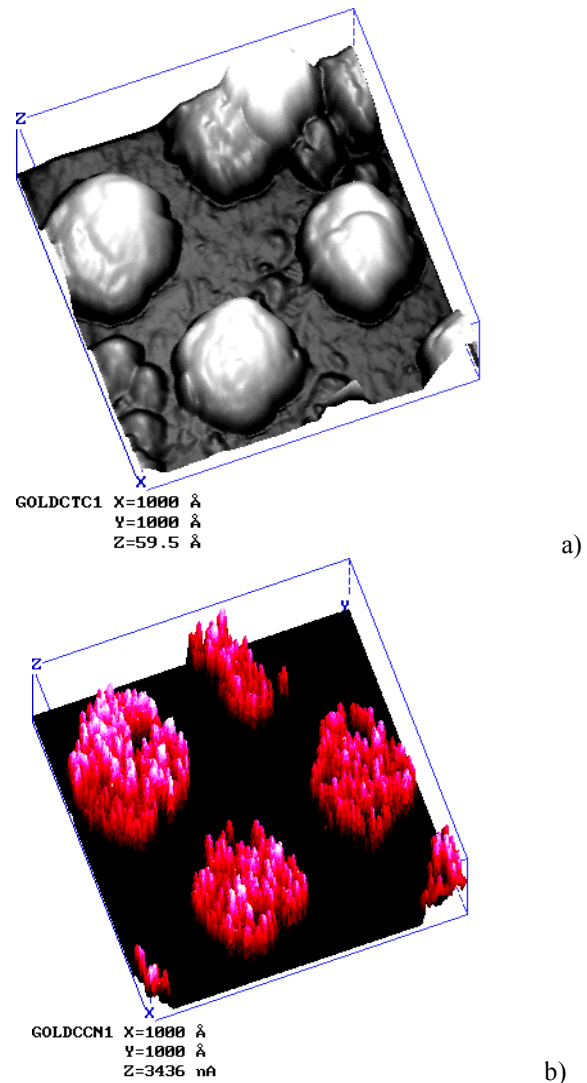


Fig. 3.

It's why the MDM image reflects the true picture of surface layers and their characteristics. The wide opportunities of MDM allows to obtain the results exclusive on the informational content, resolution and trustworthiness with high efficiency and reproducibility.

-
- | | |
|--|---|
| [1] G. Binnig, H. Rohrer. Helv. Phys. Acta. 1982, v. 55, pp. 726-735.
[2] R.Z. Bakhtizin. Sorosovskiy obrazovatelskiy j., 2000, t. 6, № 11, s. 1. (in Russian).
[3] S.P. Molchanov and etc. Patent № 2145055, Russia Federation. | [4] S.P. Molchanov, V.V. Dremov. All-Russian conference "Probe microscopy 99", Nizhny Novgorod, march 1999
[5] S.P. Molchanov, I.A. Chernova-Kharaeva, S.H. Abdullayeva, S.D. Alekperov. I International Scientific Seminar "Light in Nanosize Solids", Baku, 2004, September 22-28 (Proceeding of the Conference, pp. 47-48). |
|--|---|

S.P. Molçanov, S.H. Abdullayeva, İ.A. Çernova-Haraeva, İ.C. Ələkbərov

RASTR ZOND MİKROSKOPİYASININ ÇOX PARAMETRLİ METODİKASI

Rastr zond mikroskopu "ForceMaster-402MD" (Rusya) konstruktiv və funksional olaraq işləmə prinsipi müxtəlif olan iki cihazı özündə birləşdirir – rast tunnel mikroskopu və atom-güclü mikroskopu. Bütün bunlar istənilən cismin və dielektrikin səthində misilsiz dəqiq tədqiqatların aparılmasına imkan verir. Bu cihaz unikal çox parametrlü metodika ilə təchiz olunmuşdur (metod patentləşdirilib), hansı ki, səthin topoqrafiyası ilə birlikdə obyektin bölünmə növünün təyin edilmə xəritəsini almağa imkan verir (elektrikkeçirmə və s.).

С.П. Молчанов, С.Г. Абдуллаева, И.А. Чернова-Хараева, С.Д. Алекперов

**МЕТОД МНОГОПАРАМЕТРОВОГО РЕЖИМА В СКАНИРУЮЩЕЙ ЗОНДОВОЙ
МИКРОСКОПИИ**

Сканирующий зондовый микроскоп “ForceMaster-402MD” (Россия) конструктивно и функционально объединяет в себе два прибора с различным принципом работы – сканирующий туннельный микроскоп и атомно-силовой микроскоп. Все это позволяет с необходимой детальностью исследовать поверхности любых веществ с любой степенью проводимости, а также поверхности любых диэлектриков. Этот прибор оснащен уникальной, так называемой многопараметровой методикой (метод запатентован), которая дает возможность одновременно с топографией исследуемой поверхности получать карты распределения электрических, магнитных и поляризационных характеристик поверхности.

Received: 12.01.05

VISCOSEITY METHOD FOR THE DESCRIBING OF DYNAMICAL SYSTEMS

E.A. AKHUNDOVA

*Institute of Physics of National Academy of Sciences of Azerbaijan,
Az-1143, H. Javid av., 33*

Three types of nonlinear partial differential equations of polynomial form are considered and explicit substitutions of dependent variables, which transform the equations under study to linear equations, are obtained. Some nonlinear second order partial differential equations, which can be solved by the viscosity method, are also obtained

Introduction

The problem of finding exactly solvable nonlinear partial differential equations has very popular after discovering the inverse scattering method [1] and it still attracts the attention of many authors[2]. There are also some other methods of obtaining exact solutions of nonlinear equations: see [3-6]. However, in spite of variety of forms, all methods know till now are based after all on the very simple idea-to reduce the problem of solving the given nonlinear equation by means of some transformations to the problem of solving a more simple equation, which has been already studied. In the most of cases, people try to reduce nonlinear problems to linear ones because the theory of linear equations is well elaborated, although sometimes the reduction to a more simple nonlinear equation is also used.

Therefore, the following important and interesting problem arises: to describe the class of nonlinear equations which can be reduced by means of some transformations to linear equations.

One of possible ways of solving this problem is to apply all kinds of transformations to a given class of linear equations and to analyze the nonlinear equations thus obtained [7-8]. Of course, this class of equations is very small in comparison with the class of all exactly solvable equations. Nonetheless, we know this small class contains some physically interesting equations, for example, the Burgers-

Hopf equation [9]. We hope that the methodical study of all possible substitutions of variables and the initial linear equations may lead to some new exactly solvable nonlinear equations being of physical interest.

In this paper, we investigate some nonlinear equations obtained from linear partial differential equations of the second order by substitutions of dependent variables.

Nonlinear forms of linear equations

Since equations occurring in physical applications contain the derivatives with respect to the time variable t , as a rule, not higher than of the second order, we consider the nonlinear forms of the following general linear partial differential equation of the second order

$$a\psi_t + b\psi_{kt} + c\psi_{tt} + d\psi_{xx} = 0 \quad (1)$$

where a, b, c and d are arbitrary functions of variables x and t .

Making the substitution

$$\psi = \exp(\alpha\varphi + \beta\varphi_x + \gamma\varphi_t) \quad (2)$$

we obtain the following equation (we confine ourselves to the equations of polynomial type):

$$\begin{aligned} & a(\alpha\varphi_t + \beta\varphi_{xt} + \gamma\varphi_{tt}) + b(\alpha^2\varphi_t \cdot \varphi_x + \alpha\gamma\varphi_{tt}\varphi_x + \alpha\beta\varphi_t\varphi_{xx} + \beta^2\varphi_{xt} + \beta\gamma\varphi_{tt} \cdot \varphi_{xx} + \gamma^2\varphi_{tt}\varphi_{xx} + \alpha\gamma\varphi_t\varphi_{xt} + \\ & + \beta\gamma\varphi_{xt} + \alpha\varphi_{xt} + \beta\varphi_{xt} + \gamma\varphi_{tt}) + c(\alpha^2\varphi_t^2 + \beta^2\varphi_{xt}^2 + \gamma^2\varphi_{tt}^2 + 2\alpha\beta\varphi_{xt}\varphi_t + 2\alpha\gamma\varphi_{tt}\varphi_t + 2\beta\gamma\varphi_{xt}\varphi_{tt} + \alpha\varphi_{tt} + \\ & + \beta\varphi_{xtt} + \gamma\varphi_{ttt}) + d(\alpha^2\varphi_x^2 + \beta^2\varphi_{xx}^2 + \gamma^2\varphi_{tx}^2 + 2\alpha\beta\varphi_{xx}\varphi_x + 2\alpha\gamma\varphi_{tx}\varphi_x + 2\beta\gamma\varphi_{xx}\varphi_{tx} + \alpha\varphi_{xx} + \beta\varphi_{xxx} + \gamma\varphi_{txx}) = 0 \end{aligned} \quad (3)$$

$$\varphi_{xxx} + \varphi_{xtt} + N(\varphi_{xx}, \varphi_{tt}, \varphi_{xt}, \varphi_x, \varphi_t, \dots) = 0 \quad (6)$$

(and symmetrically $x \leftrightarrow t$)

It is not difficult to show that the equation of type (4) is obtained from eq.(3) provided

$$b=c=\gamma=0 \quad (7)$$

that is, we have the following equation:

$$a(\alpha\varphi_t + \beta\varphi_{xt}) + d(\alpha^2\varphi_x^2 + \beta^2\varphi_{xx}^2 + 2\alpha\beta\varphi_{xx}\varphi_x + \alpha\varphi_{xx} + \beta\varphi_{xxx}) = 0 \quad (8)$$

which is reduced to the equation

$$a\psi_t + d\psi_{xx} = 0 \quad (9)$$

by the replacement

$$\psi = \exp(\alpha\varphi + \beta\varphi_x) \quad (10)$$

The equation of type (5) is obtained from eq.(8) provided either

$$\text{b)} \quad b=c=\beta=0 \quad (12)$$

a) $d=c=\gamma=0$

(11)

In the first case, we obtain the equation

$$a(\alpha\varphi_t + \beta\varphi_{xt}) + (\alpha^2\varphi_t\varphi_x + \alpha\beta(\varphi_{xt}\varphi_x + \varphi_t\varphi_{xx}) + \beta^2\varphi_{xt}\varphi_{xx} + \alpha\varphi_{xt} + \beta\varphi_{xxt}) = 0 \quad (13)$$

which is reduced to the equation

$$a\psi_t + b\psi_{xt} = 0 \quad (14)$$

by the substitution

$$\psi = \exp(\alpha\varphi + \beta\varphi_x) \quad (15)$$

In the second case, we have the equation

$$a(\alpha\varphi_t + \gamma\varphi_{tt}) + d[(\alpha\varphi_x + \gamma\varphi_{tx})^2 + \alpha\varphi_{xx} + \gamma\varphi_{txx}] \quad (16)$$

which is reduced to the equation

$$a\psi_t + d\psi_{xx} = 0 \quad (17)$$

$$a(\alpha\varphi_t + \beta\varphi_{xt}) + c[(\alpha\varphi_t + \beta\varphi_{xt})^2 + d(\varphi_{tt} + \varphi_{xx}) + (\alpha\varphi_x + \beta\varphi_{xx})^2 + \beta(\varphi_{xxx} + \varphi_{xtt})] = 0 \quad (21)$$

which is reduced to the equation

$$a\psi_t + c(\psi_{xx} + \psi_{tt}) = 0 \quad (22)$$

by the replacement

$$a[\varphi_t + \beta(\varphi_{xt} - \varphi_{tt})] + b[\alpha^2(\varphi_t\varphi_x + \varphi_x^2) + \alpha\beta(\varphi_{xt}\varphi_x - \varphi_{tt}\varphi_x + \varphi_t\varphi_{xx} - \varphi_t\varphi_{xt} + 2\varphi_{xx}\varphi_x - 2\varphi_{tx}\varphi_x) + \beta^2(\varphi_{xt}\varphi_{xx} - \varphi_{tt}\varphi_{xx} + \varphi_{tt}\varphi_{tx} - \varphi_{xt}\varphi_{xx}^2 - \varphi_{tx}^2 - 2\varphi_{xx}\varphi_{tx}) + \alpha(\varphi_{xt} + \varphi_{xx}) + \beta(\varphi_{xxx} - \varphi_{xtt})] = 0 \quad (24)$$

which is reduced to the equation

$$a\psi_t + b(\psi_{xt} + \psi_{xx}) = 0 \quad (25)$$

by the replacement

$$\psi = \exp(\alpha\varphi + \beta\varphi_x - \beta\varphi_t) \quad (26)$$

The viscosity method

Let us investigate in detail equation (8). It is convenient to introduce a new notation

$$\begin{aligned} a\alpha &= \alpha & d\beta &= k \\ a\beta &= N & d\beta &= c \end{aligned} \quad (27)$$

The equation (8) assumes the following form

$$L\varphi_t + N\varphi_{xt} + \frac{L^2k}{N^2}\varphi_x^2 + k\varphi_{xx}^2 + 2\frac{Lk}{N}\varphi_{xx}\varphi_x + \frac{LC}{N}\varphi_{xx} + C\varphi_{xxx} = 0 \quad (28)$$

Apparently, using the substitution $x' = \alpha x$ one can always equate the coefficients L and N . Then the equation (8) assumes the form

$$C(\varphi_{xxx} + \varphi_{xx}) + 2k\varphi_{xx}\varphi_x + k\varphi_{xx}^2 + k\varphi_x^2 + N(\varphi_t + \varphi_{xt}) = 0 \quad (29)$$

Accordingly, equations (9) and (10) rewritten as follows:

$$N\varphi_t + C\varphi_{xx} = 0 \quad (9a)$$

$$\psi = \exp\left[\frac{k}{c}(\varphi + \varphi_x)\right] \quad (10a)$$

VISCOSITY METHOD FOR THE DESCRIBING OF DYNAMICAL SYSTEMS

Now let us note that the equation (29) can be used to find the solution of following equation:

$$2K\varphi_{xx}\varphi_x + k\varphi_{xx}^2 + k\varphi_x^2 + N(\varphi_t + \varphi_{xt}) = 0 \quad (30)$$

Indeed, if φ_c is a solution of equation (29) then the function

$$\varphi = l \lim_{c \rightarrow 0} \varphi_c \quad (31)$$

can be considered as a formal solution of eq. (30).

Such a method of solving equations is often called "the viscosity method".

Let us write the explicit forms of some other equations, which can be solved by this method.

Making analogical (27) substitutions and equating the coefficients L_i and N_i ($i=1,2,3,4$)

one can rewrite the equations (13), (16), (21), (24) correspondingly and obtain ($c_i \rightarrow 0$) equations, which can be solved by the viscosity method

$$K_1(\varphi_{xt}\varphi_{xx} + \varphi_{xi}\varphi_x + \varphi_t\varphi_x) + N_1(\varphi_t + \varphi_{xt}) = 0 \quad (13')$$

$$K_2(2\varphi_{tx}\varphi_x + \varphi_{tx}^2 + \varphi_x^2) + N_2(\varphi_t + \varphi_{xt}) = 0 \quad (16')$$

$$K_3(2\varphi_{xx}\varphi_x + \varphi_{xx}^2 + \varphi_x^2 + 2\varphi_{xt}\varphi_t + \varphi_{xt}^2 + \varphi_t^2) + N_3(\varphi_t + \varphi_{xt}) = 0 \quad (21')$$

$$K_4(\varphi_t\varphi_x + 2\varphi_x^2 - \varphi_{tt}\varphi_x + \varphi_t\varphi_{xx} - \varphi_t\varphi_{xt} + 2\varphi_{xx}\varphi_x - \varphi_{tx}\varphi_x - \varphi_{tt}\varphi_{xx} + \varphi_{tt}\varphi_{tx} - \varphi_{xt} + \varphi_{tx}^2 - \varphi_{xx}\varphi_{tx}) + N_4(\varphi_t + \varphi_{xt} - \varphi_{tt}) = 0 \quad (24')$$

In conclusion we note, that general properties, exact solutions and soliton-like solutions of obtained equations will be discussed in another paper.

The author expresses his acknowledgements to Prof. V.I.Man'ko and Doc. V.V.Dodonov for useful discussions.

- | | |
|--|--|
| [1] C.S.Gardner, J.M.Greene, M.D.Kruskal and R.M.Miura. Phys. Rev.Lett., 1967, v.19, p.1095.
[2] L.D.Faddeev. Modern Problem of Mathematics, 1974, v.3,p.93, Moscow, (in Russian)
[3] F.Calogero. Nuovo Cimento, 1976, vol. 31B, p.229
[4] J.Dziarmaga, Phys. Rev. Lett.,1998, vol.81, №8, p.1551.
[5] V.V.Dubrovskyi, A.N.Tipko, UMN,2001,t.56, vip.3. s.163. | [6] K.Takemura, Journ. of Phys.A,2002, vol.35,№41, p.8867.
[7] V.V.Dodonov and V.I.Man'ko. P.N.Lebedev Phys. Instit. Preprint №209, 1977.
[8] E.A.Akhundova, V.V.Dodonov, V.I.Man'ko. P.N.Lebedev Phys. Instit. Preprint №225, 1978.
[9] E.Hopf Commun Pure Appl. Math., 1950,vol.3, p.201. |
|--|--|

E.A. Axundova

KVANT DİNAMİK SİSTEMLƏRİ TƏSVİRİNDE QATILAŞMA METODU

Polinomşəkilli fərdi törəmələrdə qeyri-xətti differensial tənliklərin üç növünə baxılıb və araşdırılan tənlikləri xətti tənliklərə gətirən asılı dəyişənlərin əvəzolunmasının dəqiq ifadəsi alınmışdır. Həmçinin qatlaşma metodu ilə həll edilə bilən II dərəcəli fərdi törəməli bəzi differensial tənliklər alınmışdır.

Э.А. Ахундова

МЕТОД ВЯЗКОСТИ В ОПИСАНИИ КВАНТОВЫХ ДИНАМИЧЕСКИХ СИСТЕМ

Рассмотрены три типа нелинейных дифференциальных уравнений в частных производных полиномиального вида и получены явные выражения замен зависимых переменных, которые сводят исследуемые уравнения к линейным. Также получены некоторые дифференциальные уравнения в частных производных второго порядка, которые могут быть решены методом вязкости.

Received: 24.03.05

PHASE TRANSITIONS IN CuAgS_{0.5}Se_{0.5}

Yu.G. ASADOV, R.B. BAYKULOV, Yu.I. ALIYEV

*Institute of Physics of National Academy of Sciences of Azerbaijan,
Az-1143, H. Javid av., 33*

CuAgS_{0.5}Se_{0.5} monocrystals were synthesized and grown. Phase transitions were investigated by high temperature x-ray analysis. It's been shown, that at room temperature crystals have two phases, and one of the phases has structure of Cu_{1.96}S and the other of CuAgSe. Both phases at 695 K turn to single FCC lattice with parameter $a=6.356 \text{ \AA}$.

In [1] it has been determined that CuAgS crystals at room temperature are crystallized into orthorhombic structure with lattice parameters $a=4.06 \text{ \AA}$, $b=6.66 \text{ \AA}$, $c=7.99 \text{ \AA}$, space group D¹⁷_{2h} – Cmcm, Z=4, $\rho=6.4 \text{ g/cm}^3$. The only thing about polymorphism mentioned in [1], is that at 366 K low temperature orthorhombic modification turns to hexagonal one that is identical to β -Cu₂S ($a=4.005 \text{ \AA}$, $c=6.806 \text{ \AA}$, Z=2, space group P6₃/mmm)[2].

In [3] phase transitions in CuAgS were investigated. It has been shown that low temperature orthorhombic modification at 400 K turns to hexagonal and the hexagonal one in its part turns at 705 K to high temperature FCC with $a=5.7288 \text{ \AA}$. Crystal turns back to its initial state when cooled.

Partial replacement of 50% Se atoms by Te atoms and its influence on phase transitions in CuAgS_{0.5}Te_{0.5} were also investigated in [3]. It has been shown that at room temperature CuAgS_{0.5}Te_{0.5} consist of three phases, one of them iden-

tical, as regards lattice size, to low temperature monocline Cu_{1.96}S [4], another one has lattice of low temperature orthorhombic phase of Cu₂Te [5] and the last one has lattice of low temperature orthorhombic CuAgS [1]. CuAgS_{0.5}Te_{0.5} consist of three phases and at 720±1 K turns to single FCC phase with lattice parameter $a=6.531 \text{ \AA}$.

In present paper the influence of partial replacement of 50% of S atoms by Se atoms on structure and temperatures of phase transitions in CuAgS_{0.5}Se_{0.5} has been investigated. The conditions of crystal synthesis and growth did not differ from those of CuAgS and CuAgS_{0.5}Te_{0.5} [3].

An X-ray diffractometric temperature investigation was conducted in a “DRON-3M” diffractometer with a temperature attachment URVT-2000 in vacuum (10^{-1} Pa). Angular resolution was $\approx 0.1^\circ$. Diffraction angles were measured with an accuracy $\Delta\theta=\pm 0.02^\circ$.

Table 1

XRD data for CuAgS_{0.5}Se_{0.5} (Fe-filtered, CoK α radiation, $\lambda_\alpha=1.7902 \text{ \AA}$, 55kV, 12mA).

T, K	Θ	I/I ₀	D _{exp.} Å	CuAgSe		Ag ₂ Se		Lattice Parameters, Å
				d _{calc.} Å	hkl	d _{calc.} Å	Hkl	
293	1	2	3	4	5	6	7	9
	18° 00'	30	2.897	2.898	243	2.890	150	Cu _{1.96} S Monocline $a=26.897$ $b=15.515$ $c=13.585$ $Z=8$ S.G. P2 _{1/n} $\rho_x=5.870 \text{ g/cm}^3$
	19° 30'	80	2.682	2.690	10 0 0	2.681	042	
	20° 24'	100	2.568	2.569	044			
	21° 36'	50	2.432	2.437	162			
	23° 30'	70	2.245	2.245	942			
	25° 06'	40	2.110	2.111	326			
	25° 36'	50	2.072	2.073	11 2 3			
	26° 36'	60	1.999	1.998	645	2.012	220	
	28° 24'	90	1.882	1.882	027	1.890	191	
	31° 24'	40	1.718	1.717	275, 390	1.710	0 10 2	
	33° 42'	50	1.163	1.614	038			
	37° 24'	10	1.474	1.473	908, 286			
	39° 06'	30	1.419	1.419	938	1.411	243	
373	41° 24'	10	1.354	1.354	078, 1 0 10			S.G. D ⁷ _{2h} – P4/nmm $Z=10$ $\rho_x=7.895 \text{ g/cm}^3$
	45° 54'	10	1.247	1.246	0 5 10	1.247	0 10 4	
	48° 00'	20	1.205	1.205	0 6 10	1.204	115	
	17° 55'	30	2.909	2.910	243	2.909	150	
	19° 28'	80	2.686	2.686	10 0 0	2.684	042	
	20° 19'	100	2.578	2.579	044			
	21° 27'	45	2.448	2.447	132			
	23° 28'	70	2.248	2.248	942			
	25° 00'	40	2.118	2.118	326			
	25° 33'	50	2.075	2.074	11 2 3			
	26° 32'	60	2.004	2.004	645	2.014	220	
	28° 18'	90	1.888	1.888	027	1.906	191	
	31° 17'	35	1.724	1.724	275, 390	1.724	0 10 2	
	33° 34'	45	1.619	1.619	038			
	37° 17'	10	1.478	1.478	908			
	38° 59'	25	1.423	1.423	938	1.411	243	

PHASE TRANSITIONS IN CuAgS_{0.5}Se_{0.5}

	41° 12'	10	1.359	1.359	1 0 10			
	45° 44'	10	1.250	1.250	0 5 10	1.250	0 10 4	
	47° 46'	20	1.209	1.209	0 6 10	1.201	115	
473	17° 49'	30	2.925	2.926	243	2.925	150	$\text{Cu}_{1.96}\text{S}$ $a=26.905$ $b=15.852$ $c=13.753$ $\rho_x=5.673 \text{ g/cm}^3$
	19° 26'	75	2.691	2.691	10 0 0	2.712	042	
	20° 10'	100	2.596	2.597	044			
	21° 22'	50	2.456	2.456	162			
	23° 24'	70	2.254	2.255	942			
	24° 45'	40	2.138	2.138	326			
	25° 27'	50	2.083	2.082	11 2 3			
	26° 30'	60	2.006	2.006	645	2.030	220	
	28° 00'	90	1.907	1.908	027	1.915	191	
	31° 05'	40	1.734	1.734	275, 390	1.734	0 10 2	
	33° 12'	50	1.635	1.635	038			
	36° 55'	10	1.490	1.490	908, 286			
	38° 37'	30	1.434	1.434	938	1.425	243	
	40° 39'	10	1.374	1.374	078, 1 0 10			
	45° 11'	10	1.262	1.262	0 5 10	1.262	0 10 4	
	47° 12'	20	1.220	1.221	0 6 10	1.216	115	
573	17° 47'	30	2.931	2.931	243	1.931	150	$\text{Cu}_{1.96}\text{S}$ $a=26.936$ $b=15.893$ $c=13.775$ $\rho_x=5.643 \text{ g/cm}^3$
	19° 24'	80	2.694	2.964	10 0 0	1.716	042	
	20° 07'	100	2.602	2.602	044			
	21° 20'	45	2.460	2.460	162			
	23° 22'	70	2.257	2.258	942			
	24° 42'	40	2.142	2.142	326			
	25° 25'	50	2.086	2.085	11 2 5			
	26° 17'	60	2.022	2.021	645	2.039	220	
	27° 56'	90	1.911	1.910	027	1.923	191	
	31° 02'	35	1.736	1.737	275	1.741	0 10 2	
	33° 08'	45	1.638	1.638	038			
	36° 51'	10	1.493	1.493	908			
	38° 32'	25	1.437	1.437	938	1.430	243	
	40° 35'	10	1.376	1.376	1 0 10			
	45° 06'	10	1.264	1.264	0 5 10	1.266	0 10 4	
	47° 06'	20	1.222	1.222	0 6 10	1.218	115	
673	17° 44'	30	2.939	2.937	243	2.939	150	$\text{Cu}_{1.96}\text{S}$ $a=26.936$ $b=15.893$ $c=13.775$ $\rho_x=5.620 \text{ g/cm}^3$
	19° 23'	80	2.697	2.696	10 0 0	2.720	042	
	20° 05'	100	2.606	2.606	044			
	21° 15'	50	2.466	2.467	162			
	23° 20'	70	2.260	1.260	942			
	24° 40'	40	2.145	1.145	326			
	25° 24'	50	2.087	2.087	11 2 3			
	26° 15'	60	2.024	2.024	645	2.039	220	
	27° 54'	90	1.913	1.913	027	1.923	191	
	30° 57'	40	1.740	1.740	275	1.741	0 10 2	
	33° 05'	50	1.640	1.640	038			
	36° 48'	10	1.494	1.494	908			
	38° 29'	30	1.438	1.438	938	1.430	243	
	40° 32'	10	1.377	1.377	1 0 10			
	45° 01'	10	1.266	1.266	0 5 10	1.266	0 10 4	
	47° 00'	20	1.224	1.244	0 6 10	1.220	115	
773	16° 19'	40	3.176	3.185	200			FCC $a=6.356$ S.G. Fm3m $Z=4$ $\rho_x=6.376 \text{ g/cm}^3$
	23° 30'	65	2.246	2.245	220			
	27° 52'	100	1.915	1.915	311			
	29° 12'	70	1.834	1.835	222			
	34° 19'	30	1.588	1.588	400			
	37° 54'	80	1.457	1.458	331			
	39° 04'	30	1.420	1.420	420			
	43° 39'	50	1.297	1.297	422			
	47° 04'	90	1.222	1.223	333, 511			
873	16° 16'	40	3.196	1.182	200			FCC $a=6.363$ $\rho_x=6.355 \text{ g/cm}^3$
	23° 27'	65	2.250	1.250	220			
	27° 49'	100	1.918	1.919	311			
	29° 10'	70	1.837	1.837	222			
	34° 16'	30	1.590	1.591	400			
	37° 51'	80	1.459	1.460	331			
	39° 02'	30	1.422	1.423	420			

	43° 36'	50	1.298	1.299	422		
	47° 01'	40	1.224	1.225	333		
973	16° 13'	40	3.205	1.186	200		FCC $a=6.372$ $\rho_x=6.328 \text{ g/cm}^3$
	23° 24'	65	2.254	1.253	220		
	27° 46'	100	1.921	1.921	311		
	29° 07'	70	1.840	1.840	222		
	34° 13'	30	1.592	1.593	400		
	37° 49'	80	1.460	1.462	331		
	39° 00'	30	1.422	1.425	420		
	43° 33'	50	1.299	1.301	422		
	46° 58'	90	1.225	1.226	333		

At 293 K the XRD patterns from $5 \times 5 \times 1$ mm arbitrary oriented $\text{AgCuS}_{0.5}\text{Se}_{0.5}$ single-crystal showed 16 diffraction peaks. Indexing of patterns confirms existence of two phases, the first is identical to monocline $\text{Cu}_{1.96}\text{S}$ [4], the second – to low temperature orthorhombic CuAgSe [6].

All 16 diffraction peaks (Table 1) can be indexed on the basis of lattice parameters of orthorhombic $\text{Cu}_{1.96}\text{S}$, 8 of them also can be indexed on the basis of orthorhombic CuAgSe .

After the patterns were recorded at room temperature, the furnace was turned on and reference recordings were taken

every 100 K without disturbing the original crystal orientation. The sample temperature prior to every record was kept constant for 40 minutes.

At 773 K 9 peaks were recorded that belong to high temperature FCC modification with $a=6.356 \text{ \AA}$, $Z=4$, space group Fm3m. The transition temperature was determined from disappeared peaks when both phases turn to FCC at $T_i=695 \pm 2$ K.

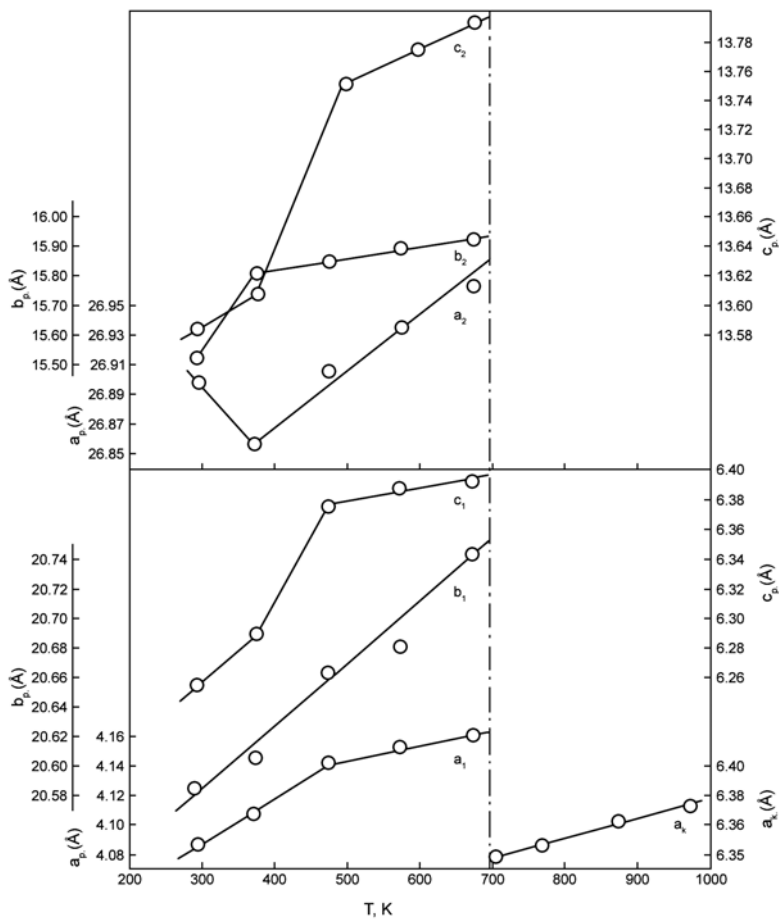


Fig. 1. Temperature dependence of lattice parameters in $\text{CuAgS}_{0.5}\text{Se}_{0.5}$

Fig 1 shows temperature dependence of lattice parameters. As we see, lattice parameters a_1 , b_1 , c_1 of monocline $\text{Cu}_{1.96}\text{S}$ deviate from linearity at 373 K, parameters b_1 and c_1 quickly increase and a_1 decreases and linearly grows after 373 K. Lattice parameters a_2 and c_2 of modifications identical to orthorhombic CuAgSe structure, deviate from linearity at

473 K. In spite of such changing in lattice parameters of both phases with temperature, there is not much difference in number and intensity of diffraction peaks.

Table 2 contains coefficients of thermal expansion calculated using temperature dependence of lattice parameters. As we can see, the thermal expansion for modification identical

to Cu_{1.96}S along [010] significantly differ from that along [100] and [001] ($\alpha_{[100]} < \alpha_{[010]} > \alpha_{[001]}$). It's significant that in low temperature monocline modification, S atom layers form hexagonal close packages and Cu atoms are distributed

among them in 3 different ways. In this structure 51 of Cu atoms distributed in distorted triangles, 9 – in tetrahedral spaces and one is in double coordination. Some of Ag atoms might replace Cu atoms.

Table 2

Thermal expansion coefficients for CuAgS_{0.5}Se_{0.5}

Modification	Temperature K	$\alpha_{[100]} 10^{-6} K^{-1}$	$\alpha_{[010]} 10^{-6} K^{-1}$	$\alpha_{[001]} 10^{-6} K^{-1}$	$\bar{\alpha} = \frac{\sum \alpha_i}{3} \cdot 10^{-6} K^{-1}$
Orthorhomb. Cu _{1.96} S	293-373	-19.05	238.48	21.16	80.20
	293-473	1.65	120.67	68.70	63.67
	293-573	5.18	87.01	49.95	47.38
	293-673	6.46	68.86	40.29	38.54
Orthorhomb. CuAgSe	293-373	64.24	79.75	197.21	113.73
	293-473	76.14	35.44	87.65	66.41
	293-573	57.69	28.18	61.47	49.11
	293-673	47.66	28.71	46.97	41.11
FCC CuAgS _{0.5} Se _{0.5}	773-873	0.11			0.11
	773-973	0.13			0.13

In CuAgSe lattice, Ag atoms situated in planes perpendicular to c axis. Near each of them, there are 4 Ag atoms at 2.96 Å and 6 Se atoms at 2.67 Å (4 Se), 3.59 Å (1 Se), 3.64 Å (1 Se). Se atoms form elongated tetrahedrons in which Cu atoms situated. Distance between Se atoms is Se-Se=3.30 Å, between Cu and Se is from 2.06 Å to 2.50 Å and the least one is Cu-Ag=2.98 Å.

Thermal expansion coefficient of phase crystallized as CuAgSe structure has anisotropy along basic crystallographic directions ($\alpha_{[100]} \approx \alpha_{[010]} > \alpha_{[001]}$). Strong anisotropy of thermal expansion of both phases is one of the main reasons of thermal instability of low temperature phase. We should note, that monocline Cu_{1.96}S at 377 K turns to FCC phase with

$a=5.707$ Å and CuAgSe at 504 K turns to FCC phase ($a=5.082$ Å) as well. In our case that doesn't happen, i.e. both phases (Cu_{1.96}S and CuAgSe) turn to FCC phase ($a=6.356$ Å) at 695 K at the same time.

At room temperature CuAgS_{0.5}Se_{0.5} crystals consist of 2 phases and while heated, as seen from thermal expansion anisotropy, deform each other. The nucleus of high temperature FCC phase is formed in the interface of these two phases and grows at the expense of both phases. When cooled, FCC phase splits in two and crystal turns to initial state. Phase transitions are reversible and take place by single-poly crystal model.

-
- [1] J. Frueh, Zeits. Krist. 1955, 106, p. 299.
 [2] N.B. Belov, V.A. Butuzov, Докл. АН СССР, 1964, т.54, №8, с. 717.
 [3] F.Yu. Asadov, R.B. Baykulov, S.S. Gamidova, F.G. Magerramova, Vtoraya mejdunarodnaya konferentsiya po fizike kristallov «Kristallographiya XXI veka» posveshennaya pamjati M.P. Shaskolskoy, 2003.
 [4] H. T. Evans. Zeits. Krist., 1979, 150, p. 299.
 [5] J. Patzak, Z. Metallkund., 1956, 47, p. 433.
 [6] J. Frueh, G. K. Czamanske, C. H. Knight, Zeits. Krist., 1957, 108, p. 389.

Y.H. Əsədov, R.B. Baykulov, Y.İ. Əliyev

CuAgS_{0.5}Se_{0.5} KRİSTALINDA POLİMORF KEÇİD

CuAgS_{0.5}Se_{0.5} tərkibi sintez edilmiş və monokristalı alınmışdır. Yüksek temperatur difraktometrik metodu ilə polimorf keçid tədqiq edilmiş və göstərilmişdir ki, otaq temperaturunda kristal iki fazalıdır. Fazalardan biri Cu_{1.96}S strukturasını, digəri isə AgCuSe-nin strukturasını qəbul edir. Hər iki faza 695 K-də səthinə mərkəzləşmiş kubik fazaya keçir.

Ю.Г. Асадов, Р.Б. Байкулов, Ю.И. Алиев

ПОЛИМОРФНЫЕ ПРЕВРАЩЕНИЯ В CuAgS_{0.5}Se_{0.5}

Синтезированы и выращены монокристаллы CuAgS_{0.5}Se_{0.5}. Высокотемпературным рентгенографическим методом исследованы полиморфные превращения. Показано, что при комнатной температуре кристаллы - двухфазные, одна из фаз принимает структуру Cu_{1.96}S, а другая - CuAgSe. Обе фазы при 695 К превращаются в единую ГЦК модификацию с параметром $a=6.356$ Å.

Received: 09.02.05

SCISSORS MODE IN THE γ -SOFT NUCLEUS ^{134}Ba

E. GULİYEV

Institute of Physics, Academy of Science of Azerbaijan, H.Cavid avenue 33, Baku, Azerbaijan

F. ERTUĞRA

Physics Department, Faculty of Arts and Sciences, Sakarya University, Adapazari, Turkey

M. GÜNER

Mathematics Department, Faculty of Arts and Sciences, Sakarya University, Adapazari, Turkey

Z. DEMİR

Electric and Electronic Department, Faculty of Engineering, Sakarya University, Adapazari, Turkey

In this study the scissors mode is investigated for γ -soft nucleus ^{134}Ba . Calculations have been made using Quasiparticle Random Phase Approximation method. With the selection of suitable separable effective isoscalar and isovector forces, rotational invariance is restored for the description of the M1 modes. Our calculations show that, results obtained here are in a good agreement with the experimental data. In this work, contribution of $\Delta K=0$ branch of $I^\pi=I^+$ states to scissors mode region has been investigated, as well. Calculations show that most of the M1 transitions have $\Delta K=1$ character.

I. INTRODUCTION

Recently, great success has been achieved in the measurement of nuclear excitations with low multipolarity [1]. One of them is the observation of strong low-lying magnetic dipole excitations in deformed nuclei, which are frequently referred to as a scissors mode. The study of these excitations gives valuable information about nuclear structure and nucleon-nucleon forces at low energy. In a geometrical picture [2] the scissors mode is visualized as a counter rotational oscillation of the deformed proton body against the deformed neutron body in the intrinsic frame of reference. This mode was first observed in high-resolution electron scattering experiments in Darmstadt [3]. A series of subsequent nuclear resonance fluorescence (NRF) experiments (see e.g., Refs [4]) established the systematic of this common mode in deformed even-even nuclei at excitation energies around 3 MeV. The remarkable features of the scissors mode obtained from experimental results are the quadratic dependence of the summed $B(\text{M}1)$ values on the ground state deformation parameter δ and the strong fragmentation of the M1 strength about the pairing gap up to 4 MeV excitation energy [5-8]. Properties of scissors mode have been investigated for deformed nuclei in detail. Recently the scissors mode was observed in ^{196}Pt [9]. This was the first observation of the scissors mode in a deformed nucleus with a soft triaxiality. After than this mode else has been obtained for nucleus from another wide region of γ -soft triaxiality for ^{134}Ba [10]. In spite of the nature of scissors mode is an open question in nuclei near shell closures where the simple geometrical picture of a scissors-like motion of deformed proton and neutron bodies breaks down. There were only some more experiments else for nucleus from these regions [11]. Unfortunately explicit parity determination is not upper degree in those experiments. Therefore, only with the advent of the new generation of experimental facility with improved detection characteristics it is possible to investigate in detail the fine structure of the M1 response [12]. Earlier, the scissors mode calculations for ^{134}Ba [13]

had been made using RPA method. In that work, the broken symmetry of the nuclear Hamiltonian is reached by adding to it only some effective isoscalar forces [13]. However, here certain difficulties immediately arise when the isovector quadrupole coupling constant is chosen. Generally, an isovector dependence of effective forces can arise from the breaking of rotational invariance by the isovector term in the mean-field potential.

Based on these observations the aim of the present work is to investigate the nature of the scissors mode of nucleus ^{134}Ba using RPA method, where broken rotational invariance restored adding effective isoscalar and isovector forces [8]. This approach is self-consistent, since the coupling constants and matrix elements of the effective interactions are, in turn, connected with the characteristics of the deformed field. This method of restoring broken symmetries successfully has been applied to the well deformed and spherical nuclei were restored rotational or transitional invariance [8,14-17]. Here we also investigate the contribution $\Delta K=0$ branch of $I^\pi=I^+$ states to the scissors mode region.

II. THEORY

A detailed description $I^\pi;K=I^+;I$ states generated by the isovector spin-spin interactions in rotational invariant Quasiparticle Random Phase Approximation (QRPA) was given in Ref [8]. There, by the selection of suitable separable effective isoscalar and isovector forces, rotational invariance is restored for the description of the M1 modes for $\Delta K=1$ branches without introducing any additional parameters. In this approximation, the model Hamiltonian of the system can be written

$$H = H_{\text{sqp}} + h_0 + h_1 + V_{\sigma\tau} \quad (1)$$

where H_{sqp} is the quasiparticle Hamiltonian with pairing interactions, h_0 and h_1 describe the effective isoscalar and isovector interactions restoring the rotational invariance of the quasiparticle Hamiltonian which are important only for $\Delta K=1$ branch of the I^+ states.

Here we followed the methods and notations of Ref.[8]. According to Ref.[8] the rotational invariance of the single-quasiparticle Hamiltonian can be restored with the aid of a separable isoscalar and isovector effective interaction of the form

$$h_0 = -\frac{1}{2\gamma_0} \sum_{\mu} [H_{sqp} - V_1, J_{\mu}]^+ [H_{sqp} - V_1, J_{\mu}] \quad (2)$$

$$h_1 = -\frac{1}{2\gamma_1} \sum_{\mu} [V_1, J_{\mu}]^+ [V_1, J_{\mu}] \quad (3)$$

where, V_1 is the isovector part of nuclear potential and J_{ν} are the spherical components of the total angular momentum for the $K^{\pi}=I^+$ excitations. Here, γ_0 and γ_1 are the coupling parameters. $V_{\sigma\tau}$ isovector spin-spin interactions that generated the I^+ states in the deformed nuclei have the form

$$V_{\sigma\tau} = \frac{1}{2} \chi_{\sigma\tau} \sum_{i \neq j} \vec{\sigma}_i \vec{\sigma}_j \vec{\tau}_i \vec{\tau}_j \quad (4)$$

where, $\vec{\sigma}$ and $\vec{\tau}$ are the Pauli matrices that represent the spin and the isospin, respectively.

Due to the symmetries of the effective restoring forces, spin- spin interactions and the magnetic dipole operator, the most characteristic quantity of I^+ state is the reduced $M1$ transition probability, which can be written in the form [8]

$$\begin{aligned} B(M1; 0^+ \rightarrow 1_i^+) &= \\ &= \frac{3}{4\pi} \left| R_p(\omega_i) + \sum_{\tau} (g_s^{\tau} - g_l^{\tau}) R_s^{\tau}(\omega_i) \right|^2 \mu_N^2 \end{aligned} \quad (5)$$

Here g_s and g_l are the spin and orbital gyromagnetic ratios of the free nucleons, respectively.

The energy-weighted sum rules for $M1$ transitions are given as

$$2 \sum_i \omega_i B(M1; 0^+ \rightarrow 1_i^+) = [\vec{\mu}^+, [H, \vec{\mu}]]_{RPA} \quad (6)$$

In the RPA, right-hand side of the this sum rule can be obtained

$$\begin{aligned} [\vec{\mu}^+, [H, \vec{\mu}]]_{RPA} &= \frac{3}{4\pi} [\gamma_p + \sum_{\tau} (g_s^{\tau} - g_l^{\tau}) \delta^{\tau} - \\ &- \frac{(\gamma_p - \gamma_l^p)^2}{\gamma - \gamma_1} - \frac{\gamma_l^{p2}}{\gamma_1}] \mu_N^2 \end{aligned} \quad (7)$$

where

$$\begin{aligned} \gamma_{\tau} &= 2 \sum_{\mu} {}^{(\tau)} \varepsilon_{\mu} L_{\mu}^2 j_{\mu}^2 ; \\ \delta_{\tau} &= 2 \sum_{\mu} {}^{(\tau)} \varepsilon_{\mu} L_{\mu}^2 j_{\mu} s_{\mu} . \end{aligned}$$

Since the effective forces h_0 and h_1 are not commutative with the $J_{\pm 1}$ operators besides the H_{sqp} part of the Hamiltonian, they also contribute to the sum rules (7). In this formula, the last two, which represent the contributions of the isoscalar and isovector effectively restoring forces to the sum rule, are important.

Another important quantity of the orbital I^+ states is excitation energies. In order to establish the average energy of the $M1$ strength below 4 MeV we use the energy weighted and not energy weighted sum rules,

$$\overline{\omega} = \frac{\sum_i \omega_i B(M1, \omega_i)}{\sum_i B(M1, \omega_i)} . \quad (8)$$

III. RESULTS AND DISCUSSION

In numerical calculations, the experimental value of deformation parameter $\delta=0.161$ of the ^{134}Ba were taken from the ref.[18]. The Nilsson single-particle energies were obtained from Warsaw deformed Wood-Saxon potential [19]. All energy levels from the bottom of the potential well to 6 MeV were considered for neutrons and protons. The pair-interaction constants Δ and λ were chosen in accordance with Soloviev [20]. For the strength parameter of the isovector spin -spin interactions we used $\chi_o=40/\text{MeV}$, which has been obtained from magnetic moments calculations. To show important restoration broken symmetry we present here result of calculation obtained without any restoration, result taken from ref [21] where restored only broken isoscalar forces and result of calculation obtained using restored broken isoscalar and isovector forces of the mean field potential. The calculated I^+ excitation energies and the corresponding $B(M1)$ values are shown in Fig.1. As can be seen in Fig. 1 calculations made without any restoration gives for scissors mode summed $B(M1)=4.163 \mu_N^2$ strength with 8 levels.

The results obtained using only isoscalar restoring forces taken from Ref.[21] give summed $B(M1)=0.49 \mu_N^2$ with only 2 levels (in Ref[21], the level obtained at the energy $E=395 \text{ keV}$ has not been interpreted as scissors mode level). Despite the fact that the results above give the scissors mode like distribution, they are not in agreement with the experimental results.

According to Ref.[8] using isoscalar and isovector restoring forces to restoration the broken rotational invariants, we obtain the sum $\sum_i B(M1; 0_1^+ \rightarrow 1_i^+) = 0.60 \mu_N^2$ with 10 levels, where ratio $l/s>1$. These levels can be interpreted as a scissors mode. Comparison this result with the results above we observe that the consideration of the isoscalar and isovector restoring forces causes the splitting of the states with large $B(M1)$ strengths and fragments the $M1$ strength into more levels.

Where experiment obtained the total $M1$ strength summed over all states, where $J^{\pi}=I^+$ is at least tentatively assigned, amounts to $\sum_i B(M1; 0_1^+ \rightarrow 1_i^+) = 0.56 \mu_N^2$ strength with 6 levels [10] (Fig.1). Due to the low cross sections, firm assignments of

spins and parities were not possible for many levels [10]. Although the experiment had been performed in correct spin and parity for only one state, it was assumed that some of the other states were also scissors mode states. So the total strength of the scissors mode in ^{134}Ba presumably does not deviate too much from the value $\sum_i B(M1; 0_1^+ \rightarrow 1_i^+) = 0.56\mu_N^2$. But for correct determination of scissors mode strength in this region the parity measurement is necessary.

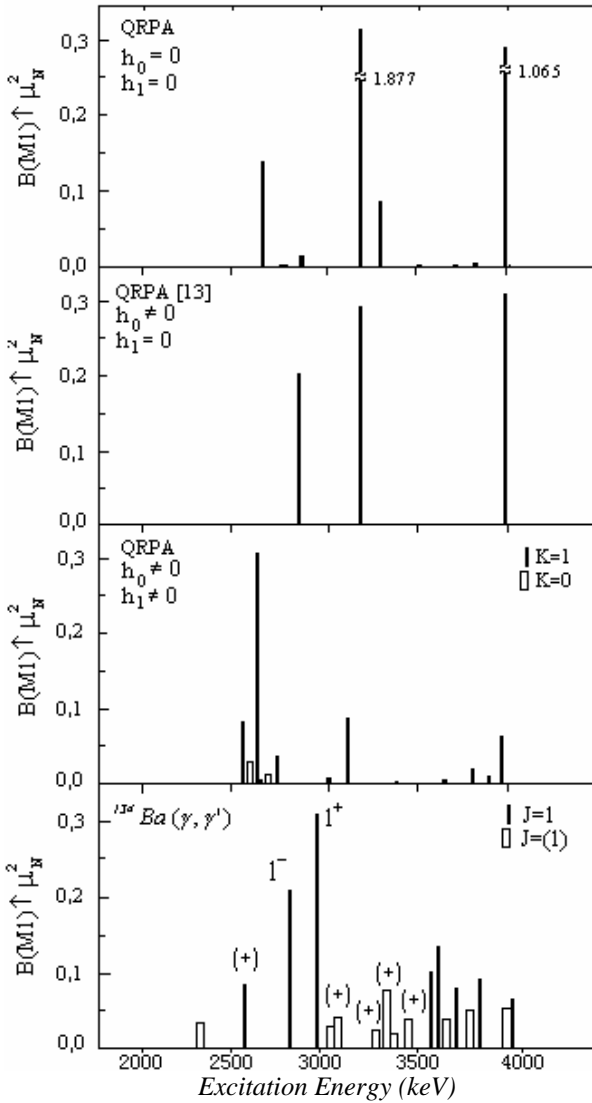


Fig. 1. Spectral distribution of the dipole excitations strength in the ^{134}Ba nucleus

Our theoretical calculations gives for ^{134}Ba several collective I^+ state (mainly $\Delta K=1$ branch) in the energy interval 2.5- 4 MeV with an energy centroid $\bar{E}=2.9$ MeV. Also experiment show dipole strength distribution in ^{134}Ba extracted from the measured photon scattering cross sections in the energy range up to 4MeV with an energy centroid $\bar{E}=2.987$ MeV. As can be seen results obtained in this work are in good agreement with experiment. Comparison results are given in Table 1.

Table 1. Comparison RPA calculation with Experimental Results of $I^\pi; K=1^+$; I states of ^{134}Ba

RPA Calculations [21]	RPA Calculation (This Work)	Experimental Results [10]			
\bar{E} (MeV)	$\sum_i B(M1)$ μ_N^2	\bar{E} (MeV)	$\sum_i B(M1)$ μ_N^2	\bar{E} (MeV)	$\sum_i B(M1)$ μ_N^2
3.07	0.49	2.9	0.6	2.987	0.56(4)

Our results is also in a good agreement with empirical sum rule for the excitations strength of the scissors mode obtained from the $B(E2)$ value

$$B(M1)_{sc} \hat{=} \frac{10.6}{Z^2} B(E2; 0_1^+ \rightarrow 2_1^+) \quad (9)$$

This has been formulated in Ref.[22]. From the known $B(E2)$ values of ^{134}Ba , using formula (9) we have obtained $B(M1)_{sc} \hat{=} 0.61(2) \mu_N^2$, which is in agreement with the our theoretical value and experiment.

As can be seen in Fig1., the experiment shows the I^+ state at energy $E=2939$ keV with a relatively large M1 excitation strength of $B(M1; 0^+ \rightarrow I^+) = 0.307 \mu_N^2$. This level is only one level where made correct parity and multipolarity determination. The corresponding excitation obtained from our calculation at energy $E=2612$ keV with $B(M1; 0^+ \rightarrow I^+) = 0.305 \mu_N^2$. Also theory predicts 1^+ state at energy $E=2583$ keV, with excitation strength of $B(M1) = 0.083 \mu_N^2$, so experiment gives spin one state at energy $E=2571$ keV, with excitation strength of $B(M1) = 0.081 \mu_N^2$ which can be attributed to magnetic dipole transition. According with the results obtained here we can say experimental observed spin one state at energy $E=2571$ keV may have positive parity.

Furthermore, above an excitation energy of 3500 keV experimentally eight states where observed, four of them with spin assignment $J=1$. Experiment according to Ref. [21] were restored only isoscalar forces and expected that the magnetic dipole excitations above 3500 keV have a low orbit-to-spin ratio and thus do not belong to the scissors mode. However our rotational invariant RPA calculation predicts three high orbit-to-spin ratio ($I/s > 1$) levels with summed excitation strength of $B(M1) \hat{=} 0.086 \mu_N^2$. It has been shown that some of observed strengths in experiment above 3500 keV are in orbital character. This situation shows that without any correct spin determination it is no right makes any comment.

Here we also made calculation for $\Delta K=0$ branch of $I^\pi=1^+$ states. The obtained summed $B(M1)$ value for $\Delta K=0$ is $B(M1; K^\pi=0^+) = 0.045 \mu_N^2$ with only two strength (Fig.1). Our results showed that likely the deformed nuclei [23] in γ -soft nuclei, all stronger M1 transitions were $\Delta K=1$ character. Where $\Delta K=0$ branch take only 8 % of all strength.

IV. CONCLUSION

Results obtained here show that using isovector and isoscalar effective forces fragmented the scissors mode of appropriate with fragmentation with deformed rare earth nuclei but gives the scissors mode strength amounts to about 1/5 of the strength in typical deformed nuclei. These results are suitable with experiment. Besides this, our calculations show the important consideration of the isovector restorating forces in calculations. These results point out, the choice of the isoscalar and isovector forces in a self-consistent manner based on the rotational invariance of the Hamiltonian makes it possible to treat the scissors mode more rigorously without any extra quadrupole-quadrupole interaction parameter and results

gained in this case has been found to be in a close proximity to the experimental data.

Recent experiments show that the scissors mode is fundamental excitation mode of γ -soft nuclei. Our theoretical calculations give same results and show that above 3500 keV it is possible to obtain scissors mode levels. Our calculations also show that all stronger magnetic dipole strengths are from $\Delta K=1$.

ACKNOWLEDGEMENTS

We wish to express our thanks to Prof. Dr. A.A. Kuliev and Dr. I. Okur for his most careful reading of the manuscript and useful comments.

-
- [1] A.Richter, Prog. Part. Nucl. Phys. 34, 1995, 261
 - [2] N. Lo Iudice. Phys. Rev. Lett. 41, 1978, 1532.
 - [3] D.Bohle et al. Phys. Lett. B137, 1984, 27.
 - [4] U. Kneissl et al. Prog. Part. Nucl. Phys. 37, 1996, 349.
 - [5] W. Ziegler et al. Phys. Rev. Lett. 65, 1990, 2515.
 - [6] J. Margraf et al. Phys. Rev. C 47, 1993, 1474.
 - [7] P. von Neumann-Cosel et al. Phys. Rev. Lett. 75, 1995, 4178.
 - [8] A.A.Kuliev et al. Int. Journ. of Mod. Phys. E 9, 2000, 249.
 - [9] P von Brentano et al. Phys. Rev. Lett. 76, 1996, 2029.
 - [10] H. Maser et al. Phys. Rev. C 54, 1996, R2129.
 - [11] R.-D. Herzberg et al. Phys. Rev. C 60, 1999, 051307.
 - [12] E.Guliyev et al. Int. Journ. of Mod. Phys. E 11, 2002, 501.
 - [13] H. Harter, Phys. Lett. B 205, 1988, 174.
 - [14] N. Pyatov and D. Salamov Nucleonika 22, 1977, 127.
 - [15] A.A. Kuliev et al. Jour. of Phys. G 28, 2002, 407.
 - [16] E. Guliyev et al. Phys. Lett. B 532, 2002, 173.
 - [17] Linnemann et al. Phys. Lett. B 554, 2003, 15.
 - [18] S. Raman et al. Atomic Data and Nuclear Data Tables, 2001, 78.
 - [19] J. Dudek, T.Werner, Journ. Phys. G 4, 1978, 1543.
 - [20] V.G. Soloviev "Theory of Complex Nuclei" Pergamon Press, New York, 1976.
 - [21] H.Harter et al. Phys. Lett. 1988, B205, 174.
 - [22] N.Pietralla et al. Phys. Rev. C 52, 1995, R2317.
 - [23] M. Scheck et al. Phys. Rev., 2003, C 67, 064313

Ə. Guliyev, F. Ertuğral, M. Güner, Z. Demir

γ -SOFT BÖLGƏSINDƏ YERLƏŞƏN ^{134}Ba NÜVƏSİNİN QAYÇI MOD HƏYƏCANLANMALARI

Məqalədə qayçı modu (scissors mode) səviyyələri γ -soft nüvəsi olan ^{134}Ba nüvəsi üçün tədqiq edilmişdir. Hesablamalar QRPA (Quasiparticle Random Phase Approximation) yanaşması bazasında aparılmışdır. Uyğun izoskalar və izovektor effektiv qüvvətləri seçilərək $M1$ səviyyələri üçün rotasion invariantlıq bərpa edilmişdir. Məqalədə əldə edilən nəticələr təcrübə nəticələrlə uyğunluq təşkil edir. Bundan başqa $I^\pi=1^+$ həyəcanlanmaların $\Delta K=0$ budağının qayçı modu bölgəsinə əlavəsi də tədqiq edilmişdir. Hesablamalar $M1$ səviyyələrin bir çoxunun $\Delta K=1$ budağına aid olduğunu göstərdi.

Е. Гулиев, Ф. Ертуграл, М. Гунер, З. Демир

НОЖНИЧНАЯ МОДА СОСТОЯНИЯ ДЛЯ ЯДРА ^{134}Ba ИЗ РЕГИОНА γ -СОФТ

В статье была изучена ножничная мода (scissors mode) состояния для ядра из региона γ -софт ^{134}Ba . Вычисления были произведены в рамках QRPA (Quasiparticle Random Phase Approximation). Для $M1$ переходов с выбором соответствующих изоскалярных и изовекторных эффективных сил была реставрирована нарушенная ротационная инвариантность. Результаты, полученные здесь, соответствуют данным, полученным из экспериментов. Кроме того, здесь было произведено вычисление для $\Delta K=0$ ветви $I^\pi=1^+$ возбуждения. Было показано, что большинство из $M1$ состояний принадлежит ветви $\Delta K=1$.

Received: 23.02.2005

COLLECTIVE 1^+ STATES IN $^{176,178}\text{Hf}$ DEFORMED NUCLEI

H. YAKUT, M. BEKTAŞOĞLU, F. ERTUĞRAL AND R. AKKAYA

*Physics Department, Faculty of Arts and Sciences, Sakarya University,
54100 Serdivan, Adapazarı, Turkey*

In this study, properties of the collective $I^\pi = 1^+$ ($K=0$ and $K=1$) states, generated by the residual paired and isovector spin-spin interactions, in the deformed nuclei $^{176,178}\text{Hf}$ are investigated in the Quasiparticle Random Phase Approximation (QRPA) method using the deformed Saxon-Woods Potential. Furthermore, contribution of $M1$ transition matrix element to the energy weighted sum rules and energy distribution of $M1$ excitation strength functions were investigated for these states. We have observed that the low-lying 1^+ states have weak correlations and small value of $B(M1, 0 \rightarrow 1)$, and the collective 1^+ states with larger values of $B(M1)$ are in the energy region 8-10 MeV for $K = 0$ and 10-12 MeV for $K = 1$. We have also shown that the number of states for $K = 0$ is less than $K = 1$ states.

INTRODUCTION

Magnetic dipole excitations in heavy nuclei are of considerable interest in modern nuclear structure physics. Both low lying orbital and high lying magnetic resonance excitations were studied systematically to test nuclear models. An outstanding example is the so-called $M1$ scissors mode to which most attention was paid in the past. This low-lying orbital 1^+ states were first observed in ^{156}Gd in high resolution inelastic (e, e') reactions in 1984 [1]. Two of the important properties of these states are their low energy ($\omega \leq 4$ MeV) and having a value for their reduced magnetic dipole probability $B(0^+ \rightarrow 1^+)$ in the interval $0.6-1.8 \mu_N^2$. The different aspects of the magnetic dipole transition of 1^+ states have been investigation in inelastic proton scattering at small angles for the nuclei ^{154}Sm , ^{156}Gd and ^{164}Dy [2]. Before these experimental studies, existence of a state with the energy $E=3.18$ MeV and $B(M1, 0^+ \rightarrow 1^+) = 1.8 \mu_N^2$ in the nucleus ^{168}Er was observed in theoretical calculations using quasiparticle model in the framework of RPA and taking into account the residual paired and spin-spin interactions [3]. Calculations have shown that collective states in the energy range 2-4 MeV and occur in the nuclei ^{154}Sm and ^{168}Er [4]. These states expected by the theory were experimentally studied using (γ, γ') resonance scattering reactions and a state with $E=3.39$ MeV and $B(M1) = (0.71 \pm 0.08) \mu_N^2$ was observed in the nucleus ^{168}Er [5].

Recently, magnetic dipole resonances ($I^\pi = 1^+$) have been experimentally found in wide region from light spherical nuclei up to actinides [6-11]. These experiments shown that a very broad $M1$ resonance at energies between 7 and 11 MeV exists in heavy spherical and deformed nuclei.

Spin-spin interactions in the spherical even-even nuclei happen in connection with the particle hole transitions between the spin-orbital elements of the neutron-neutron and proton-proton single particle states [12]. Unlike the potential of spherical nuclei, the picture is more complicated. In such case, the magnetic quantum number of every J-shell splits into excitations characterized by the angular momentum projection on the symmetry axis $K=0$ and $K=1$. Due to split mentioned, shell structure of the nucleus is destroyed and this causes an increase in the density of 1^+ states ($\rho \approx 10$ MeV $^{-1}$). Based on the information given, two independent branches

of 1^+ states, namely $K=0$ and $K=1$, exist due to axial symmetry in deformed nuclei. $K=0$ corresponds to the spin vibrations along with the symmetry axis, and $K=1$ corresponds to the perpendicular ones. $K=1$ branch is easy to investigate in photon scattering experiments since electromagnetic waves are transverse. Results of such experiments have shown that in low energy spectroscopic region $K=1$ states are denser compare to $K=0$ levels.

The well-known Random Phase Approximation (RPA) is one the most popular method in theoretical microscopic study of nuclear structure and describes many-body systems. In nuclear physics RPA has been exploited to model properties of the excited states that allows to calculate intensities of various nuclear reactions, including decay probability of electromagnetic, beta and double beta decay. For the nuclei away from closed shells there appear static pairing correlations within the quasi-particle representation is usually referred to as quasi-particle version of RPA(QRPA), which consider the quasi-particle correlations and excitations.

In this study, properties of $I^\pi = 1^+$ ($K=0$ and $K=1$) spin-vibration states in the even-even $^{176,178}\text{Hf}$ isotopes were studied using QRPA method. Contribution of $M1$ transition matrix element to the energy weighted sum rules and energy distribution of $M1$ excitation strength functions were investigated for these states.

THEORY

For a system with large number of particles, like nucleus, it is difficult to solve the Schrödinger equation due to large number of the degrees of freedom. Therefore, in the microscopic model, it is assumed that neutron and proton in the nucleus move in a common field produced by them and assumed that they interact with each other. It is based on the Shell model. In this model the component of the effective force responsible for the excitations is taken into account in the microscopic calculations.

Assuming that 1^+ states are produced by the spin-spin forces in deformed nuclei, Hamiltonian of the system can be chosen as

$$H = H_{sqp} + V_{\sigma\tau} \quad (1)$$

where H_{sqp} is the single quasi-particle Hamiltonian represented by

$$H_{sqp} = \sum_{s\tau} \varepsilon_s(\tau) (\alpha_s^+(\tau) \alpha_s(\tau) + \alpha_{\tilde{s}}^+(\tau) \alpha_{\tilde{s}}(\tau)) \quad (2)$$

In this expression, $\varepsilon_s = \sqrt{(E_s - \lambda)^2 + \Delta^2}$ is quasi-particle energy of the nucleons, and E_s is energy of the average field. Δ and λ are the gap and chemical potential parameters of the super fluid model, respectively. $\alpha^+(\alpha^-)$ are the quasi-particle creation(annihilation) operators.

The second term in Eq. 1

$$V_{\sigma\tau} = \frac{1}{2} \chi_{\sigma\tau} \sum_{i\neq j} \sigma_i \sigma_j \tau_i^z \tau_j^z \quad (3)$$

represents the isovector spin-spin interactions. Here, σ and τ are spin and isotropic Pauli matrices, respectively. All the unexplained expressions used here are given in Ref. [13].

The isovector spin-spin interactions can be written in terms of particle operators:

$$V_{\sigma\tau} = \chi_{\sigma\tau} \sum_{\mu=0,\pm 1} D_\mu^+ D_\mu^- \quad (4)$$

In case of $\chi_{np} = \chi_{pn} = q\chi$ and $\chi_{nn} = \chi_{pp} = \chi$ $q=-1$. In the quasi-particle representation the D_μ operator splits up into quasi-boson and scattering terms in the form

$$D_\mu(\tau) = \sum_{ss'} \sigma_{ss'} \left\{ \mu_{ss'} B_{ss'} + \frac{1}{\sqrt{2}} L_{ss'} (C_{ss'}^+ + C_{ss'}^-) \right\} + \sum_{ss'} \sigma_{\tilde{s}\tilde{s}'} \left\{ \mu_{ss'} \bar{B}_{ss'} - \frac{1}{\sqrt{2}} L_{ss'} (\bar{C}_{ss'}^+ + \bar{C}_{ss'}^-) \right\} \quad (5)$$

$$B_{ss'} = \sum_{\rho=\pm 1} \rho \alpha_{s\rho}^+ \alpha_{s'\rho}^- \quad B_{ss'}^+ = \sum_{\rho=\pm 1} \rho \alpha_{s'\rho}^+ \alpha_{s\rho}^- \quad (7)$$

Here, $M_{ss'} = u_s u_{s'} + v_s v_{s'}$ and $L_{ss'} = u_s v_{s'} + u_{s'} v_s$ are the Bogoliubov canonical transformation parameters, expressed through u_s and v_s , $D_\mu^{(\nu)} = \langle s | D_\mu | s' \rangle$ are single-particle matrix elements of the Pauli spin operator, and

$$C_{ss'} = \frac{1}{\sqrt{2}} \sum_{\rho=\pm 1} \rho \alpha_{s'\rho}^+ \alpha_{s-\rho}^- , \quad C_{ss'}^+ = \frac{1}{\sqrt{2}} \sum_{\rho=\pm 1} \rho \alpha_{s-\rho}^+ \alpha_{s'\rho}^- \quad (6)$$

are the quasi-particle operators. In RPA, collective 1^+ states are considered as one-phonon excitations given by

$$|\psi_i\rangle = Q_i^+ |\psi_0\rangle = \frac{1}{\sqrt{2}} \left[\sum_{n\neq i} \{\psi_{ss'}^i C_{ss'}^+ - \varphi_{ss'}^i C_{ss'}^-\} + \sum_{prot.} \{\psi_{vv'}^i C_{vv'}^+ - \varphi_{vv'}^i C_{vv'}^-\} \right] |\psi_0\rangle \quad (8)$$

where Q_i^+ is the phonon creation operator, $|\psi_0\rangle$ is the phonon vacuum. The two quasi-particle amplitudes $\psi_{ss'}$ and $\varphi_{ss'}$ are normalized by

$$\sum_{\mu\tau} [\psi_\mu^i(\tau) - \varphi_\mu^i(\tau)] = 1 \quad (9)$$

The dispersion equation for the excitation frequency w is obtained in the form

$$(1 + \chi F_n)(1 + \chi F_p) - q^2 \chi^2 F_n F_p = 0 \quad (10)$$

using a variational method and

$$\delta \left\{ \langle \psi | Q_i H Q_i^+ | \psi \rangle - \langle \psi | H | \psi \rangle - \omega_i \left(\sum_i (\psi_s^i)^2 - \varphi_s^i)^2 \right) - 1 \right\} = 0 \quad (11),$$

together with the RPA procedure. The roots of this equation gives the energy of 1^+ states.

MAGNETIC PROPERTIES OF THE COLLECTIVE 1^+ STATES

The characteristic quantity of the spin vibrational 1^+ states is the probability of the M1 transitions. The M1 transition operator is given by

where $\vec{\mu}$ is the magnetic dipole operator expressed as

$$\vec{\mu} = \sum_{\tau,i} [(g_s^\tau - g_l^\tau) \vec{s}_i^\tau + g_l^\tau \vec{J}_i^\tau] \quad (13)$$

In this equation, J is the total angular momentum operator, g_s^{τ} ve g_l^{τ} are the orbital and spin g factors of the

nucleons, respectively. Using Eqs. 8, 12 and 13, the M1 transition probability for the state 1⁺ can be written as

$$B(M1, 0 \rightarrow 1^+) = \frac{3}{16\pi} \left[\sum_{npt.} \mu_{ss'}^n L_{ss'} g_{ss'} + \sum_{prot.} \mu_{vv'}^p L_{vv'} g_{vv'} \right] \quad (14)$$

where $\mu_{ss'}^{(\tau)}$, μ are the single-particle matrix elements of the magnetic dipole operator.

SUM RULE

In quantum mechanics, the probability of a transition from one state to another is bounded by some definite relations called sum rules. There are two kinds of sum rules; energy-weighted (EWSR) and non-energy-weighted sum rule (NEWSR). The sum rules are used in the microscopic nuclear theory in order to investigate the properties of collective excitations. These rules, in case of an arbitrary potential, allow one to calculate the vibration of the giant dipole and quadrupole resonant energy.

For the case of M1 transitions, the EWSR is written as

$$\frac{1}{4} \langle \psi_0 | [\vec{\mu}, [H, \vec{\mu}]] \psi_0 \rangle = \frac{8}{3} \pi \sum_i \omega_i B_i (M1, 0^+ \rightarrow 1^+) \quad (15)$$

and we are specifically interested in the energy region of saturation of the right-hand side of Eq. 15, namely the energy dependence of the function

$$\chi_n(\omega_i) = \frac{8}{3} \pi \sum_i \omega_i B_i (M1, 0^+ \rightarrow 1^+) \quad (16)$$

The left-hand side of Eq. 15 does not depend on the strength parameter χ , and represents the quasi-particle estimate of the sum rule. Thus, the sum rules help one make conclusions about the accuracy of RPA solutions, while the

contribution of different 1⁺ states to the sum rule is given by the function χ .

NUMERICAL CALCULATIONS AND DISCUSSION

In calculations, the single-particle model is used taking the deformed Saxon-Woods potential as the average field potential. The Schrodinger Eq. is solved by means of the method mentioned in Ref. [14]. Calculations are performed for ^{176,178}Hf isotopes, the deformation parameters and interaction constants are taken from Ref. [15] and Ref. [16], respectively. For this reason, throughout this study, the RPA method with harmonic approach is used. The isovector spin-spin interaction constant is chosen as $\chi_{\sigma\tau} = 40/A$ [17].

Table 1.

Ton-pair correlation parameters and the deformation parameters for ^{176,178}Hf isotopes

A	N	δ^2	Δ_n	Δ_p	λ_n	λ_p
176	104	0.2731	0.655	0.75	-4.139	-6.098
178	106	0.2563	0.72	0.75	-3.664	-6.412

Calculations have shown that, small probability of the M1 transition from the ground state to the 1⁺ excitation levels appear in the energy region up to 5 MeV. Information on the low energy 1⁺ ($K=0$ and $K=1$) levels and the state structure of them for ^{176,178}Hf in the spectroscopic region is given in Table 2 and 3.

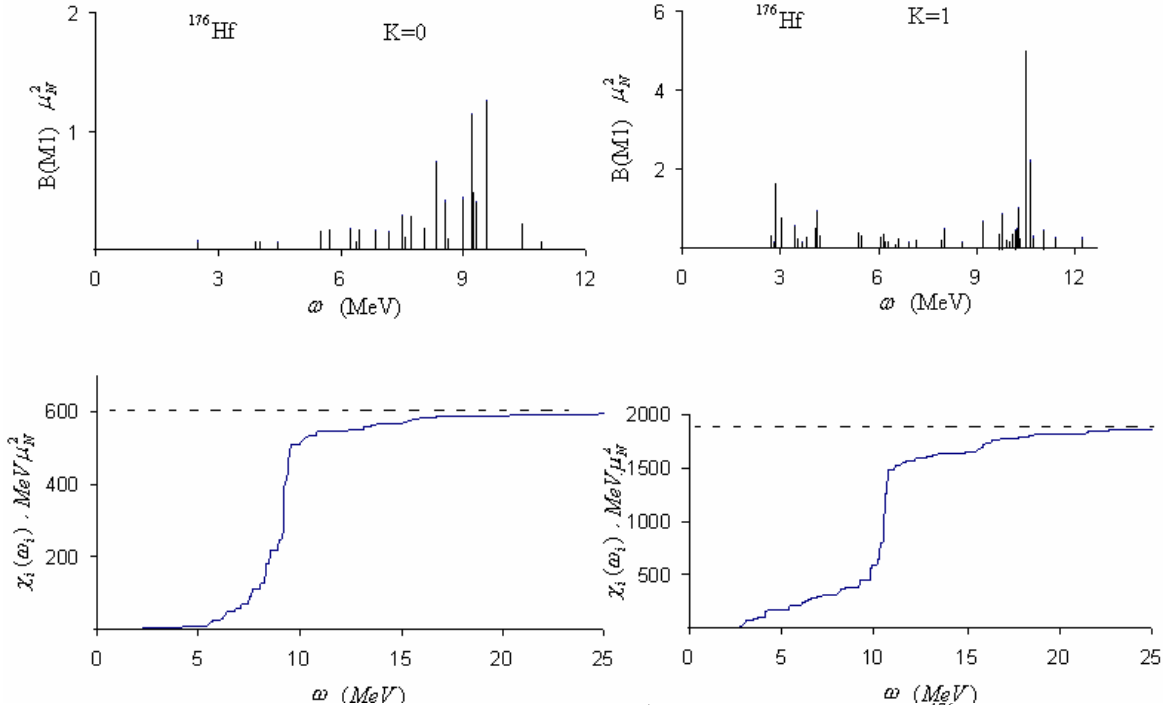


Fig. 1. Energy diagram of $B(M1)$ values (above) and sum rule for the 1⁺ states with $K=0$ and $K=1$ in ¹⁷⁶Hf. The left -hand side of the sum rule is shown by dotted line. The solid line corresponds to the function χ_i [Eq. 16].

COLLECTIVE 1⁺ STATES IN ^{176,178}Hf DEFORMED NUCLEI

Table 2.
The characteristic 1⁺ (K=0 and K=1) states and the transition probability B(M1) for ¹⁷⁶Hf in the spectroscopic energy region.

¹⁷⁶ Hf K=0				¹⁷⁶ Hf K=1			
Energy ω (MeV)	B(M1) (μ_N^2)	Amplitudes ψ_μ	Structure of states	Energy ω (MeV)	B(M1) (μ_N^2)	Amplitudes ψ_μ	Structure of states
5.717	0.159	-0.187 0.280 0.215 0.135 0.553	nn512-503 nn512-752 pp530-550 pp541-532 pp411-402	2.509	2.519	0.705	pp523-514
8.332	0.726	0.364 -0.236 -0.165 0.146 0.238 0.122 -0.186 -0.329	nn640-631 nn642-633 pp501-530 pp530-521 pp541-521 pp532-523 pp523-514 pp413-404	3.199	0.208	-0.704	pp550-532
8.544	0.399	0.278 -0.507 -0.132 -0.130 -0.263 -0.118	nn530-750 nn640-631 nn532-501 nn642-633 pp523-514 pp413-404	3.355	1.110	0.687	pp411-402
8.974	0.432	-0.529 -0.428	nn514-505 pp523-514	3.623	0.689	0.112 -0.149 0.658	nn660-631 nn631-642 pp413-404
9.228	1.144	-0.415 -0.102 -0.346 0.162 -0.190 0.287	nn530-501 nn642-633 nn514-505 pp431-640 pp532-512 pp523-514	4.417	0.722	-0.704	pp411-400
9.264	0.488	0.554 -0.191 0.279 -0.148 0.174	nn530-501 nn514-505 pp431-640 pp532-512 pp523-514	4.496	0.509	-0.704	pp411-402
9.540	1.252	-0.131 0.638 0.165	nn514-505 pp532-512 pp523-514	5.299	0.470	0.128 0.184	nn622-633 pp530-550
				6.530	0.435	0.183 -0.209 0.162 -0.240 0.221 0.132	nn651-651 nn501-523 nn613-624 nn505-505 pp530-532 pp532-523
				9.775	1.602	0.319 0.109 0.369 0.173	pp521-541 pp532-514 pp422-404 pp503-514
				9.981	0.527	0.224 -0.266 0.101 0.572	nn550-750 pp521-541 pp532-514 pp503-514
				10.350	1.529	0.462 0.212 -0.102 0.300 -0.192 -0.120	pp530-521 pp550-512 pp521-541 pp541-512 pp532-514 pp503-514
				10.600	4.028	0.178 -0.291 -0.107 0.113 -0.177 0.193 0.234 -0.144 -0.114	nn523-505 pp530-521 pp521-541 pp640-660 pp541-512 pp532-503 pp521-512 pp532-514 pp503-514
				10.640	0.666	-0.113 -0.645 -0.131	nn550-501 pp532-503 pp521-512
				10.784	0.854	-0.248 -0.613	nn523-505 pp640-660

Table 3.
The characteristic 1^+ ($K=0$ and $K=1$) states and the transition probability $B(M1)$ for ^{178}Hf in the spectroscopic energy region.

^{178}Hf $K=0$				^{178}Hf $K=1$			
Energy ω (MeV)	$B(M1)$ (μ_N^2)	Amplitudes ψ_μ	Structure of states	Energy ω (MeV)	$B(M1)$ (μ_N^2)	Amplitudes ψ_μ	Structure of states
5.716	0.194	-0.141 -0.354 0.556 -0.135 0.122	nn512-503 pp530-550 pp420-411 pp541-532 pp411-402	8.032	0.469	0.111 -0.458 -0.131 -0.131 0.294 0.107 0.237	nn660-651 nn631-651 pp550-301 pp420-400 pp420-402 pp541-523 pp512-523
6.341	0.415	-0.103 -0.148 -0.107 0.642	nn651-642 nn642-622 pp530-550 pp541-532	8.140	0.435	0.381 0.124 0.529	nn631-651 pp541-523 pp512-523
7.581	0.379	0.111 -0.164 0.124 0.367 -0.405 0.131 0.299	nn640-651 nn651-642 nn523-752 nn642-633 nn633-613 pp420-400 pp532-523	9.727	0.650	0.168 0.141 0.111 0.626	nn530-512 pp521-541 pp431-651 pp422-404
8.126	0.289	-0.137 -0.233 -0.182 -0.325 -0.114 0.480	nn640-631 nn642-633 pp530-521 pp541-521 pp523-514 pp413-404	9.820	1.780	0.516 0.137 -0.274	pp521-541 pp532-514 pp422-404
8.277	0.435	-0.411 -0.180 -0.153 -0.177 -0.451	nn640-631 nn642-633 pp541-521 pp523-514 pp413-404	10.029	0.707	-0.152 0.583 -0.241 0.200	nn530-510 nn510-532 pp521-541 pp532-514
9.026	2.293	0.237 0.132 -0.132 -0.109 -0.163 0.124 -0.239 0.476 -0.104	nn530-501 nn640-631 nn532-761 nn651-642 nn642-633 pp532-523 pp532-512 pp523-514 pp413-404	10.042	0.923	-0.421 -0.379 -0.247 0.256	nn530-510 nn510-532 pp521-541 pp532-514
9.363	1.018	0.651 0.157	pp532-512 pp523-514	10.058	0.909	0.543 -0.127 -0.217 0.298	nn530-510 nn510-532 pp521-541 pp532-514
9.746	0.116	0.551 0.433	nn514-505 pp550-510	10.254	1.856	-0.332 0.200 -0.139 -0.199 -0.403 0.135	pp301-521 pp530-521 pp521-541 pp411-422 pp532-514 pp503-514
9.756	0.160	0.420 -0.560	nn514-505 pp550-510	10.461	0.404	-0.357 -0.293 -0.212 0.450	pp530-521 pp411-431 pp541-512 pp503-514
				10.593	1.508	0.437 0.208 -0.192 -0.117 -0.307	nn642-402 nn503-514 pp530-521 pp541-512 pp503-514
				10.604	0.933	-0.552 -0.142 0.200 -0.219	nn642-402 pp530-521 pp532-303 pp503-514

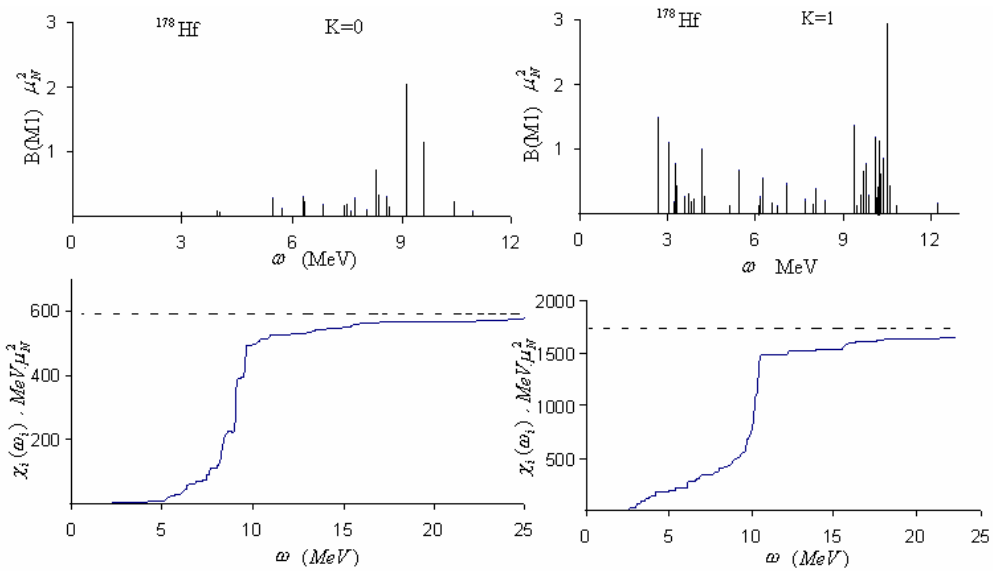


Fig. 2. Energy diagram of $B(\text{M1})$ values (above) and sum rule for the 1^+ states with $K=0$ and $K=1$ in ^{178}Hf . The left -hand side of the sum rule is shown by dotted line. The solid line corresponds to the function χ_i [Eq. 16].

Results of the calculations for $^{176,178}\text{Hf}$ nuclei are given in Figure 1 and 2. Probability of $B(\text{M1})$ transition as a function of energy for $I^\pi = 1^+$ ($K=0$ and $K=1$) excitations are shown in Fig. 1. As seen in the figure, there are several collective states with large transition probabilities ($B(\text{M1}) = (1.2 - 3.4)\mu_N^2$) exist for $\omega \leq 4$ MeV for these isotopes. There are many states between 4 and 12 MeV and

the most collective energy interval where these states are pached is 8-10 MeV for $K=0$ and 10-12 MeV for $K=1$.

ACKNOWLEDGMENT

We would like to acknowledge useful conversation with Prof. Dr. A. A. Kuliev and Dr. E. Gulyev.

-
- | | |
|---|---|
| [1] D.Bohle <i>et al.</i> Phys. Lett. B137, 1984, 27. | [12] Bohr and B. Mottelson, "Nuclear Structure"v.2, Benjamin, New York, Amsterdam, 1974. |
| [2] C. Djalali <i>et al.</i> Phys. Lett. B164, 1985, 269. | [13] F. Ertuğral, E. Gulyev, R. Akkaya and H.M. Tütüncü, Baküworkshop, Eylül 2004 |
| [3] N. Lo Iudice Phys. Rev. Lett. 1978, 41, 1532. | [14] F. A. Gareev, S. P. Ivanova and B. N. Kalinkin, Izv. Akad. Nauk SSSR (ser. fiz.) 32 (1968) 1960. |
| [4] U. Hartmann <i>et al.</i> Nucl. Phys. A 465, 1987, 25. | [15] S. Raman <i>et al.</i> Atomic Data and Nuclear Data Tables 78, 2001, 1. |
| [5] Willis <i>et al.</i> Nucl. Phys. Rev. A 499, 1989, 367. | [16] J. Margraf <i>et al.</i> , Phys. Rev. C 47 1993, 1474. |
| [6] J. Margraf <i>et al.</i> Phys. Rev. C 47, 1993, 1474. | [17] A. Nojarov and A. Faessler, Nucl. Phys. A 484, 1988, 1; Nucl. Phys. A 492, 1989, 105; Phys. Rev. C 41, 1990, 1243. |
| [7] R. D. Heil <i>et al.</i> Nucl. Phys. A 476, 1988, 39. | |
| [8] A.Richter. Nucl. Phys. A 507, 1990, 99. | |
| [9] B.S. Ishkanov <i>et al.</i> Phys. Of Atomic Nucl. 59, 1996, 1109. | |
| [10] H. Maser <i>et al.</i> Phys. Rev. C 54, 1996, R2129. | |
| [11] P. von Brentano <i>et al.</i> Phys. Rev. Lett. 76, 1996, 2029. | |

H. Yakut, M. Bektaşoğlu, F.Ertuğral, R. Akkaya, P. Akkaya

DEFORMASIYA OLMUŞ $^{176,178}\text{Hf}$ NÜVƏLƏRİNİN COLLEKTİV 1^+ SƏVIYYƏLƏRI

Məqalədə qalıq cütlənmə və izovektor spin-spin qarşılıqlı təsirləri tərəfindən yaradıldığı fərz edilən $I^\pi=1^+$ ($K=0$ və $K=1$) səviyyələrinin xüsusiyyətləri QRPA yanaşmasında deformasiya olmuş Saxon-Woods potensialı istifadə edilərək öyrənilmişdir. Ayrıca bu səviyyələrin M1 matris elemntlərinin enerji ağırlıqlı cəmləmə qanunlarına əlavəsi və M1 səviyyələrinin güc funksiyalarının enerji yayılması da öyrənilmişdir. Hesablamalar aşağı enerjilərdəki 1^+ səviyyələrinin zəif korellasiona və kiçik ehtimala sahib olduğunu göstərdi. $K=0$ budağının ən böyük ehtimallı səviyyələri 8-10 MeV bölgəsində, $K=1$ budağı üçün isə 10-12 MeV bölgəsində olduğu təyin edildi. Ayrıca $K=1$ budağına aid olan səviyyələrin sayının $K=0$ budağından daha çox olduğunu göstərildi.

Х. Якут, М. Бекташоглу, Ф.Ертуграли, Р. Аккайя

КОЛЛЕКТИВНЫЕ 1^+ СОСТОЯНИЯ ДЕФОРМИРОВАННЫХ ЯДЕР $^{176,178}\text{Hf}$

В статье было изучено свойство $I^\pi=1^+$ ($K=0$ и $K=1$) состояний, взаимодействующих посредством остаточных парных и изовекторных спин-спиновых взаимодействий для ядер $^{176,178}\text{Hf}$ в приближении случайных фаз (СФ) с использованием деформированного потенциала Саксона- Вуда. Кроме того, для этих состояний были изучены вклад M1 матричных

COLLECTIVE 1^+ STATES IN $^{176,178}\text{Hf}$ DEFORMED NUCLEI

элементов в закон энерговесомого суммирования и энергетическое распределение силовых функций для этих состояний. Вычисления показали, что низколежащие 1^+ состояния слабо коррелированы и маловероятны, так как для $K=0$ ветви возбуждения более вероятные состояния лежат в интервале 8-10 MeВ, а для $K=1$ ветви более вероятные состояния лежат в интервале 10-12 MeВ. Кроме того, было показано, что число состояний из ветви $K=1$ больше числа состояний из ветви $K=0$.

Received: 09.02.2005

QURĞUŞUN SELEN ƏSASINDA ALINMIŞ ƏRİNTİLƏRİN FİZİKİ XASSƏLƏRİNİN TƏDQİQİ (300 K)

**M.Ə. ƏLİCANOV, N.M. ORUCOV, A.O. MEHRABOV, S.M. ƏLİCANOVA,
N.U. İBAYEV**

*AZ-1073, Azərbaycan Memarlıq və İnşaat İnstitutu, Bakı, Ayna Sultanova küçəsi 5,,
1143, Bakı, Hüseyn Cavid, 33, MEA Kimya problemləri İnstitutu*

Qurğuşun selen birləşməsində CrSe-nin həll olma sahəsi müəyyən edilmiş, bərk məhlul sahəsindəki ərintilərin: 2,4,6 mol% tərkibli nümunələrin fiziki xassələri 300K temperaturda ölçülülmüşdür. PbSe birləşməsində olduğu kimi onun əsasındaki nümunələr də kub quruluşa malik olub, elektron tip yarımkəcəricilərdir. Həm əsas komponentin (PbSe) və onun əsasındaki ərintilərin: Termoelektrik parametrləri (Termo e.h.q., istilikkeçirmə, elektrikkeçirmə) ölçülülmüşdür. Holl effektini ölçməklə yükdaşıyıcıların konsentrasiyası və yürüklüyü hesablanmışdır.

$\text{Al}^{\text{IV}}\text{Bi}^{\text{IV}}$ tipli birləşmələr yarımkəcərici materiallar kimi geniş öyrənilmiş və hal-hazırda öyrənilməkdədir. Bu birləşmələr əsasında alınmış ərintilər praktiki və elmi cəhətdən tədqiqatçıları daha çox maraqlandırır. Həmin tip birləşmələrdən PbSe və onun əsasındaki ərintilər termofotoelektrik material kimi yarımkəcəricilər texnikasında geniş tətbiq olunur. PbSe sistemində 1361K temperaturunda əriyən bir konkurent birləşmə halını alır. Bu birləşmə kub quruluşda kristallaşaraq, kiçik qadağan olunmuş zolağa malik yarımkəcəricilərə aid olur [1,2].

Fiziki kimyəvi analiz metodlarından istifadə etmək $(\text{PbSe})_{1-x} \text{CrSe}_x$ sistemində PbSe tərəfdən 8 mol%-ə qədər (300K) bərk məhlul sahəsi müəyyən edilmişdir. PbSe birləşməsinin və 2,4,6 mol % CrSe tərkibli nümunələrin fiziki xassələri 300K temperaturunda ölçülülmüşdür. Cədvəl 1-də göstərilmişdir ki, kristal qəfəs sabiti tərkibdən asılı

olaraq artır və 6 mol% CrSe tərkibli nümunə üçün 6.31 Å olur. Bu artım Pb və Ni atomlarının ion radiuslarının müxtəlif olması ilə əlaqədardır. Elektrikkeçirmənin qiyməti PbSe üçün $362 \text{ om}^{-1}\text{sm}^{-1}$ olduğu halda, 6 mol % CrSe tərkibli nümunə üçün azalaraq $267 \text{ om}^{-1}\text{sm}^{-1}$ olur. Termo-e.h.q.nin qiyməti əksinə 282 mkv/dər ilə 312 mkv/dər qiymətləri arasında dəyişərək artır. İstilikkeçirmə tərkibdən asılı olaraq azalır, $12,62 \text{ Wt sm.dər}$ (PbSe üçün) isə $10,96 \text{ Wt/(sm.dər)}$ (6mol% CrSe tərkibli nümunə üçün) qiymətləri arasında dəyişir. Bu hal, bərk məhlul sahəsi üçün xarakterikdir. Yük daşıyıcıların komppensasiyası $4.7 \cdot 10^{18} \text{ sm}^{-3}$ ilə $6.6 \cdot 10^{19} \text{ sm}^{-3}$ qiymətləri arasında artdığı halda yükdaşıyıcıların yürüklüyü $958 \text{ sm}^2/(\text{v.san})$ ilə $972 \text{ sm}^2/(\text{v.san})$ arasında azalır. Bu isə tamamilə qanuna uyğun hesab edilə bilər.

($\text{PbSe})_{1-x}(\text{Cr Se})_x$ sistemli ərintilərin fiziki xassələri (300K)

Cədvəl №1

Tərkib, $(\text{PbSe})_{1-x}$ $(\text{CrSe})_x$	Qəfəs sabiti, $\sigma, \text{Å}$	Elektrik- keçirmə $\sigma, \text{om}^{-1}\text{sm}^{-1}$	Termo- ehq. $\alpha, \text{mkv/dər}$	İstilikkeçirmə $\chi, \text{Bm/dereca}$ ($\text{sm}^2/\text{dereca}$)	Yükdaşıyıcıların konsentrasiyası, n, sm^{-3}	Yükdaşıyıcı-ların yürüklüyü, $\mu, \text{sm}^2/(\text{b.sah})$	Qadağan olunmuş zolağın eni $\Delta E, \text{eV}$	Keciriciliyin tipi, n, g
0,00	6,14	362	282	12,62	$4,7 \cdot 10^{18}$	958	0,30	pp
0,02	—	326	276	12,23	$8,2 \cdot 10^{18}$	916	0,36	pp
0,04	6,21	285	297	11,46	$2,2 \cdot 10^{19}$	876	0,43	pp
0,06	6,31	267	312	10,96	$6,6 \cdot 10^{19}$	792	0,51	pp

Tədqiq olunmuş nümunələr üçün qadağan olunmuş zolağın eni hesablanmış və onun 0,30 ev ilə 0,51 ev qıymətləri arasında dəyişdiyi müəyyən olunmuşdur. ΔE -nin tərkibdən asılı olaraq belə dəyişməsi, qəfəs sabitinin

dəyişməsi ilə əlaqədardır. Termoelektrik hərəkət qüvvəsinin işarəsinin dəyişməsinə görə PbSe-nin «P» tip, onun əsasındaki ərintilərin isə «n» tip keçiriciyə malik olduğu müəyyən edilmişdir. Keçiriciliyinin tipinin

dəyişməsi qurğusunun (Pb^{+2}) və $Cr(Cr^{+3})$ atomlarının elektrik mənfilinin müxtəlifliyi ilə izah oluna bilər.

Elektrikkeçirmə və termo e.h.q.-nin tərkibdən asılı olaraq dəyişməsi yüksəlyicilərin konsentrasiyası və yürüklüğünün qiymətlərinin $CrSe$ -nin miqdarının $PbSe$ -də artması ilçə əlaqələndirilir. Keçiriciliyin tipinin dəyişməsi

qürüşün (Pb^{+2}) və Cr (Cr^{+3}) atomlarının elektromənfilinin müxtəlifliyi ilə izah olunur. Elektrikkeçirmə və termo-e.h.q.-nin tərkibdən asılı olaraq dəyişməsi yüksəlyicilərin konsentrasiyası və yürüklüğünün qiymətlərinin $CrCe$ -nin miqdarının $PbSe$ -də artması ilə əlaqələndirilir.

- [1] Yu.P. Paviç, V.A. Efimova, I.A. Smirnova. Metodi issledovaniya poluprovodnikov v primenenie xalkogenidov svintsa $PbTe$, $PbSe$, PbS . Moskva, izdatelstvo Nauka, 1968, 394 s.

- [2] M.A. Alidjanov. Zakonomernost svoystv v soedineniyax $A^{IV}B^{IV}$. Moskva, izdatelstvo VNITI, 1987, 96s.

М.А. Алиджанов, Н.М. Оруджев, А.О. Мехрабов, С.М. Алиджанова, Н.И. Ибаев

ИССЛЕДОВАНИЕ ФИЗИЧЕСКИХ СВОЙСТВ ПРИМЕСЕЙ, ПОЛУЧЕННЫХ НА ОСНОВЕ PbSe

Определена область твердого раствора на основе соединения селенида свинца, которая составляет до 6 мол % $PbSe$. Измерены физические свойства соединений $PbSe$ и сплавов содержащих 2,4 и 6 мол % $CrSe$ при 300 К.

Сплавы на основе $PbSe$ имеют кубическую структуру и являются полупроводниками электронного типа.

Измерены термоэлектрические параметры (термо э.д.с., теплопроводность, электропроводность), как основного компонента ($PbSe$) так и сплавов на его основе. Вычислены концентрация и подвижность носителей заряда на основе измерения эффекта Холла.

М.А. Алиджанов, Н.М. Оруджев, А.О. Мехрабов, С.М. Алиджанова, Н.И. Ибаев

INVESTIGATION OF IMPURITY PHYSICAL PROPERTIES OBTAINED ON THE BASE OF PbSe

The region of the solid solution based on plumbum selenide compound, which compounds up to 6 moth % of $CrSe$. Physical properties of $PbSe$ compound and alloys containing 2.4 and 6 moth % $CrSe$ at 300 K are measured.

Alloys based on $PbSe$ have cubic structure and are electronic type semiconductors.

Thermo-electric parameters (thermo edc, thermal conductivity, electric conduction) of the main component ($PbSe$) and alloys based on it are measured. Concentration and mobility of current carriers based on Hall effect measurement are calculated.

Received: 07.01.05

Fizika

**Azərbaycan Milli Elmlər Akademiyası
Fizika İnstitutu**

MÜNDƏRİCAT

Arakəsməli qazboşalmasının təsiri şəraitində dəri, sənaye tullantı sularının seolitdə təmizlənməsi.	M.Ə. Həsənov	3
Se-Te xalkoqenid şüşəvari yarımkəciri sistemlərdə həcmli yüklə məhdudlaşdırılmış cərəyanlar.S.İ. Mehdiyeva, A.İ. İsayev, G.A. Məmmədov, Z.A. Aqamaliyev	6	
Mayelərin xüsusi səthəmələgəlmə istiliyi.E.Ə. Eyyazov, A.U. Mahmudov, A.A. Abuşova, Y.M. Abbasov	9	
PbTe monokristallarının daxili sürtünmə və sürüşmə modulunun xüsusiyyətlərinin tədqiqi.O.İ. Davaraşvili, M.İ. Enukaşvili, N.P. Kekelidze, Q.Ş. Darsavelidze, L.L. Qabriçidze, E.R. Kuteliya, V.P. Zlomanov, O.İ. Tananayeva, T.S. Mamedov, N.D. Əhmədzadə, L.N. Teser	12	
Tirozinhidroksilaza N-sonlu domeninin Met1-Arq16 fragmentin quruluşunun nəzəri modeli.N.N. Mustafayeva, İ.N. Əliyeva, N.M. Qocayev	15	
Sinqlet-triplet antiferromaqnitlərdə işığın səth kollektiv oyanmaları ilə udulmasının xətti nəzəriyyəsi.A. M. Süleymanov	20	
Relaksasiya müddətinin mayelərin istilik tutumuna təsiri.Q.T. Həsənov, A.N. Məmmədova	25	
Modernizə edilmiş bridcmen üsulu ilə alınan Ge-Si bərk məhlullarında gallium aşqarının kristallaşma oxu boyunca paylanması.L.Ə. Qubatova, Z.M. Zeynalov, H.X. Əjdərov	28	
Qann effektinin qeyri-xətti nəzəriyyəsi.E.R. Həsənov, R.K. Qasimova	31	
TIB ¹¹¹ C ^{V1} ₂ anizotrop monokristallarında laylar arasındaki energi maniələrinin təyini.S.N. Mustafayeva	36	
In _{1-x} Ga _x As bərk məhlullarının istilik xassələri.R.N. Rəhimov	38	
Əks rabitələri ikeda modelində inversion xaoc sinxronlaşması. E.M. Şahverdiyev, R.A. Nuriyev, E.M. Hüseynova, L.H. Həşimovab R.H. Həşimov	42	
Asetilasetonun n-heptandakı məhlullarında ifrat yüksək tezlikli şüalanma zamanı əksolunmayan udulma effekti.M.İ. Vəliyev, R.M. Qasimov, Ç.O. Qacar	45	
Plazmali ionmənbəyinə malik kütlə spektrometrlərində ikinji növ ionların nisbi həssaslığının təyini.K.Z. Nuriyev	49	
FeGalnS ₄ - də termo-e.h.q. və Xoll effekti.N.N. Niftiyev, O.B. Tağıyev, F.M. Məmmədov	54	
Rastr zond mikroskopisişinin çox parametrli metodikası.S.P. Molçanov, S.H. Abdullayeva, İ.A. Çernova-Haraeva, I.C. Ələkbərov	56	
Kvant dinamik sistemləri təsvirində qatılışma metodu.E.A. Axundova	59	
CuAgS _{0.5} Se _{0.5} kristalında polimorf kecid.Y.H. Əsədov, R.B. Baykulov, Y.İ. Əliyev	62	
γ-soft bölgəsində yerləşən ¹³⁴ Ba nüvəsinin qayçı mod həyəcanlanmaları.Ə. Guliyev, F. Ertuğral, M. Güner, Z. Demir	66	
Deformasiya olmuş ^{176,178} Hf nüvələrinin kollektiv 1 ⁺ səviyyələri.H. Yakut, M. Bektaoğlu, F. Ertuğral, R. Akkaya, R. Akkaya	70	
Qurmuşun selen əsasında alınmış ərintilərin fiziki xassələrinin tədqiqi (300 K).M.Ə. Əlicanov, N.M. Orucov, A.O. Mehrabov, S.M. Əlicanova, N.U. İbayev	77	

СОДЕРЖАНИЕ

Использование цеолита для адсорбционной очистки кожевенных производственных сточных вод при воздействии электрических разрядов.	М.А. Гасанов	3
Токи, ограниченные объемным зарядом, в халькогенидных стеклообразных полупроводниках системы Se – Te.	С.И. Мехтиева, А.И. Исаев, Э.А. Мамедов, З.А. Агамалиев	6
Удельная теплота поверхностообразования жидкостей.	Э.А. Эйвазов, А.У. Махмудов, А.А. Абушова, Я.М. Абасов	9
Исследование особенностей внутреннего трения и модуля сдвига в монокристаллах теллурида свинца. О.И. Даварашвили, М.И. Енукашвили, Н.П. Кекелидзе, Г.Ш. Дарсавелидзе, Л.Л. Габричидзе, Э.Р. Кутелия, В.П. Зломанов, О.И. Тананаева, Т.С. Мамедов, Н.Д. Ахмедзаде, Л.Н. Тесер		12
Теоретическая модель структуры структуры фрагмента MET1-ARG16 N-концевого домена тирозингидроксилазы.	Н.Н. Мустафаева, И.Н. Алиева, Н.М. Годжаев	15
Линейная теория поглощения света поверхностными коллективными возбуждениями в синглет-триплетных антиферромагнетиках.	А. М. Сулейманов	20
Влияние времени релаксации на теплоемкость жидкостей.	Г.Т. Гасанов, А.Н. Мамедова	25
Распределение примеси галлия вдоль оси кристаллизации твердых растворов Ge-Si, выращенных модернизированным методом Бриджмена.	Л.А. Губатова, З.М. Зейналов, Г.Х. Аждаров	28
Нелинейная теория эффекта Ганна.	Э.Р. Гасанов, Р.К. Гасымова	31
Определение межслоевого энергетического барьера в анизотропных монокристаллах TLB ^{III} C ₂ ^{VI}	С.Н. Мустафаева	36
Теплопроводность твердых растворов In _{1-x} Ga _x As.	Р.Н. Рагимов	38
Инверсионная хаотическая синхронизация в модели Икеды с несколькими обратными связями.	Э.М. Шахвердиев, Р.А. Нуриев, Е.М. Гусейнова, Л.Г. Гашимова Р.Г. Гашимов	42
Эффект безотражательного поглощения сверхвысокочастотного излучения в растворах ацетил-акетона в н-гептане.	М.И. Велиев, Р.М. Касимов, Ч.О. Каджар	45
Метод расчета относительной интенсивности вторичных ионов в масс-спектрометрах с плазменными источниками ионов.	К.З. Нуриев	49
Термо – э.д.с.и эффект Холла в FeGaInS ₄	Н.Н. Нифтиев, О.Б. Тагиев, Ф.М. Мамедов	54
Метод многопараметрового режима в сканирующей зондовой микроскопии.	С.П. Молчанов, С.Г. Абдуллаева, И.А. Чернова-Хараева, С.Д. Алекперов	56
Метод вязкости в описании квантовых динамических систем.	Э.А. Ахундова	59
Полиморфные превращения в CuAgS _{0.5} Se _{0.5}	Ю.Г. Асадов, Р.Б. Байкулов, Ю.И. Алиев	62
Ножничная мода состояния для ядра ¹³⁴ Ba из региона γ -софт	Е. Гулиев, Ф. Ертуграл, М. Гунер, З. Демир	66
Коллективные 1 ⁺ состояния деформированных ядер ^{176,178} Hf.	Х. Яакут, М. Бекташогли, Ф. Ертуграл, Р. Аккайа	70
Исследование физических свойств примесей, полученных на основе селенида свинца (300К).	М.А. Алиджанов, Н.М. Оруджов, А.О. Мехрабов, С.М. Алиджанова, Н.У. Ибаев	77

CONTENTS

The use of zeolite for adsorption purification of the leather manufacturing waters at the electric discharge influence.....	M.A. Gasanov	3
The currents, limited by volume charge in the chalcogenide glassy semiconductors of Se-Te system..... S.I. Mekhtieva, A.L. Isayev, E.A. Mamedov, Z.A. Agamaliyev		6
The specific heat of the surface formation of liquids..... E.A. Evzakov, A.A. Abushova, Y.M. Abasov, A.U. Makmudov		9
The investigation of the peculiarities of the internal friction and the shear modulus in the lead telluride monocrystal..... O. Davarashvili, M. Enukashvili, N. Kekelidze, G. Darsavelidze, L. Gabrichidze, E. Kuteliya, V.P. Zlomanov, O.I. Tananaeva, N. Ahmedzade, L.Tecer, T. Mamedov		12
The theoretical model of the Met1-Arg16 segment structure from N-terminus of tyrosine hydroxylase domain	N.N. Mustafayeva, I.N. Aliyeva, N.M. Gojayev	15
Linear theory of the light absorption by the surface collective excitations in singlet – triplet antiferromagnets..... A. M. Suleymanov		20
The influence of the relaxation time on the liquid heat capacity	G.T. Gasanov, A.N. Mamedova	25
Axial Ga- impurity distribution in Ge-Si, solid solutions, grown by the modernized Bridgmen method..... L.A. Gubatova, , Z.M. Zeynalov, G.H. Ajdarov		28
The nonlinear theory of gun's effect..... E.R. Gasanov, R.K. Gasimova		31
The interlayer energy barrier in the anisotropic TiB ^{III} C ₂ ^{VI} monocrystals	S.N. Mustafaeva	36
Thermal conductivity of In _{1-x} Ga _x As solid solution..... R.N. Rahimov		38
Inverse chaos synchronization in the multi-feedback Ikeda model..... E.M. Shahverdiev, R.A. Nuriev, E.M. Huseynova, L.H. Hashimova, R.H. Hashimov		42
Effect of non-reflective absorption of microwave radiation in solutions of acetyl acetone in N-heptanes. M.I. Valiyev, R.M. Kasimov, Ch.O. Kadjar		45
The method for calculation of relative intensity of the secondary ions in mass-spectrometers with plasma type ions source..... K.Z. Nuriyev		49
Thermoelectromotive force and Hall effect in FeGaInS ₄ N.N. Niftiyev, O.B. Tagiyev, F.M. Mamedov		54
Multi Data Mode method in the scanning probe microscopy..... S.P. Molchanov, I.A. Chernova-Kharaeva, S.H. Abdullayeva, S.D. Alekperov		56
Viscosity method for the describing of dynamical systems..... E.A. Akhundova		59
Phase transitions in CuAgS _{0.5} Se _{0.5} Yu.G. Asadov, R.B. Baykulov, Yu.I. Aliyev		62
Scissors Mode In the γ -soft Nucleus ¹³⁴ Ba	E. Guliyev, F. Ertugra, M. Güner, Z. Demir	66
Collective 1 ⁺ states in ^{176,178} Hf deformed nuclei. I. H. Yakut, M. Bektasoğlu, F. Ertuğral and R. Akkaya		70
Investigation of impurity physical properties obtained on the base of PbSe. M.A. Aljanov, N.M. Orucov, A.O. Mehrabov, S.M. Aljanova, N.I. Ibayev		77